

# **Novel Photocatalytic Organic Synthesis: Cyclization and *N*-Alkylation of Nitroaromatic Compounds**

Von der Naturwissenschaftlichen Fakultät  
der Gottfried Wilhelm Leibniz Universität Hannover  
zur Erlangung des Grades

**Doktor der Naturwissenschaften**  
**Dr. rer. nat.**

genehmigte Dissertation

von

**Amer Hakki, Madjistir**

Geboren am 08.01.1978 in Damaskus, Syrien

**2013**

Referent: Prof. Dr. rer. nat. Detlef W. Bahnemann

Koreferent: Prof. Dr. rer. nat. Jürgen Caro

Tag der Promotion: 17. April 2013

## **Erklärung zur Dissertation**

Hierdurch erkläre ich, dass ich meine Dissertation mit dem Titel „**Novel Photocatalytic Organic Synthesis: Cyclization and *N*-Alkylation of Nitroaromatic Compounds**“ während meiner Tätigkeit als wissenschaftler Mitarbeiter am Institut für Technische Chemie der Gottfried Wilhelm Leibniz Universität Hannover selbständig verfasst und die benutzten Hilfsmittel und Quellen sowie gegebenenfalls die zu Hilfeleistungen herangezogenen Institutionen vollständig angegeben habe.

Die Dissertation wurde nicht schon als Masterarbeit, Diplomarbeit oder andere Prüfungsarbeit verwendet.

Hannover, 17. April 2013

Amer Hakki

## **Acknowledgements**

I am absolutely indebted to my supervisor Prof. Dr. Detlef Bahnemann. His brilliant academic guidance, patience, time, enthusiasm and support are greatly appreciated.

I would like also to express my deepest gratitude to Dr. Ralf Dillert for his tremendous efforts and his great scientific discussion.

I thank the Deutscher Akademischer Austauschdienst (DAAD), Bonn, Germany, for granting me the Ph.D scholarship and the Department of Chemistry, Damascus University, Damascus, Syria, for the extension of a scholarship.

My sincere thanks to Prof. Claus Rüscher and his team at the Institut für Mineralogie, Leibniz Universität Hannover for their help in the FTIR and the TGA measurements.

Dr. Armin Feldhoff, Mr. Frank Steinbach, and Dr. Oliver Merka at the Institut für Physikalische Chemie, Leibniz Universität Hannover are also gratefully acknowledged for their help in the TEM and XRD measurements.

Furthermore I thank Mr. Hendrik Fullriede at the Institut für Anorganische Chemie, Leibniz Universität Hannover for the NMR measurements.

I would like to extend my appreciation and thanks to all members of Prof. Bahnemann's group for their assistance in the lab related issues and for the friendly atmosphere of work.

Many thanks to all my friends especially Mahmoud Jaweesh, Anas Ajaj, and Viola Elenius.

I am deeply grateful to my parents, brothers and sister for their support whenever they are needed.

Finally many thanks to my wife for her understanding, patience and emotional support.

## Contents

<b>Contents.....</b>	<b>i</b>
<b>List of Figures.....</b>	<b>v</b>
<b>List of Tables.....</b>	<b>viii</b>
<b>Abstract.....</b>	<b>xi</b>
<b>Kurzzusammenfassung.....</b>	<b>xiii</b>
<b>1 Introduction .....</b>	<b>1</b>
1.1 Historical and theoretical background .....	1
1.2 Principles of photocatalytic reactions .....	6
1.2.1 Band bending at the semiconductor - electrolyte interface .....	6
1.2.2 Photoelectrochemical cells .....	8
1.2.3 Redox reaction on photoexcited TiO <sub>2</sub> particles.....	9
1.2.4 Energetic considerations.....	12
1.2.5 Solvent considerations.....	15
1.3 Modification of the surface of TiO <sub>2</sub> with precious metals.....	16
1.4 TiO <sub>2</sub> -based photocatalytic organic synthesis .....	18
1.4.1 Photocatalytic oxidation reactions employed for organic synthesis.....	18
1.4.2 Photocatalytic reduction reactions employed for organic synthesis.....	23
1.4.2.1 Photocatalytic reduction of nitroaromatic compounds.....	24
1.4.2.2 Effect of the modification of TiO <sub>2</sub> on the photocatalytic reduction of nitroaromatic compounds .....	27
1.5 Objectives of the study.....	29
<b>2 Materials and experimental methods .....</b>	<b>32</b>
2.1 Materials .....	32
2.2 Modification of the TiO <sub>2</sub> powders .....	32
2.2.1 Modification of TiO <sub>2</sub> with arenesulfonic acid functionalized mesoporous SiO <sub>2</sub> ..	32
2.2.2 Modification of TiO <sub>2</sub> with Pt nanoparticles .....	33
2.2.2.1 Photocatalytic deposition method .....	33
2.2.2.2 Mixing of solids method using colloidal Pt suspensions .....	33

2.2.3	Modification of TiO <sub>2</sub> with other precious metal nanoparticles .....	34
2.2.4	Modification of TiO <sub>2</sub> with bimetallic Ag-Pt nanoparticles .....	34
2.3	Characterizations of the prepared materials .....	34
2.3.1	Transmission electron microscopy .....	34
2.3.2	Specific surface area measurements .....	35
2.3.3	Infrared spectroscopy .....	35
2.3.4	Diffuse reflectance spectroscopy .....	35
2.3.5	Thermogravimetric measurements .....	35
2.3.6	X-ray diffraction .....	36
2.3.7	Acidic sites determination .....	36
2.3.8	Acidic capacity measurements .....	36
2.4	Photocatalytic reaction procedure .....	36
2.5	Dark reaction procedure .....	37
2.6	Analysis of the reaction mixture .....	38
2.6.1	Gas chromatography-mass spectroscopy measurements .....	38
2.6.2	Gas chromatography-flame ionization detector measurements .....	38
2.6.3	Gas chromatography- thermal conductivity detector measurments .....	39
2.6.4	Nuclear magnetic resonance spectroscopy .....	39
<b>3</b>	<b>Results .....</b>	<b>40</b>
3.1	General reaction sequence for the photocatalytic conversion of nitroaromatic compounds (NACs) .....	40
3.2	Photocatalytic conversion of the nitroaromatic compounds over bare TiO <sub>2</sub> .....	41
3.2.1	Effect of TiO <sub>2</sub> type on the photocatalytic conversion of the nitroaromatic compounds .....	43
3.2.2	Effect of the addition of an acid as a co-catalyst .....	47
3.2.2.1	Photocatalytic conversion of the nitroaromatic compound in ethanol .....	47
3.2.2.2	Photocatalytic conversion of different nitroaromatic compounds and different alcohols .....	48
3.3	Photocatalytic conversion of the nitroaromatic compounds over modified TiO <sub>2</sub> .....	51
3.3.1	TiO <sub>2</sub> Modified with acid functionalized SiO <sub>2</sub> .....	51

3.3.1.1	Characterization of the prepared catalysts.....	52
3.3.1.2	Photocatalytic activity of the newly prepared photocatalysts for the conversion of nitroaromatic compounds .....	57
3.3.2	TiO <sub>2</sub> modified with precious metals nanoparticles.....	59
3.3.2.1	Comparison of different precious metals loaded on the surface of TiO <sub>2</sub> .....	59
3.3.2.2	Effect of the type of TiO <sub>2</sub> supporting the Pt particles .....	61
3.3.2.3	Effect of the loaded amount of Pt.....	63
3.3.2.4	Influence of the light intensity.....	65
3.3.2.5	<i>N</i> -alkylation reactions of nitroaromatic compounds in different alcohols .....	66
3.3.2.6	Modification of the surface of TiO <sub>2</sub> with bimetallic platinum-silver nanoparticles.....	68
<b>4</b>	<b>Discussion .....</b>	<b>73</b>
4.1	Reduction of the nitroaromatic compounds .....	73
4.2	Effect of TiO <sub>2</sub> type on the photocatalytic conversion of the nitroaromatic compounds .....	81
4.3	Effect of the addition of an acid as a co-catalyst .....	84
4.4	Immobilization of Brønsted acid and TiO <sub>2</sub> into one heterogeneous photocatalyst.....	86
4.5	Discussion of the reaction mechanism.....	88
4.6	Effect of the deposition of metal nanoparticles on the surface of TiO <sub>2</sub> on the photocatalytic reaction of the nitroaromatic compounds.....	91
4.7	Effect of different parameters on the selectivity of the photocatalytic <i>N</i> -alkylation reaction.....	94
4.7.1	Effect of the type of TiO <sub>2</sub> .....	94
4.7.2	Effect of the platinization method .....	95
4.7.3	Effect of the loaded amount of Pt.....	95
4.7.4	Effect of the light intensity .....	97
4.7.5	Effect of the type of the loaded metal.....	98
4.8	Effect of the deposition of bimetallic (Pt-Ag) nanoparticles .....	99
4.9	<i>N</i> -alkylation of various nitroaromatic compounds by different alcohols .....	101
<b>5</b>	<b>Summary and conclusions .....</b>	<b>103</b>
<b>6</b>	<b>References.....</b>	<b>106</b>

---

<b>7</b>	<b>Appendix.....</b>	<b>121</b>
7.1	Names, structures, and abbreviations of the studied and the produced compounds .	121
7.2	List of abbreviations and symbols .....	126
7.3	Publications.....	128
7.4	Presentations .....	129
7.5	Curriculum vitae .....	130



---

## List of Figures

- Figure 1.1:** Schematic representation of different reaction processes activated by light: (a) direct photochemical reaction, (b) indirect photochemical reaction via energy transfer (photosensitization), (c) indirect photochemical reaction via species transfer (chemical reaction) where the sensitizer S is deactivated, and (d) indirect photochemical reaction via species transfer (chemical reaction) where the sensitizer S is regenerated (photocatalytic reaction). ..... 2
- Figure 1.2:** Schematic diagrams of the energy levels of: (a) intrinsic, (b) n-type, and (c) p-type semiconductors. The band bending in: (d) n-type semiconductor, and (e) p-type semiconductor in equilibrium with an electrolyte in the dark. .... 7
- Figure 1.3:** Band diagram for a PEC cell based on an n-type semiconducting photoanode that is electrically connected to a metal counter electrode; in equilibrium in the dark (a) and under illumination (b). Illumination raises the Fermi level and decreases the band bending. Near the semiconductor/electrolyte interface, the Fermi level splits into quasi-Fermi levels,  $E_{F,n}^*$  and  $E_{F,p}^*$ , for the electrons and holes, respectively[51]. ..... 8
- Figure 1.4:** Schematic description of the redox reaction photocatalyzed by a semiconductor as well as other fates of the photogenerated charge carriers. The circle represents a semiconductor particle, wherein A and D are the electron acceptor and donor, respectively. .... 10
- Figure 1.5:** Schematic description of the antenna effect induced by a network structure of semiconductor particles[56]. .... 12
- Figure 1.6:** Positions of the energy levels at the interface of an n-type semiconductor and a redox couple in an electrolyte[51]. .... 14
- Figure 1.7:** Schematic representation of the photocatalytic oxidation of alcohols in the absence (current doubling) or the presence of oxygen (radical chain mechanism)[105]. 22
- Figure 1.8:** Schematic illustration of the reduction of a nitroaromatic compound to an aminoaromatic compound. .... 25
- Figure 1.9:** Schematic illustration of the synthesis of quinolines and N-alkylated compounds starting from the photocatalytically formed aminoaromatic compounds and aldehydes. .... 29
- Figure 2.1:** Schematic view of the employed photocatalytic reaction system. .... 37
- Figure 3.1:** General reaction sequence for the photocatalytic conversion of the nitroaromatic compounds. A list of compounds with their names and corresponding symbols is provided in the Appendix. (e and h are not used in the symbols because they are usually used for the electron and the hole, respectively, in the discussion). .... 40

- Figure 3.2:** GC chromatograms obtained at different irradiation times of the reaction mixture (reaction conditions: 100  $\mu\text{mol}$  m-nitrotoluene (**1a**) and 25 mg  $\text{TiO}_2$  in 10 ml EtOH, 60 mW UV(A)/ $\text{cm}^2$ , 25  $^\circ\text{C}$ , under Ar atmosphere)..... 41
- Figure 3.3:** Time course of: photocatalytic conversion of (**1a**) ( $\bullet$ ); photocatalytic formation of: (**1c**) ( $\blacksquare$ ), (**1f**) ( $\blacklozenge$ ), (**1j**) ( $\blacktriangle$ ); and ( $\circ$ ) summation (reaction conditions: 100  $\mu\text{mol}$  (**1a**) and 25 mg  $\text{TiO}_2$  in 10 ml EtOH, 60 mW UV(A)/ $\text{cm}^2$ , 25  $^\circ\text{C}$ , under Ar atmosphere). Experimental error of the analysis is calculated to be 0.5%..... 42
- Figure 3.4:** Time courses of the: (A) consumption of m-nitrotoluene (**1a**), (B) production of the aminoaromatic compound (**1c**), (C) production of the imine (**1f**), and (D) production of the quinoline (**1j**); employing: UV100 ( $\blacksquare$ ), rutile ( $\bullet$ ), P25 ( $\blacklozenge$ ), and mesoporous anatase ( $\blacktriangledown$ ). (reaction conditions: 100  $\mu\text{mol}$  (**1a**) and 25 mg  $\text{TiO}_2$  in 10 ml EtOH, 60 mW UV(A)/ $\text{cm}^2$ , 25  $^\circ\text{C}$ , under Ar atmosphere)..... 44
- Figure 3.5:** Infrared spectra of bare  $\text{TiO}_2$ ; (a) UV100, (b) P25, (c) mesoporous anatase, and (d) rutile..... 46
- Figure 3.6:** Infrared spectra of  $\text{TiO}_2$  powders treated with pyridine vapor; (a) UV100, (b) P25, (c) mesoporous anatase, and (d) rutile. .... 46
- Figure 3.7:** Yield of the photocatalytically produced quinoline (**1j**) at: different p-TsOH concentrations (reaction conditions: 100  $\mu\text{mol}$  (**1a**), 25 mg  $\text{TiO}_2$ , and the required amounts of p-TsOH in 10 ml EtOH, 60 mW UV(A)/ $\text{cm}^2$ , 25  $^\circ\text{C}$ , under Ar atmosphere). .... 47
- Figure 3.8:** GC-MS chromatograms obtained after 4 hours irradiation of the reaction mixtures: (A) **1a**, (B) **6a**, (C) **3a**, (D) **2a**, and (E) p-NPh. The MS spectra refer to the peaks labeled with ( $\star$ ). (reaction conditions: 100  $\mu\text{mol}$  of nitroaromatic compound, 25 mg  $\text{TiO}_2$ , and (5 mol%) p-TsOH in 10 ml EtOH, 20 mW UV(A)/ $\text{cm}^2$ , 25  $^\circ\text{C}$ , under Ar atmosphere) ..... 49
- Figure 3.9:** FT-IR spectra of  $\text{TiO}_2$  (A),  $\text{SiO}_2$  (B), and extracted arenesulfonic modified  $\text{SiO}_2$ - $\text{TiO}_2$  samples with different Ar- $\text{SO}_3\text{H}$  molar ratios: 0 (C), 0.03 (D), 0.06 (E), 0.1 (F). (I) enlarged region from 1350-1650  $\text{cm}^{-1}$ , and (II) enlarged region from 990-1200  $\text{cm}^{-1}$ ..... 54
- Figure 3.10:** TGA and DTA measurements of: (a) the extracted arenesulfonic modified  $\text{SiO}_2$ - $\text{TiO}_2$  sample  $\text{T}_1\text{S}_1\text{Ar}_{0.1}$ , (b) extracted  $\text{TiO}_2$  modified with mesoporous silica, and (c)  $\text{TiO}_2$  modified with mesoporous silica calcined at 450  $^\circ\text{C}$  for 4h. .... 55
- Figure 3.11:** EDXS elemental map of: (a) silicon, (b) titanium, and (c) sulfur in the extracted arenesulfonic modified  $\text{SiO}_2$ - $\text{TiO}_2$  (sample  $\text{T}_1\text{S}_1\text{Ar}_{0.1}$ ); (d) TEM image of the porous  $\text{SiO}_2$  matrix in the same sample (e) Dark-field TEM micrograph showing the nanocrystalline  $\text{TiO}_2$  deposited on the  $\text{SiO}_2$  matrix; (f) HRTEM image of the sample

- showing the anatase polycrystallites on the surface of the sample  $T_1S_1Ar_{0.1}$ . The Fourier transformation (FFT) is shown as inset. .... 56
- Figure 3.12:** XRD patterns of: (A) pure  $SiO_2$ , (B)  $SiO_2-TiO_2$  (sample  $T_1S_1$ ), and (C) arenesulfonic modified  $SiO_2-TiO_2$  sample  $T_1S_1Ar_{0.03}$ . .... 57
- Figure 3.13:** Time-dependent change in the amounts of substrate and products during the photoirradiation of (**1a**) in EtOH: (**1a**) ( $\bullet$ ), (**1c**) ( $\blacksquare$ ), (**1f**) ( $\blacklozenge$ ), (**1l**) ( $\star$ ), (**1m**) ( $\star$ ), and ( $\circ$ ) summation (reaction conditions: 100  $\mu\text{mol}$  (**1a**) and 25 mg  $Pt_{0.5}/TiO_2$  in 10 ml EtOH, 60 mW UV(A)/ $\text{cm}^2$ , 25  $^\circ\text{C}$ , under Ar atmosphere). .... 60
- Figure 3.14:** Selectivity of the reaction products obtained upon illumination of the ethanolic solutions of m-nitrotoluene (**1a**) in the presence of Schachtleben Hombikat UV100 loaded with different amounts of Pt. .... 63
- Figure 3.15:** TEM images of Hombikat UV100 samples containing different amounts of Pt: (a)  $Pt_{0.3}/TiO_2$  (c)  $Pt_{0.5}/TiO_2$ , and (d)  $Pt_{1.0}/TiO_2$ . (b) HRTEM image of  $Pt_{0.3}/TiO_2$ . .... 64
- Figure 3.16:** Time-dependent change in the concentrations of **1a** (empty symbols) and **1l** (filled symbols) in the presence of  $Pt_{0.5}/TiO_2$  UV100 at different light intensities: 60  $\text{mW}/\text{cm}^2$  ( $\blacklozenge$ ), 30  $\text{mW}/\text{cm}^2$  ( $\blacksquare$ ), and 15  $\text{mW}/\text{cm}^2$  ( $\blacktriangle$ ). (reaction conditions: 100  $\mu\text{mol}$  (**1a**) and 25 mg  $Pt_{0.5}/TiO_2$  UV100 in 10 ml EtOH, 25  $^\circ\text{C}$ , under Ar atmosphere). .... 65
- Figure 3.17:** Time-dependent change in the amount of N-ethyl-m-toluidine (**1l**) during the photoirradiation of (**1a**) in EtOH in the presence of  $Ag_n/Pt_m/TiO_2$ : bare  $TiO_2$  ( $\blacksquare$ ),  $Pt_{0.5}/TiO_2$  ( $\bullet$ ),  $Ag_{0.1}/Pt_{0.5}/TiO_2$  ( $\blacktriangle$ ),  $Ag_{0.3}/Pt_{0.5}/TiO_2$  ( $\blacktriangledown$ ),  $Ag_{0.5}/Pt_{0.5}/TiO_2$  ( $\blacklozenge$ ),  $Ag_{1.0}/Pt_{0.5}/TiO_2$  ( $\blacktriangleleft$ ), (reaction conditions: 100  $\mu\text{mol}$  (**1a**) and 25 mg  $Ag_n/Pt_m/TiO_2$  in 10 ml EtOH, 60 mW UV(A)/ $\text{cm}^2$ , 25  $^\circ\text{C}$ , under Ar atmosphere). .... 68
- Figure 3.18:** Time-dependent change in the amount of the N-ethyl-m-toluidine (**1l**) during the photoirradiation of (**1a**) in EtOH in the presence of  $Pt_m/Ag_n/TiO_2$ :  $Ag_{0.5}/TiO_2$  ( $\blacksquare$ ),  $Pt_{0.1}/Ag_{0.5}/TiO_2$  ( $\bullet$ ),  $Pt_{0.3}/Ag_{0.5}/TiO_2$  ( $\blacktriangle$ ),  $Pt_{0.5}/Ag_{0.5}/TiO_2$  ( $\blacktriangledown$ ), (reaction conditions: 100  $\mu\text{mol}$  (**1a**) and 25 mg  $Pt_m/Ag_n/TiO_2$  in 10 ml EtOH, 60 mW UV(A)/ $\text{cm}^2$ , 25  $^\circ\text{C}$ , under Ar atmosphere). .... 69
- Figure 3.19:** Diffuse reflectance spectra of bare  $TiO_2$  (Schachtleben Hombikat UV100) and of  $TiO_2$  (Schachtleben Hombikat UV100) photocatalytically modified with bimetallic (Pt-Ag) nanoparticles: (a)  $Ag_{m(m=0-1.0)}/Pt_{0.5}/TiO_2$  and (b)  $Pt_{n(n=0-0.5)}/Ag_{0.5}/TiO_2$ . .... 71
- Figure 3.20:** Dark Field-TEM image of  $Ag_{0.5}/Pt_{0.5}/TiO_2$  sample (a) and HRTEM image of the same sample (b). .... 72
- Figure 4.1:** Suggested overall reaction steps of the photocatalytic conversion of the NACs. 73
- Figure 4.2:** Schematic representation of the proposed steps for the photocatalytic reduction of m-nitrotoluene dissolved in ethanol at an irradiated  $TiO_2$  particle, (1)

---

photogeneration of charge carriers,  $e^-$  and  $h^+$ ; (2) trapping of  $e^-$ ; (3) first oxidation step of EtOH by trapped hole; (4) formation of acetaldehyde through electron injection into the conduction band of  $TiO_2$  (current-doubling); (5) reduction of m-nitrotoluene to m-nitrosotoluene by two of the CB electrons; (6) reduction of m-nitrosotoluene to m-(hydroxyamino)toluene by two of the CB electrons; (7) reduction of m-(hydroxyamino)toluene to m-toluidine by two of the CB electrons; (8) recombination channel. Note: For simplicity, the electrons (trapped and injected) required for total reduction of the nitro group to the amino group is presented as  $6e^-$  in the CB. .... 74

**Figure 4.3:** Proposed reaction mechanism for the Lewis acid-catalyzed formation of the imine on the surface of  $TiO_2$ . .... 80

**Figure 4.4:** ATR-FTIR spectra of  $TiO_2$  layers in contact with pyridine in acetonitrile solution (100 mM). Solid lines and dotted lines refer to non irradiated and UV(A) irradiated samples, respectively. (a)  $TiO_2$  rutile, (b)  $TiO_2$  UV100, and (c)  $TiO_2$  P25. .... 84

**Figure 4.5:** Schematic presentation of the formation of the vinyl ether and its addition to the imine to form the quinoline compound. .... 85

**Figure 4.6:** Splitting of alcohol from the ethoxy-1,2,3,4-tetrahydroquinoline molecule to form the dihydroquinoline derivative. .... 86

**Figure 4.7:** Pathways of the photocatalytic formation of the quinoline compounds from NACs and alcohols. .... 88

**Figure 4.8:** Pathway A in **Figure 4.7**. .... 89

**Figure 4.9:** Pathway B in **Figure 4.7**. .... 90

**Figure 4.10:** Pathway C in **Figure 4.7**. .... 91

**Figure 4.11:** Proposed mechanism for the one-pot N-alkylation of m-nitrotoluene promoted by  $TiO_2$  loaded with metal nano particles catalyst under photoirradiation. ... 102

**Figure 5.1:** Schematic summarization of the fates of the nitroaromatic compounds in alcohols upon illumination in the presence of different bare or modified  $TiO_2$  photocatalysts. .... 103

**List of Tables**

**Table 1.1:** Examples of commonly used homogeneous photocatalysts[6]. .... 3

**Table 1.2:** Approximate band positions of some common semiconductors[60]. .... 13

**Table 1.3:** Examples of photocatalytic oxidation reactions ..... 19

**Table 1.4:** Examples of photocatalytic reduction reactions ..... 24

---

<b>Table 1.5:</b> Formal potentials for the couple $\text{RNO}_2/\text{RNO}_2^{\bullet-}$ for some nitroaromatic compounds[121].....	26
<b>Table 3.1:</b> Physical properties of the employed photocatalysts.....	43
<b>Table 3.2:</b> Photocatalytic conversion of different NACs in different alcohols in the presence of $\text{TiO}_2$ and p-TsOH as co-catalyst. ....	50
<b>Table 3.3:</b> Physical and chemical properties of the prepared catalysts. ....	52
<b>Table 3.4:</b> Conversion of m-nitrotoluene ( <b>1a</b> ) and yields of m-toluidine and 2,7-dimethylquinoline ( <b>1j</b> ) obtained upon the illumination of EtOH solutions containing m-nitrotoluene and the corresponding catalyst. ....	58
<b>Table 3.5:</b> Photocatalytic conversion of m-nitrotoluene with EtOH employing different metal loaded on $\text{TiO}_2$ UV100.....	61
<b>Table 3.6:</b> Photocatalytic conversion of m-nitrotoluene with EtOH employing different Pt loaded $\text{TiO}_2$ .....	62
<b>Table 3.7:</b> Photocatalytic N-alkylation of nitroaromatic compounds in different alcohols employing 1%Pt/ $\text{TiO}_2$ . ....	66
<b>Table 3.8:</b> Amount of the photocatalytically generated hydrogen during the photocatalytic reduction of m-nitrotoluene employing different ( $\text{Ag}_m\text{-Pt}_n$ )/ $\text{TiO}_2$ photocatalysts. ....	70
<b>Table 4.1:</b> Photonic efficiencies $\xi$ (%) of the photocatalytic reduction of m-nitrotoluene in ethanol over different type of $\text{TiO}_2$ powders with their respective BET surface area . ...	78
<b>Table 4.2:</b> Selectivity of the photocatalytic reduction of m-nitrotoluene employing different $\text{TiO}_2$ photocatalysts under UV(A) irradiation. ....	81
<b>Table 4.3:</b> Photonic efficiencies $\xi$ (%) of the photocatalytic reduction of m-nitrotoluene ( <b>1a</b> ) and the photocatalytic $\text{H}_2$ evolution in ethanol over bare $\text{TiO}_2$ UV100 or Pt0.5/ $\text{TiO}_2$ UV100. ....	94
<b>Table 4.4:</b> N-alkylation of the m-toluidine ( <b>1c</b> ) with acetaldehyde in the presence of different metal loaded $\text{TiO}_2$ .....	99



---

**Abstract**

The photocatalytic conversion of nitroaromatic compounds in alcohols employing TiO<sub>2</sub>-based photocatalysts has been studied. The light-induced conversion of *m*-nitrotoluene dissolved in ethanol under Argon has been chosen as a model reaction. The effect of the type of the employed TiO<sub>2</sub> (Sachtleben Hombikat UV100 as anatase, Cristal Global R34 as rutile, Evonik-Degussa Aeroxide P25 as anatase-rutile mixture, and home-made mesoporous anatase) on the reaction products has been investigated. Moreover, TiO<sub>2</sub> was modified either with acids or with various precious metals in order to investigate the effect of these modifications on the reaction sequence and products.

Acid modified TiO<sub>2</sub> was successfully prepared via the co-condensation of 2-(4-chlorosulfonylphenyl)ethyltrimethoxysilane (CSPTMS) and tetraethyl orthosilicate (TEOS) in the presence of commercially available Sachtleben Hombikat UV100 TiO<sub>2</sub> particles. The resulting bifunctional catalysts were characterized by TEM and BET measurements, and by FT-IR, TGA, and acid-base titration method.

For the modification of bare TiO<sub>2</sub> with noble metals, different precious metals (Pt, Pd, Au, and Ag) have been photocatalytically deposited on the surface of TiO<sub>2</sub> particles. Moreover, the influences of various parameters including the loaded amount of Pt and its particle size, the platinization method, and the light intensity on the selectivity of the photocatalytic reaction have been studied by employing platinized Sachtleben Hombikat UV100 TiO<sub>2</sub> particles. Furthermore, bimetallic (Ag-Pt) modified Sachtleben Hombikat UV100 TiO<sub>2</sub> photocatalysts have been prepared and tested for the same model reaction.

Upon irradiation of the ethanolic solution of *m*-nitrotoluene in the absence of oxygen gas and in the presence of the photocatalyst, different products are obtained according to the applied photocatalyst. It is found that the surface properties of the photocatalyst play an important role in the reaction pathway and thus in the selectivity of the products. In all cases,

---

a simultaneous reduction of the nitroaromatic compound and an oxidation of the alcohol are induced by the photogenerated electrons and holes, respectively. An imine is then produced upon condensation of the generated aldehyde and aminoaromatic compounds. Rutile is found to be more selective towards the primary aminoaromatic compound (*m*-toluidine) while anatase photocatalysts yield a higher amount from the imine (*N*-ethylidene-3-methylaniline). A cyclization reaction of the produced imine to generate methyl quinoline is observed when Aeroxide P25 or acid modified Sachtleben Hombikat UV100 is used as the photocatalyst.

On the other hand, *N*-alkylation reactions of the nitroaromatic compounds by alcohols take place through the combination of the photocatalytic properties of titanium dioxide and the catalytic properties of metal nanoparticles supported on its surface. Among the employed precious metals, Pt/TiO<sub>2</sub>(UV100) exhibits a superior selectivity towards the formation of mono *N*-alkylated products. By increasing the loaded amount of Pt the selectivity towards mono *N*-alkylated products increases reaching the highest selectivity when (1wt%)Pt/TiO<sub>2</sub> was employed. Moreover, Pt/TiO<sub>2</sub> prepared by the photocatalytic deposition method was found to be more active and selective than the one obtained through a mixed solids synthesis method. Changing the light intensity does not affect the reaction selectivity but it affects the required time to obtain the highest yield of the desired product. The illumination time plays an important role in the selectivity of the mono *N*-alkylation reaction, with prolonged illumination time the *N*-alkylated product completely converts into the *N,N*-dialkylated one. Loading of a small amount of Ag (0.1 wt.%) on the photocatalyst (0.5wt%)Pt/TiO<sub>2</sub>(UV100) enhances the selectivity towards the mono *N*-alkylated product resulting in similar yields as if (1wt%)Pt/TiO<sub>2</sub> was employed. However, a further increase in the amount of Ag in these bimetallic samples has negative effects on the mono *N*-alkylated product selectivity.

**Keywords:** Photocatalysts, anatase, rutile, photocatalytic reduction, photocatalytic oxidation, imine, quinoline, *N*-alkylation, reaction mechanism.



---

## Kurzzusammenfassung

Die photokatalytische Umsetzung von Nitroaromaten in Alkoholen wurde unter Verwendung verschiedener Titandioxid ( $\text{TiO}_2$ ) Photokatalysatoren untersucht. Die lichtinduzierte Umwandlung von *m*-Nitrotoluol in Ethanol unter Argon wurde als Modellreaktion ausgewählt. Die Auswirkung diverser  $\text{TiO}_2$ -Typen (Sachtleben Hombikat UV100 als Anatas, Cristal Global R34 als Rutil, Evonik-Degussa P25 Aeroxide als Anatas-Rutil-Gemisch und selbstsynthetisiertes mesoporöses Anatas) auf die Bildung der Reaktionsprodukte wurde erforscht. Außerdem wurde das  $\text{TiO}_2$  entweder mit Säure oder mit verschiedenen Edelmetallen modifiziert, um die Wirkung dieser Modifizierungen auf den Reaktionsverlauf und die Ausbildung der Produkte zu untersuchen.

Säuremodifiziertes  $\text{TiO}_2$  wurde durch die Co-Kondensation von 2-(4-Chlorsulfonylphenyl) ethyltrimethoxysilan (CSPTMS) und Tetraethylorthosilikat (TEOS) in Gegenwart von kommerziellen  $\text{TiO}_2$ -Partikeln erfolgreich hergestellt. Die resultierenden bi-funktionellen Katalysatoren wurden durch TEM, BET, FT-IR, TGA, und Säure-Base-Titration charakterisiert.

Verschiedene Edelmetalle (Pt, Pd, Au und Ag) wurden auf der Oberfläche des  $\text{TiO}_2$  photokatalytisch abgeschieden. Die Einflüsse der verschiedenen Parameter, wie die Platinmenge, die Teilchengröße der Platincluster, die Platinierungsmethode sowie der Einfluss der Lichtintensität auf die Selektivität der photokatalytischen Reaktion wurden untersucht. Weiterhin wurden Sachtleben Hombikat UV100  $\text{TiO}_2$ -Photokatalysatoren mit bimetallicen (Ag - Pt) Nanopartikeln modifiziert und für die oben beschriebene Reaktion getestet.

Je nach eingesetztem Photokatalysator wurden verschiedene Produkte bei der Bestrahlung der ethanolischen Lösung von *m*-Nitrotoluol in Abwesenheit von Sauerstoff erhalten. Es zeigte sich, dass die Oberflächeneigenschaften des Photokatalysators einen wichtigen Einfluss auf den Reaktionsweg und auf die Selektivität der Produkte haben. In allen Fällen wurde gleichzeitig die Reduktion der Nitroaromaten und die Oxidation des Alkohols durch die

---

lichterzeugten Elektronen und Löcher induziert. Hierbei wird ein Imin aus der Kondensation des photokatalytisch erzeugten Aldehyds mit den Aminoaromaten erhalten. Rutil erwies sich als selektiver für die primären Aminoaromaten (*m*-Toluidin), wohingegen auf Anatas basierte Photokatalysatoren eine höhere Menge an Iminen (*N*-Ethyliden-3-methylanilin) lieferten. Die Umsetzung des hergestellten Imins zu Methylchinolin durch eine Zyklisierungsreaktion wurde während der Verwendung von Aeroxide P25 oder säuremodifiziertem Sachtleben Hombikat UV100 beobachtet.

Andererseits erfolgten die *N*-Alkylierungsreaktionen der Nitroaromaten mit dem Alkohol durch die Kombination der photokatalytischen Eigenschaften von Titandioxid mit den katalytischen Eigenschaften der Metallnanopartikel, welche auf der TiO<sub>2</sub> Oberfläche gebunden sind. Unter den verwendeten Edelmetallen zeigte Pt auf TiO<sub>2</sub> (UV100) die höchste Selektivität für die Bildung von *N*-monoalkylierten Produkten. Die Selektivität der Bildung von *N*-monoalkylierten Produkten nahm durch das Erhöhen der aufgetragenen Pt-Menge zu. Das mittels photokatalytischer Abscheidungsverfahren hergestellte Pt/TiO<sub>2</sub> ist aktiver und selektiver als das durch das gemischte Feststoffsyntheseverfahren hergestellte Pt/TiO<sub>2</sub>. Die Veränderung der Lichtintensität beeinflusst nicht die Selektivität der Reaktion sondern lediglich die erforderliche Zeit, um die höchste Ausbeute des gewünschten Produkts zu erhalten. Zudem spielt die Bestrahlungszeit eine wichtige Rolle für die Selektivität der *N*-Monoalkylierungsreaktion, da das *N*-alkylierte Produkt bei längerer Bestrahlungszeit vollständig in das *N,N*-dialkylierte Produkt umgewandelt wird. Die Beladung mit einer kleinen Ag-Menge (0,1 Gew.%) auf den (0,5 Gew.%) Pt/TiO<sub>2</sub> (UV100) Photokatalysator verbessert die Selektivität für das *N*-monoalkylierten Produkt. Eine weitere Erhöhung der Ag-Menge in diesen Bimetallproben hat allerdings negative Auswirkungen auf die Selektivität des *N*-monoalkylierten Produktes.

**Stichworte:** Photokatalysatoren, Anatas, Rutil, photokatalytische Reduktion, photokatalytische Oxidation, Imine, Chinolin, *N*-Alkylierung, Reaktionsmechanismus.

## 1 Introduction

### 1.1 Historical and theoretical background

Up to the beginning of the 20<sup>th</sup> century scientists regarded illumination just as one of different ways available to increase the reaction rate such as heating or adding the appropriate chemicals. Until 1912 when Giacomo Luigi Ciamician (1857–1922), the founder of photochemistry and one of the pioneers of the solar energy usage for chemical synthesis[1-3] stated that: “*organic chemistry ... needs ... high temperature, inorganic acids and very strong bases, halogens, the most electropositive metals, some anhydrous metal chlorides and halogenated phosphorous compounds.... plants, on the contrary, by using small traces of carbonic acid obtained from the air, small amounts of salts subtracted from the ground, water found everywhere, and by exploiting solar light, are able to prepare easily many substances that we can badly reproduce*”. These words opened the door for scientists to learn from the plants how to utilize light to carry out chemical reactions. Subsequently, Ciamician, in collaboration with Paul Silber, devoted intensive and patient systematic work to understand the chemical effect of light. Their efforts resulted in the discovery of a range of interesting photochemical processes caused only by light not by heat[4].

In 1914 Bodenstein recognized that photochemical reactions involve electronically excited states exhibiting a reactivity different from that of the ground state[5]. These reactions, in which the reacting molecule has been previously promoted by absorption of light to an electronically excited state, are called photochemical reactions (*cf.* **Figure 1.1a**). However, activation with light does not necessarily imply that the reactant  $R$  is directly irradiated. It is also possible to promote the reagent  $R$  indirectly (photosensitization) by employing a sensitizer  $S$  that absorbs the light and transfers energy to the reagent  $R$  (*cf.* **Figure 1.1b**). Apart from such as energy transfer, the light-absorbing species  $S$  may alternatively activate the reagent  $R$  by a chemical reaction (such as an electron transfer) eventually transforming it into the final products, possibly via further intermediates (*e.g.*,  $R_{\text{int}}$ , *cf.* **Figure 1.1c**) while the

species  $S$  will be converted to the deactivated form  $S_{de}$ . However, if the deactivated species  $S_{de}$  can be regenerated by reacting with an intermediate or a substrate present in the reaction mixture (*cf.* **Figure 1.1d**) it will be appropriate to call such a process a ‘photocatalytic’ reaction[6]. Hence, the term ‘photocatalytic’ implies that light and a catalyst, that is activated by absorbing this light, are necessary to induce or accelerate a chemical transformation[7, 8].

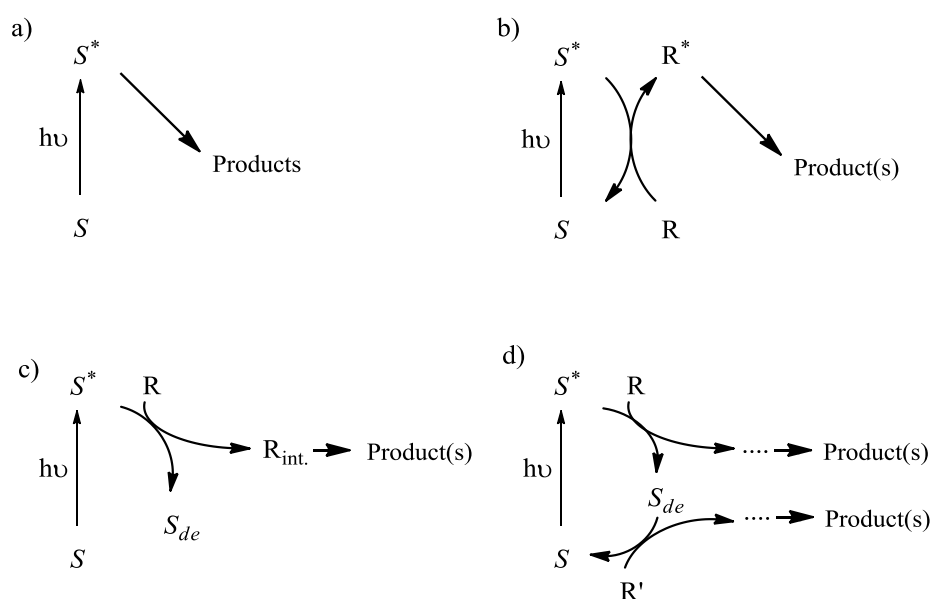


**Figure 1.1:** Schematic representation of different reaction processes activated by light: (a) direct photochemical reaction, (b) indirect photochemical reaction via energy transfer (photosensitization), (c) indirect photochemical reaction via species transfer (chemical reaction) where the sensitizer  $S$  is deactivated, and (d) indirect photochemical reaction via species transfer (chemical reaction) where the sensitizer  $S$  is regenerated (photocatalytic reaction).

In general, photocatalysts can be divided into two classes: homogeneous and heterogeneous photocatalysts. Homogeneous photocatalysts include aromatic compounds, in particular, those bearing strongly electron withdrawing substituents, quinons, and electron-poor heterocycles. **Table 1.1** shows some of the commonly used homogeneous photocatalysts together with their reduction potentials (*vs.* NHE) in the relevant excited state.

**Table 1.1:** Examples of commonly used homogeneous photocatalysts[6]

Photocatalyst	Common name	Reduction potential <sup>[a]</sup> [V] vs. NHE	Exited state
	Chloranil	3.57	Triplet
	Terephthalonitrile	2.91	Singlet
	Anthraquinone	2.40	Triplet
	Benzophenone	1.79	Triplet

[a] Values vs. SCE have been converted to the NHE scale by adding + 0.24 Volts[9]

Semiconducting transition metal oxides or sulfides, such as TiO<sub>2</sub>, ZnO, ZnS, and CdS, are examples for heterogeneous photocatalysts. Upon absorption of light with a suitable energy [10-12] these materials simultaneously act as oxidants and reductants. The respective photocatalytic reactions will then occur on the surface of these solids which can easily be separated from the reaction mixture after the completion of the reaction.

At the early 1970s, scientists started to focus on possible applications of these photocatalysts in response to challenging energy and environmental issues [12-15]. The oil crisis gave a strong impulse to the research of alternative energy sources, i.e., exploiting solar energy for the generation of suitable fuels, in particular, of molecular hydrogen through water splitting [16-18]. On the other side, concern about pollution by chemicals increased and it was proposed that photocatalysis might be employed to clean up water and air avoiding the

---

addition of more aggressive oxidants than air [11]. In addition to that, the subsequently developed photocatalytic chemical synthesis assumed to be a promising method which according to today's nomenclature belongs into the field of green – or sustainable – chemistry[5, 19].

One of the earliest reports of the photocatalytic effect of titania was published in 1921 by Renz [20], who observed that titania turned from white into a dark color upon solar illumination in the presence of organic compounds such as glycerol. The photobleaching of dyes caused by the effect of semiconductors was reported in 1928 by Keidel and by Wagner [21]. A detailed photochemical study of the bleaching of a dye (Chlorazol Sky Blue FF) on titanium dioxide in the dry state is described in the work of Goodeve and Kitchener published in 1938[22]. This process appeared at first sight to be a true case of photosensitization, because the dye was photochemically stable on various transparent substances such as barium sulphate, but showed rapid fading on  $\text{TiO}_2$  and other oxides which were found to absorb ultra-violet light[22]. Consequently, the definition ‘photocatalyst’ was not used in these reports but the term ‘photosensitizer’ was used instead. Carey *et al.*,[23] were among the first authors who used the term photocatalyst in their report in which they employed a semiconductor photocatalyst for the destruction of an organic compound in water. Later on, in 1977, Frank and Bard first examined the possibility of using  $\text{TiO}_2$  to decompose cyanide as an example of an inorganic pollutant in water[24]. One of the earliest observations concerning the photocatalytic oxidation in the gas phase was reported by McLintock and Ritchie in 1965[25]. In the middle of 1980s, researchers focused on the application of semiconductors, especially  $\text{TiO}_2$ , for the degradation of pollutants in order to purify water as well as air through the complete oxidation of all organic or inorganic pollutants. The extensive work in this field resulted in thousands of papers and reviews covering different topics such as the type of pollutant, the detailed mechanisms of the photocatalytic degradation of different organic

compounds, and the modification of the photocatalyst materials as well as the design of the photoreactors[11, 13, 14, 26-28].

Research in the field of photoelectrochemical and/or photocatalytic water splitting, as an important process for solar energy conversion, “exploded” following the demonstration of the photoelectrolysis of water employing a TiO<sub>2</sub> photoelectrode in the presence of an anodic bias under UV(A) illumination by Fujishima and Honda in 1972[29]. Following a rather quiet period in the 1990s and the early part of this century, this research area started “blooming” again today initiated by the apparent scarcity of fossil fuel.

The application of heterogeneous photocatalysis for organic synthesis is also a very attractive and significant research topic, which, however, has not been extensively studied. In particular, the fact that some reactions can only be initiated in photocatalytic reaction systems should be regarded as a significant observation with considerable implications for possible applications. Being one of the first reports in this area, Frank and Bard (1977), reported the formation of tribromoaniline after the photooxidation of Br<sup>-</sup> at TiO<sub>2</sub> in the presence of aniline[30]. In 1979, Reiche and Bard reported the photocatalytic generation of amino acids from CH<sub>4</sub>, N<sub>2</sub>, and H<sub>2</sub>O in the presence of platinized TiO<sub>2</sub>[31, 32]. The TiO<sub>2</sub> or CdS induced peptide formation from glycine was reported by Onoe et al. in 1985[33]. Fox and co-workers have also placed great emphasis on the photocatalytic organic transformation especially on the photocatalytically induced oxygenation of various organic compounds[34-36]. One example is the oxidation of 1,1-diphenylethylene dissolved in acetonitrile by O<sub>2</sub> in the presence of TiO<sub>2</sub> yielding benzophenone and CO<sub>2</sub>[34]. These authors have found that the products obtained employing TiO<sub>2</sub> as the photocatalyst are different from those obtained electrochemically on metal electrodes as well as from those generated when a homogeneous photocatalyst was used. Another example concerning the unique selectivity of heterogeneous photocatalysis is the reduction of haloethane (2-bromo-2-chloro-1,1,1-trifluoroethane) to (2-chloro-1,1-difluoroethene) by the conduction band electrons photogenerated in aqueous

colloidal suspensions of platinized titanium dioxide as reported in 1987 by Bahnemann et. al.[37]. In the middle of 1980s, Ohtani and co-workers have investigated the formation of Schiff's bases as well as the preparation of symmetrical secondary amines from primary amines employing platinized titanium dioxide suspensions in water or in organic solvents[38-40]. Other examples in the field of photocatalytic organic synthesis have also been reported such as the photocatalytic cyclization of  $\alpha,\omega$ -diamines[40], the synthesis of unsaturated *N*-phenyl- $\alpha$ -amino esters[41], the synthesis of unsaturated  $\alpha$ -cyano-homoallylamines[42], the light induced carbon-carbon bond formation [43], and the diastereoselective radical tandem addition-cyclization reactions of aromatic tertiary amines[44]. The photocatalytic organic synthesis or the respective organic transformations have been the topic of several reviews as well[5, 12, 19, 45].

## 1.2 Principles of photocatalytic reactions

The heterogeneous photocatalytic conversion of an organic compound belongs to the field of those redox reactions initiated by the absorption of a photon in the close vicinity of the surface of a solid photocatalyst to which the substrates are adsorbed. The general photocatalytic properties of suspensions of semiconducting TiO<sub>2</sub> particles are well established and have been extensively described in the literature[12, 46, 47].

### 1.2.1 Band bending at the semiconductor - electrolyte interface

Unlike metals, the electronic structure of semiconductors is characterized by the presence of a bandgap ( $E_g$ ), which is essentially an energy interval with very few electronic states (*i.e.*, with a low density of states) between the filled valence band (VB) and the nearly vacant conduction band (CB), each of which having a high density of states[48].

The Fermi level, which is defined as the energy level at which the probability of occupation by an electron is one half[49], lies in an intrinsic semiconductor at the mid-point of the band gap (*cf.* **Figure 1.2 a**). Whereas, in an n-type (negatively doped) or a p-type



(positively doped) semiconductors, the Fermi level lies just below the conduction band edge or just above the valence band edge, respectively (see **Figure 1.2** b and c).

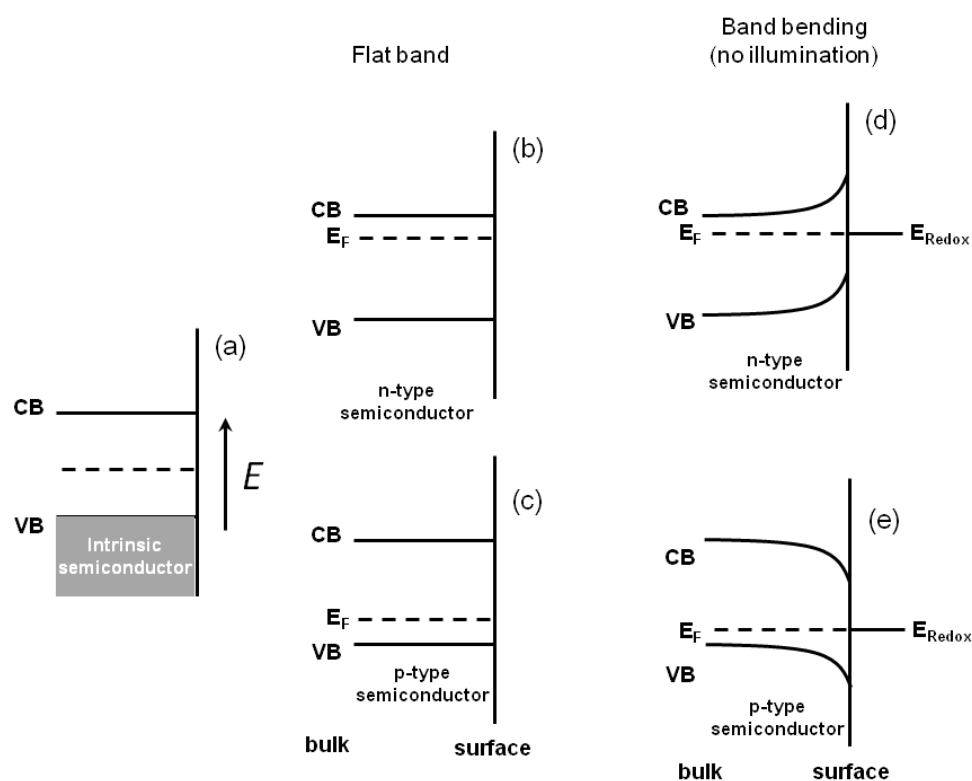


**Figure 1.2:** Schematic diagrams of the energy levels of: (a) intrinsic, (b) n-type, and (c) p-type semiconductors. The band bending in: (d) n-type semiconductor, and (e) p-type semiconductor in equilibrium with an electrolyte in the dark.

When a semiconductor surface is brought into contact with an electrolyte containing a redox couple, the mobile charge carriers will be transferred between the semiconductor and the redox system until equilibrium is attained. This will result in the movement of the redox potential to that of the bulk Fermi level to the equilibrium potential, thus the bands bend either upward (in the case of an n-type semiconductor) or downward (in the case of a p-type semiconductor) (*cf.* **Figure 1.2** d and e). Such a band bending may also occur if the surface of the semiconductor is brought into contact with adsorbed molecules (from the gas phase) or with a metal (solid phase)[50].

## 1.2.2 Photoelectrochemical cells

**Figure 1.3** shows a simplified energy diagram of a photoelectrochemical (PEC) cell based on a single photoanode and a metal counter electrode. The main component of the PEC cell is the semiconductor(s) from which the photoanode and /or the photocathode are prepared.

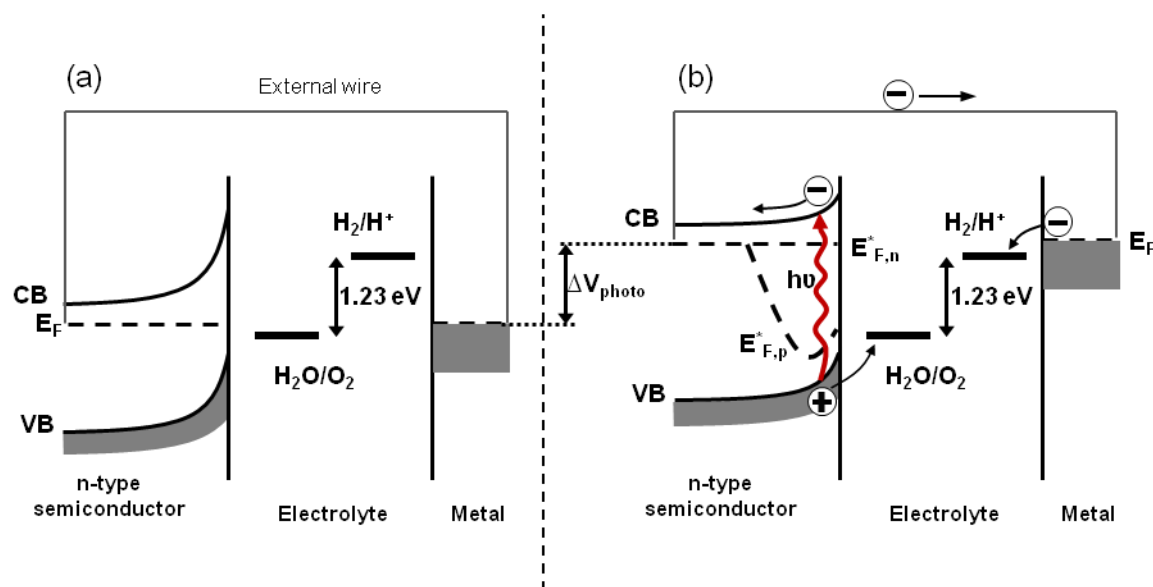


**Figure 1.3:** Band diagram for a PEC cell based on an n-type semiconducting photoanode that is electrically connected to a metal counter electrode; in equilibrium in the dark (a) and under illumination (b). Illumination raises the Fermi level and decreases the band bending. Near the semiconductor/electrolyte interface, the Fermi level splits into quasi-Fermi levels,  $E_{F,n}^*$  and  $E_{F,p}^*$  for the electrons and holes, respectively[51].

When a semiconductor surface is exposed to a photon, with energy of ( $h\nu$ ) greater or equal to its band gap energy ( $E_g$ ), an electron ( $e^-$ ) is promoted from the valence band into the conduction band, leaving a hole ( $h_{vb}^+$ ) behind (c.f. **Figure 1.3** b). The photogenerated electrons are then swept toward the conducting back contact, and are transported to the metal counter-electrode via an external wire. The positive holes are driven to the surface where they are scavenged by the reduced form (Red) of the redox relay molecule, oxidizing it to its oxidized form (Ox). The oxidized form (Ox) is reduced back to (Red) by the electrons that re-enter the cell from the external circuit. If water is oxidized to oxygen at the semiconductor

photoanode and reduced to hydrogen at the cathode, the overall photoelectrochemical reaction will be the cleavage of water[52].

In PEC, the Fermi levels of the semiconductor and metal, which are electrically connected, adjust to a value close to  $E_{ox}$ . Upon illumination, electron–hole pairs are created and the Fermi level increases with  $\Delta V_{photo}$  (*c.f.* **Figure 1.3**). Since the system is no longer in equilibrium, near the semiconductor/electrolyte interface, the Fermi level splits into quasi-Fermi levels,  $E_{F,n}^*$  and  $E_{F,p}^*$ , for electrons and holes, respectively. The quasi-Fermi levels can be given as

$$E_{F,n}^* = E_{CB} - \ln(N_C/n) ; n = n_0 + \Delta n \quad (\text{Eq. 1.1})$$

$$E_{F,p}^* = E_{VB} - \ln(N_V/p) ; p = p_0 + \Delta p \quad (\text{Eq. 1.2})$$

Here,  $N_C$  and  $N_V$  are the density of states around the conduction band edge and the top of the valence band, respectively,  $n$  and  $p$  are the concentrations of electrons and holes at a certain point in the semiconductor,  $n_0$  and  $p_0$  are the equilibrium carrier concentrations in the dark, and  $\Delta n$  and  $\Delta p$  are the additional carriers created by illumination. For an n-type semiconductor,  $n = n_0 + \Delta n \approx n_0$  and  $p = p_0 + \Delta p \approx \Delta p$  so that  $E_{F,n}^*$  remains horizontal whereas  $E_{F,p}^*$  departs from the bulk Fermi level in the active region[51].

### 1.2.3 Redox reaction on photoexcited $TiO_2$ particles

The photocatalyst particles can actually be regarded as very small photoelectrochemical cells in which the irradiation energy is used as activation energy of the redox reaction of the reductant and the oxidant[47]. At the surface of bulk semiconductor electrodes, only one species, either the electron or the hole, is available for reactions due to the band bending. However, in the photocatalytic applications very small particles (in nanometer scale) are usually employed. In this case, both photogenerated species are present on the surface of the particles, and thus both oxidative and reductive paths may occur at their surface. **Figure 1.4** shows a schematic presentation of the photocatalytic processes. Absorption of a photon with

energy of  $h\nu$  greater or equal to the bandgap energy  $E_g$  leads to the formation of electron-hole pair in the semiconductor particles.

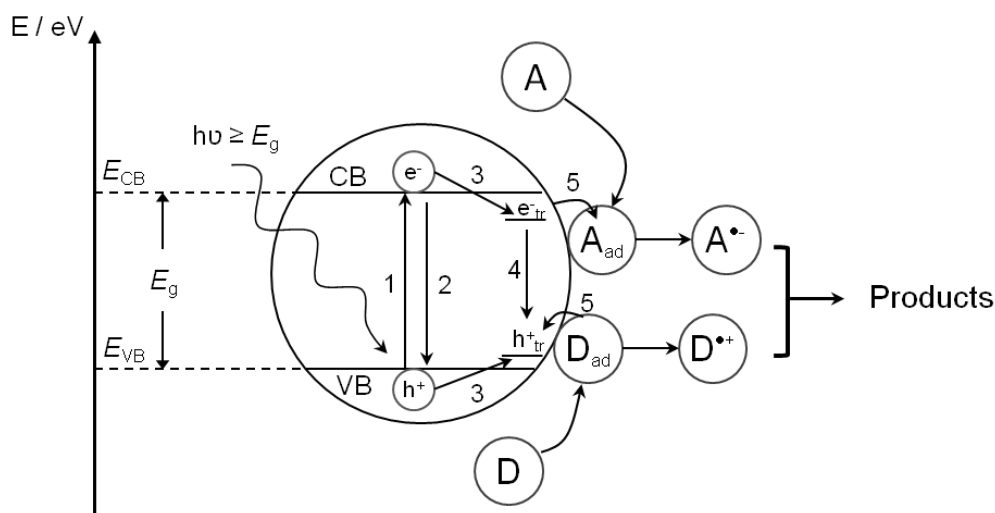


**Figure 1.4:** Schematic description of the redox reaction photocatalyzed by a semiconductor as well as other fates of the photogenerated charge carriers. The circle represents a semiconductor particle, wherein A and D are the electron acceptor and donor, respectively.

In fact, the light generated electron-hole pair may be involved in different reaction paths as illustrated in **Figure 1.4**:

- They may undergo primary recombination through radiative or non-radiative pathways (process 2 in **Figure 1.4**),
- They may be trapped at different sites on the surface of the semiconductor particle (process 3 in **Figure 1.4**). It is widely assumed that the holes are trapped at the  $\text{TiO}_2$  surface in adsorbed hydroxyl groups yielding adsorbed hydroxyl radicals (Eq. 1.3)[53].



However, Grätzel and Howe reported that the hole is trapped at a subsurface oxygen anion[54] (Eq.1.4).



On the other hand, Bahnemann *et al.* [55] have proposed, on the basis of laser flash photolysis studies on colloidal aqueous  $\text{TiO}_2$  suspensions with a mean diameter of 2.4

nm, that, in the absence of any hole scavengers, at least two types of traps have to be considered for the photogenerated holes, while the photogenerated electrons are trapped instantaneously. They defined these two types of holes as deeply trapped holes,  $h_{tr}^+$ , which are rather long-lived, and unreactive and shallowly trapped holes,  $h_{tr*}^+$ , which are in a thermally activated equilibrium with free holes and exhibit a very high oxidation potential.

- Recombination may also occur between trapped electrons and trapped holes (process 4 in **Figure 1.4**). However, this recombination is rather slow with a lifetime in the range of microseconds.
- Or, in the presence of suitable scavenger(s) adsorbed at the surface of the photocatalyst, the photogenerated electrons and/or holes may be trapped thus preventing their recombination and subsequent redox reactions will occur.

Moreover, it is worth noting that to be oxidized or reduced, it is not necessary for the charge carrier scavengers to be adsorbed on the same particle that is absorbing the photon. Wang *et al.*[56, 57] proposed that long self-assembled chains of TiO<sub>2</sub>-particles can act as antenna systems transferring the photon energy from the location of light absorption to the location of the reaction (*cf.* **Figure 1.5**). Even if the target molecule is adsorbed on a photocatalyst particle at a certain distance from the light-absorbing particle, the latter can transfer the exciton energy from particle to particle provided these particles are aggregated and exhibit the same crystallographic orientation. Once the exciton has reached the particle with the adsorbed target molecule like A or D, the latter will act as an electron or hole trap, respectively, thus inducing the separation of the original exciton.

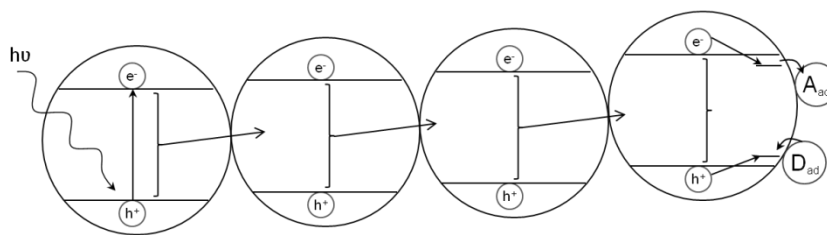


**Figure 1.5:** Schematic description of the antenna effect induced by a network structure of semiconductor particles[56].

#### 1.2.4 Energetic considerations

The attainable oxidation and reduction half reactions that can be achieved on the surface of a given semiconductor photocatalyst are limited by the positions of the band edges of this photocatalyst.

**Table 1.2** provides a list of the potentials of the band edges for those semiconductors most commonly used as photocatalysts (at pH 0 vs. NHE). As long as the oxidation potential of the adsorbed donor is lower than the valence band edge, and the reduction potential of the adsorbed acceptor is lower than the conduction band edge, electron transfer between the photo generated charge carriers and the (adsorbed) species is thermodynamically favorable. It is worth mentioning that the absolute position of the bands of metal oxide photocatalysts exhibit a nernstian shift with the change of the pH ( $-0.059 \text{ V/pH}$ ).

The band levels can also be adjusted by controlling the particle size of the employed photocatalyst. When the crystallite dimension of a semiconductor particle falls below a critical radius of approximately 10 nm, the charge carriers appear to behave quantum mechanically[11]. Thus, the bandgap increases and the band edges  $E_{CB}$  and  $E_{VB}$  shift negatively and positively, respectively, to yield larger redox potentials. For example, Kormann *et al.*[58]. have reported a red-shift in the spectra of  $\text{TiO}_2$  nanoparticles during its growth up to ( $d < 3 \text{ nm}$ ). As a result of the shift of the band edges, the use of size quantized semiconductor particles may result in increased photoefficiencies for systems in which the

rate-limiting step is charge transfer. However, in some cases the photoefficiencies decrease as the particle size decreased due to increased surface defects [11, 59].

**Table 1.2:** Approximate band positions of some common semiconductors[60].

Semiconductor	$E_{VB}$ (eV vs. NHE)	$E_{CB}$ (eV vs. NHE)	$E_g$ (eV)
TiO <sub>2</sub> (rutile)	3.0	0.0	3.0
TiO <sub>2</sub> (anatase)	3.0	-0.2	3.2
SrTiO <sub>3</sub>	3.2	-0.0	3.2
ZnO	3.0	-0.2	3.2
CdS	2.0	-0.4	2.4
CdSe	1.6	-0.1	1.7
GaP	1.2	-1.1	2.3

In water at pH = 0. Values decrease approximately 0.059 volts per unit increase in pH. Values vs. SCE are converted to NHE scale by adding + 0.24 volts[9].

The band levels, especially the conduction band edge ( $E_{cb}$ ), can also be changed by changing the crystallite phase of a given semiconductor. In the case of TiO<sub>2</sub>, for example, the flat band potential of brookite nanorods has been found to be shifted by 140mV more cathodically than the flat band potential of the anatase nanoparticles[61] whereas the flat band potential of rutile has been reported to be shifted by 200 mV more anodically than that of anatase (see **Table 1.2**). However, the potential of the valence band edges is usually calculated by subtraction of the energy gaps of TiO<sub>2</sub> (3.2, 3.0, and 3.3 eV, for anatase, rutile and brookite, respectively) from the conduction band energy, assuming that the flat band potential is equal to the potential of the conduction band edge. Hence, the valence band edge in TiO<sub>2</sub> has been reported to be almost constant at 3.0 V vs. NHE at pH 0 regardless of the crystalline phase, anatase, rutile, or brookite[61].

By carefully selecting the semiconductor, one can thus define the available redox potentials and, subsequently, one can choose appropriate molecules that can be oxidized or reduced, at the surface of this semiconductor upon illumination.

Redox species that exchange electrons with a semiconductor can either accept ( $A + e^- \rightarrow A^-$ ) or donate ( $D \rightarrow D^+ + e^-$ ) electrons. Upon electron transfer from or to adsorbed species their electronic structure changes. Upon the acceptance of electron, a previously unoccupied electronic level of the acceptor molecule becomes occupied, whereas upon electron donation an electron is removed from an occupied level. For an electron acceptor ( $A/A^-$ ), it is the energy of the lowest unoccupied level,  $E_{\text{unoc}}$ , that is of importance, whereas for an electron donor ( $D/D^+$ ) the highest occupied energy level,  $E_{\text{oc}}$ , is of importance (see **Figure 1.6**).

The redox potentials of aqueous redox couples ( $E_{\text{redox}}$ ) can be expressed as:

$$E_{A/A^-} = E_{A/A^-}^{\circ} + RT/nF \ln(a_{A^-}/a_A) \quad (\text{Eq. 1.5})$$

$$E_{D/D^+} = E_{D/D^+}^{\circ} + RT/nF \ln(a_{D^+}/a_D) \quad (\text{Eq. 1.6})$$

where  $E^{\circ}$  is the standard redox potential of the aqueous redox couple with respect to the Normal Hydrogen Electrode (NHE).

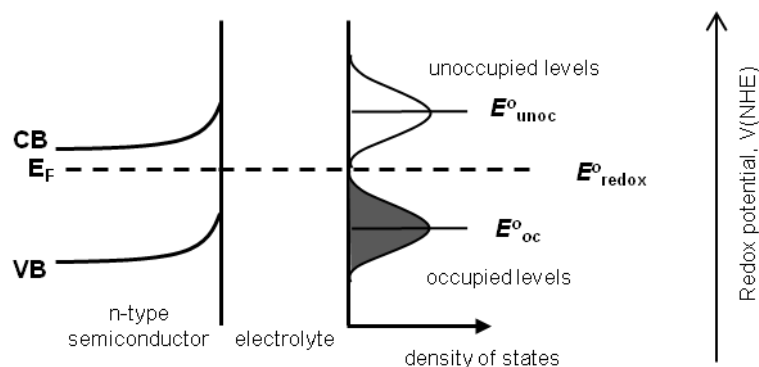


**Figure 1.6:** Positions of the energy levels at the interface of an n-type semiconductor and a redox couple in an electrolyte[51].

Therefore, the driving force for the electron transfer from or to the adsorbed species will be the difference between the energy of the band edges and the redox potential of these species. It is noteworthy that in case of a multi-electron transfer the distribution of energy states in a



---

redox couple becomes more complicated because each one-electron transfer step has a different population of the energy states.

Because of the highly positive energy level of the valence band edge in titanium dioxide, many oxidative conversions can be carried out in its aerated (or deaerated) suspensions upon irradiation. Indeed, the high oxidizing power implied by the valence band level of  $\text{TiO}_2$  (3.0 V vs. NHE) permits the oxidation of virtually a very wide range of organic compound. This turns  $\text{TiO}_2$  into an excellent photocatalyst for the purification of the contaminated water enabling the oxidation of almost any organic pollutant. However,  $\text{TiO}_2$  should be a less favorable photocatalyst from the viewpoint of organic synthesis as a result of the poor selectivity of these oxidation reactions. On the other hand, the position of the conduction band edge of  $\text{TiO}_2$  provides rather mild reduction conditions thus enabling a targeted reduction of specific organic groups.

### 1.2.5 Solvent considerations

From the viewpoint of an eco-friendly production of chemicals, one should pay attention to the choice of the solvent employed in the overall process. Water is considered to be one of the most environmentally friendly solvents in which photocatalysts such  $\text{TiO}_2$  can be easily suspended. However, because of the high positive potential of the valence-band holes of  $\text{TiO}_2$ , the direct oxidation of the adsorbed water molecules may also occur. The formation of hydroxyl radicals by the single-electron oxidation of surface-bound water molecules is well known and has been detected by different methods including EPR spectroscopy and isotopic studies[62-64]. The high reactivity of the thus formed hydroxyl radicals reduces the ability to control the reaction selectivity if the desired goal is the organic synthesis. However, the drawback of the low selectivity of an organic transformation employing water as solvent can be considerably reduced if the desired goal is the reduction of the organic substrate in the presence of a sacrificial reagent which scavenges the photogenerated holes. The

photocatalytic reduction of nitrobenzene or m-nitrobenzenesulfonic acid in acidic aqueous suspensions of titanium dioxide in the presence of oxalic acid acting as a hole scavenger are examples of such applications which, however, are rarely reported[65, 66]. On the other hand, many organic compounds are difficult to be dissolved in water because of obvious differences in polarity. To overcome these problems inert organic solvents can be used. Acetonitrile is a good candidate to be used as a solvent in photocatalytic systems because it can only be oxidized outside the potential window of the bandgap of TiO<sub>2</sub>, hence, the substrate can be selectively oxidized.

As solvents in the photocatalytic organic synthesis processes alcohols are, from an environmental point of view, more favorable than acetonitrile. Besides their ability to solve a wide range of organic substrates, alcohols will, however, be oxidized during the irradiation scavenging the photogenerated holes and generating valuable carbonyl compounds. This will result in an enhancement of the electron-hole pair separation, hence increasing the number of conduction band electrons available to drive the desired reduction reaction at the surface of the photocatalyst. Moreover, the properties of the alcohol may also affect the overall photocatalytic reaction. Brezova et al.[67] have reported that the photocatalytic reduction rate of nitrophenol is significantly affected by the solvent (alcohol) parameters, such as viscosity, polarity, and polarisability all of which affect the ability of the solvent to stabilize the charged intermediate species produced upon illumination.

### **1.3 Modification of the surface of TiO<sub>2</sub> with precious metals**

The selectivity and efficiency of a photocatalytic reaction can be improved by modifying the surface of a semiconductor particle such as TiO<sub>2</sub> with a suitable noble metal catalyst. Different metals such as silver, platinum, palladium, gold, and rhodium have been successfully deposited on the surface of TiO<sub>2</sub>[68].

Metals can be loaded on the surface of TiO<sub>2</sub> by various ways including stirring suspensions of TiO<sub>2</sub> and colloidal metal particles together, mixing TiO<sub>2</sub> with the metal simply in a mortar, or employing the so-called impregnation method. Metallic cations can also be reduced, from a thermodynamic viewpoint, by the photogenerated electrons at the surface of TiO<sub>2</sub> when their reduction potentials are less negative than the semiconductor Fermi level. This photo-loading method plays an important role in enhancing the activity of TiO<sub>2</sub>. Since the first report of the photodeposition method by Kraeutler and Bard[69], it became the most frequently employed one because it is easy and effective while it suffering, sometimes, from the poor homogeneity of the deposited metal islands.

The metal deposits on the surface of TiO<sub>2</sub> may serve different roles: Firstly, they act as sinks for the photogenerated electrons thus partially inhibiting the electron-hole recombination. This, in many cases, will improve the photocatalytic oxidation efficiency. Ismail et al.[70], reported that the rate of the photocatalytic oxidation of methanol to formaldehyde was doubled by the modification of TiO<sub>2</sub> with only 0.5wt.% of platinum. Increasing the loaded amount of the metal may, however, decrease the activity of the photocatalysts since the metal islands may also act as electron-hole recombination centres. Secondly, in the absence of O<sub>2</sub>, loading of a small amount of noble metal, *e.g.*, Pt, onto the photocatalyst enables the production of H<sub>2</sub> upon the reduction of protons in the reaction mixture[71]. Moreover, hydrogenation reactions can be also carried out when the noble metal is present as a co-catalyst on the surface of the photocatalyst. Finally, the modification of the surface of the semiconductor with the metal islands may increase the adsorbed amount of the organic substrate thus improving the photocatalytic efficiency. For example, the adsorbed amount of nitrobenzene greatly increased with the loading of Ag or Pt nanoparticles on the surface of TiO<sub>2</sub>, whereas the amount adsorbed at bare TiO<sub>2</sub> is negligibly small. This selective

adsorption of nitrobenzene resulted in a considerable increase in the activity and the selectivity of its photocatalytic reduction to aniline[72, 73].

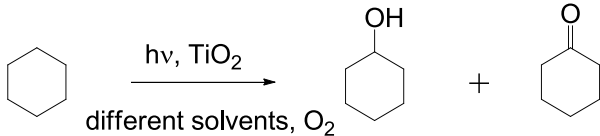
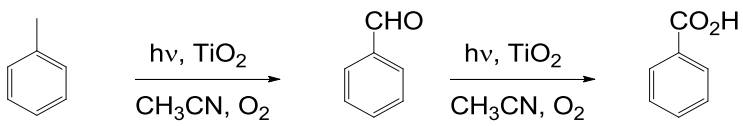
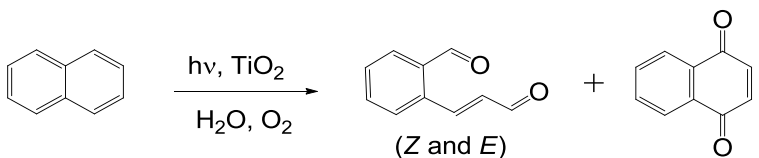
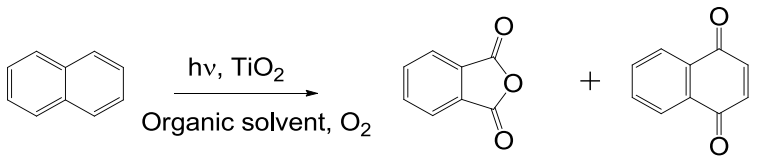
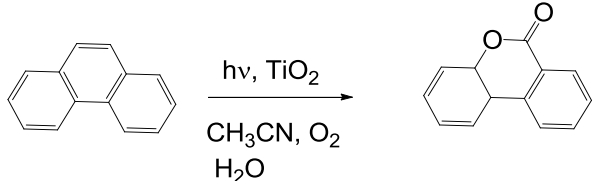
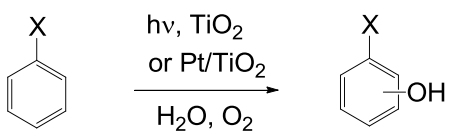
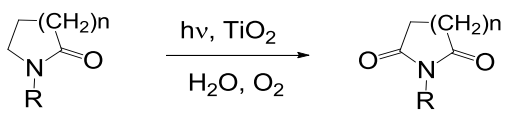
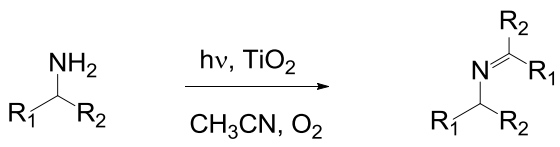
#### 1.4 TiO<sub>2</sub>-based photocatalytic organic synthesis

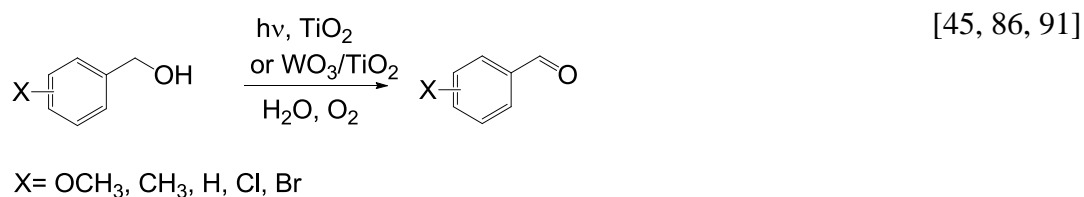
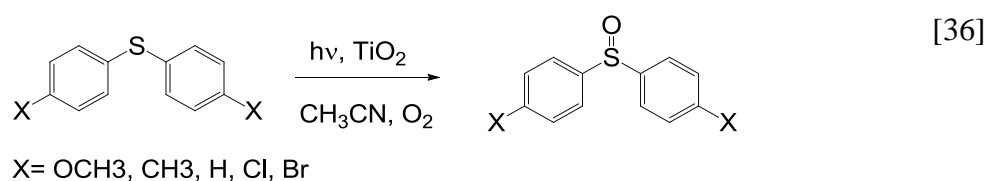
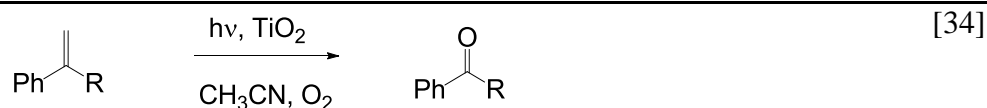
In recent years, the use of the photocatalytic method as a promising approach for green organic synthesis has attracted an increased interest owing to its unique properties[19, 74, 75]. The previously mentioned photoinduced charge separation occurring on the TiO<sub>2</sub> surface simultaneously creates both, a reduction center and an oxidation center. This unique feature allows rather complex organic transformations to be performed in one sequence without the necessity of the isolation of the intermediates[42, 43, 76-78]. Furthermore, redox reactions initiated by photogenerated electrons and holes do not produce the typical by-products encountered when employing conventional reductants or the oxidants. *E.g.*, it is well known that redox reactions carried out in the presence of permanganate or lithium aluminum hydride, respectively, lead to the formation of manganese ion or aluminum hydroxide upon completion of the oxidation or reduction process, respectively. Moreover, photocatalytic organic conversions can sometimes exhibit higher selectivity than conventional methods[79]. A variety of organic transformations mediated by the UV(A) irradiation of TiO<sub>2</sub> have been reported including oxidation and/or reduction as well as some coupling reactions[35, 38, 42, 45].

##### 1.4.1 Photocatalytic oxidation reactions employed for organic synthesis

Recently, much effort has been devoted to the application of TiO<sub>2</sub> to the selective photocatalytic oxidation of a broad range of organic compounds including hydrocarbons, aromatic compounds, and alcohols. **Table 1.3** summarizes most of these photocatalytic oxidation organic syntheses.

Table 1.3: Examples of photocatalytic oxidation reactions

Reaction	Ref.
 <p>Cyclohexane <math>\xrightarrow[\text{different solvents, O}_2]{h\nu, \text{TiO}_2}</math> Cyclohexanol + Cyclohexanone</p>	[80, 81]
 <p>Toluene <math>\xrightarrow[\text{CH}_3\text{CN, O}_2]{h\nu, \text{TiO}_2}</math> Benzaldehyde <math>\xrightarrow[\text{CH}_3\text{CN, O}_2]{h\nu, \text{TiO}_2}</math> Benzoic acid</p>	[82]
 <p>Naphthalene <math>\xrightarrow[\text{H}_2\text{O, O}_2]{h\nu, \text{TiO}_2}</math> Naphthalen-1-ol (Z and E) + Naphthalen-1,4-dione</p>	[83, 84]
 <p>Naphthalene <math>\xrightarrow[\text{Organic solvent, O}_2]{h\nu, \text{TiO}_2}</math> Naphthalen-1,4-dione + Naphthalen-1,4-dione</p>	[83]
 <p>Fluorene <math>\xrightarrow[\text{CH}_3\text{CN, O}_2, \text{H}_2\text{O}]{h\nu, \text{TiO}_2}</math> Fluorenone</p>	[85]
 <p>Substituted benzene (X) <math>\xrightarrow[\text{H}_2\text{O, O}_2]{h\nu, \text{TiO}_2 \text{ or Pt/TiO}_2}</math> Substituted phenol (X)</p> <p>X = electron-withdrawing group; <i>ortho</i>- and <i>para</i>-product  X = electron-donating group; <i>meta</i>-product</p>	[86, 87]
 <p>N-alkylsuccinimide <math>\xrightarrow[\text{H}_2\text{O, O}_2]{h\nu, \text{TiO}_2}</math> N-alkylsuccinimide</p>	[88]
 <p>Secondary amine (R<sub>1</sub>, R<sub>2</sub>) <math>\xrightarrow[\text{CH}_3\text{CN, O}_2]{h\nu, \text{TiO}_2}</math> Imine (R<sub>1</sub>, R<sub>2</sub>)</p>	[89, 90]

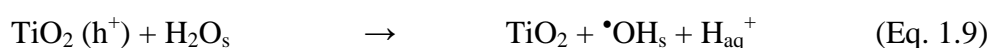
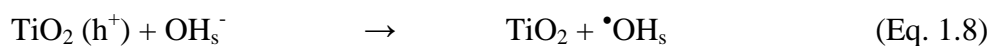


It has previously been mentioned that in photocatalytic reactions the semiconductor particle behaves practically as a microelectrode kept always under open circuit potential with the anodic and cathodic current being equal in magnitude. Thus two reactions, an oxidation and a reduction, must proceed simultaneously on the same particle surface (otherwise the particle would be charged, eventually leading to the overall reaction being stopped).

It is well known that the redox potentials of alcohols[92] are less positive than the valence band edge of TiO<sub>2</sub>, therefore, alcohols, in principle, can be photocatalytically oxidized to the corresponding carbonyl compounds[62, 93-97]. However, the “overoxidation” leading to the formation of carboxylic acids and CO<sub>2</sub> is the main drawback of this reaction. In fact, the selectivity of the photocatalytic oxidation of alcohols can be affected by several parameters such as the employed solvent (if used), the type of the employed TiO<sub>2</sub>, the presence of O<sub>2</sub>, and the structure of the alcohol.

The photocatalytic oxidation of primary, secondary, and tertiary as well as aromatic alcohols by TiO<sub>2</sub> particles suspended in their aqueous solutions has been studied extensively [18, 45, 91, 98]. In these systems, two possible mechanisms have been proposed: (1) the

direct oxidation by the photogenerated holes (Eq.1.10), or (2) the indirect oxidation (Eq.1.11) via the intermediacy of  $\bullet\text{OH}$  radicals that are produced upon the trapping of valence holes by surface  $-\text{OH}$  groups or adsorbed water molecules (Eqs. 1.8 and 1.9).[99-101].



Wang et al.[102, 103] have reported that the photocatalytic oxidation pathway of methanol, direct or indirect, depends on the molecular species adsorbed at the  $\text{TiO}_2$  surface. According to their measurements, the authors concluded that at a critical molar ratio between water and methanol of approx. 300, water is the dominant surface species and the indirect pathway, by  $\bullet\text{OH}$  radicals, is preferred. If the water content is lower than this critical ratio, the direct oxidation of methanol by the photogenerated holes will be the predominant process at the  $\text{TiO}_2$  surface.

In the presence of molecular oxygen, the corresponding aldehyde is formed via its reaction with the photocatalytically generated C-centered radical (Eq. 1.12). However, in the  $\text{O}_2$ -free system, the aldehyde is formed through the electron injection into the conduction band of  $\text{TiO}_2$ , a process called “current doubling”. Miyake et al.[104] have reported that alcohols with an  $\alpha$ -hydrogen react as current doubling reagents, while alcohols without  $\alpha$ -hydrogen do not. The photocatalytic oxidation of different neat alcohols in the presence as well as in the absence of  $\text{O}_2$  was reported by Yamagata et al.[105]. They observed that the current doubling effect disappeared upon the introduction of molecular oxygen into the system suggesting that

$O_2$  or an oxygen radical species reacts with the initially photocatalytically generated  $\alpha$ -hydroxyalkyl radicals. However, since the presence of molecular oxygen was found to enhance the formation of acetaldehyde the authors concluded that  $O_2$  participated in a radical chain mechanism during the photocatalytic oxidation of ethanol to acetaldehyde as shown in **Figure 1.7**.

**Figure 1.7.**

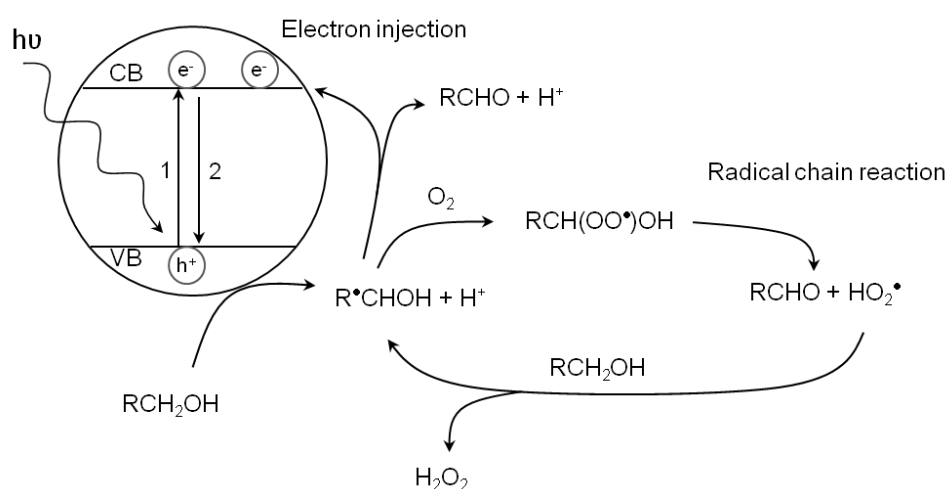


**Figure 1.7:** Schematic representation of the photocatalytic oxidation of alcohols in the absence (current doubling) or the presence of oxygen (radical chain mechanism)[105].

Therefore, alcohols carrying an  $\alpha$ -hydrogen can be used for the in situ preparation of carbonyl compounds during a photocatalytic organic synthesis. On the other hand, alcohols without  $\alpha$ -hydrogen can be used for the generation of radical species which have a relatively long life time and might subsequently undergo radical coupling reactions.

Under deaerated conditions, the photogenerated electrons will be trapped near the surface of the  $TiO_2$  particles forming trivalent titanium ( $Ti^{III}$ ) since bare  $TiO_2$  is not able to catalyze the reduction of  $H^+$  to  $H_2$ . This phenomenon has been observed by Bahnemann et al.[106] during their laser-flash photolysis study of colloidal  $TiO_2$ . However, if small precious metal islands are present on the surface of  $TiO_2$ , the photogenerated electrons will be trapped at



these metal nanoparticles facilitating the separation of the electron-hole pairs and promoting the evolution of molecular hydrogen[107].

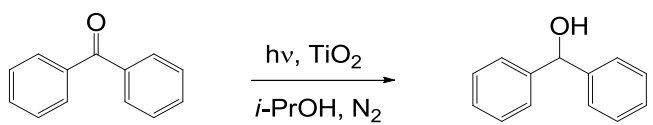
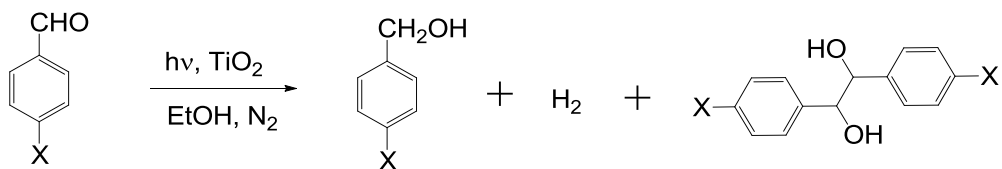
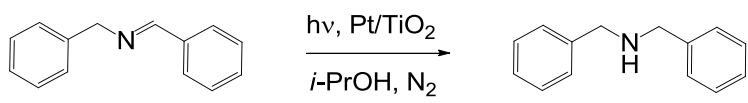
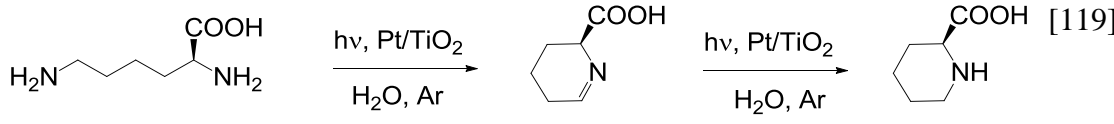
If alcoholic suspensions of TiO<sub>2</sub> are irradiated in the presence of primary or secondary amines or ammonia, the photocatalytically formed aldehydes or ketones will react with the amines to give imines, in the case of bare TiO<sub>2</sub>[108], or *N*-alkylated amines in the case of platinized TiO<sub>2</sub>[39].

### 1.4.2 Photocatalytic reduction reactions employed for organic synthesis

Reduction reactions are crucial reactions in organic chemistry that are usually conducted employing environmentally problematic species, such as borohydrides, sulfides, or iron salts. Photocatalysis seems to be a promising candidate to carry out reactions under environmentally more friendly conditions since no harmful residues are formed in the process. However, only few photocatalytic organic reductions have been reported until now. This might have two reasons: firstly, the early focus on the use of photocatalysts as powerful oxidizing agents to degrade organic pollutants; secondly, the only moderately negative potential of the conduction band electrons of most conveniently accessible semiconductors. However, the later feature ensures that the photocatalytic method will be more selective than most conventional reduction methods. Since molecular oxygen is usually found to be a relatively good electron acceptor within the reductive half reaction, it must, in most cases, be removed if other reagents are to be photocatalytically reduced.

Some examples for the photocatalytic reduction of organic compounds do exist, such as the reduction of viologens[109]; the hydrogenation of olefins[110-112], vinyl ethers[110], or  $\alpha,\beta$ -unsaturated enones[110]. Similarly, other multiple bonds can also be reduced, *e.g.*, the N=N of diaryl azo compounds[113], the C=N of Schiff bases[114], or carbonyl compounds[115-117]. Examples of these reactions are given in **Table 1.4**:

**Table 1.4:** Examples of photocatalytic reduction reactions

Reaction	Ref.
$\text{CH}_3\text{CO}_2\text{H} \xrightarrow[\text{H}_2\text{O, Ar}]{h\nu, \text{Pt/TiO}_2} \text{CH}_4 + \text{CO}_2$	[118]
$\text{CH}_3(\text{CH}_2)_5\text{CH}=\text{CH}_2 \xrightarrow[\text{EtOH, N}_2]{h\nu, \text{Pt/TiO}_2} \text{n-C}_8\text{H}_{18}$	[110]
$\text{CH}_3(\text{CH}_2)_3\text{OCH}=\text{CH}_2 \xrightarrow[\text{EtOH, N}_2]{h\nu, \text{Pt/TiO}_2} \text{CH}_3(\text{CH}_2)_3\text{OCH}_2\text{CH}_3$	[110]
	[116]
 <p>X=H, Cl, Br, CN, COCH<sub>3</sub></p>	[117]
	[114]
	[119]

### 1.4.2.1 Photocatalytic reduction of nitroaromatic compounds

Amongst the photocatalytic reduction reactions, the reduction of nitroaromatic compounds has been studied most extensively. The photocatalytic reduction of nitrobenzene and its derivatives by irradiated TiO<sub>2</sub> is particularly attractive since the products are essential precursors for a variety of biologically active compounds and important intermediates in the synthesis of polymers, pesticides, and dyes.

Several reports have been published concerning the photocatalytic conversion of nitroaromatic compounds. The yield of such a photocatalytic reaction can be considerably

enhanced by the presence of a hole scavenger that is needed to suppress the recombination between photogenerated electrons ( $e^-$ ) and holes ( $h^+$ ) within the photocatalyst particle. As mentioned previously, primary alcohols (such as methanol or ethanol) can be used as both, hole scavengers and solvent for the photocatalytic reduction of organic compounds, generating the corresponding aldehydes as oxidation products. The work of Mahdevi et al.[120] can be regarded as one of the earliest reports for this application. The authors investigated the reduction of a variety of nitroaromatic compounds to the corresponding amines and reported very high yields upon the irradiation of suspensions of  $TiO_2$  in ethanol. During the photocatalytic reduction of p-nitroacetophenone, the corresponding hydroxylamine was detected as intermediate. Inspired by this finding the authors proposed a reaction mechanism as illustrated in **Figure 1.8** involving sequential electron transfer, protonation, and dehydration. The complete reduction of a nitro compound would require six electrons and leave the same numbers of holes behind. If all of these holes are used to oxidize the alcohol employed as solvent six protons would be produced.

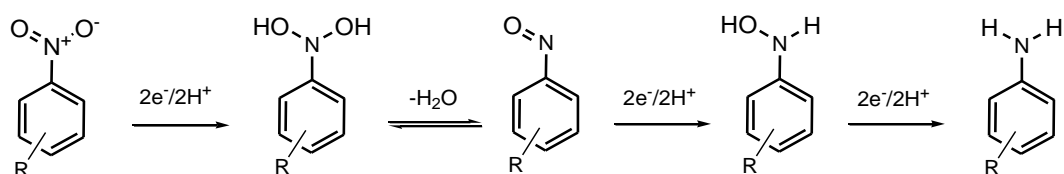


**Figure 1.8:** Schematic illustration of the reduction of a nitroaromatic compound to an aminoaromatic compound.

As explained above (1.2.2) the driving force for the heterogeneous electron transfer is the difference between the energy level of the conduction band of the semiconductor and the reduction potential of the acceptor redox couple, *i.e.*,  $RNO_2/RNO_2^{\bullet-}$ :

$$\Delta E = E_{CB} - E_{RNO_2/RNO_2^{\bullet-}} \quad (\text{Eq. 1.11})$$

The standard potentials of the one-electron reduction of some nitroaromatic compounds are given in **Table 1.5**:

**Table 1.5:** Formal potentials for the couple  $RNO_2/RNO_2^*$  for some nitroaromatic compounds[121]

Compound	Formal potential (V) vs. NHE	Conditions
<i>m</i> -NH <sub>2</sub> -Ph-NO <sub>2</sub>	-0.46	90% water/methanol, 0.02 M NaOH + 0.02 M KCl
<i>m</i> -CH <sub>3</sub> -Ph-NO <sub>2</sub>	-0.46	90% water/methanol, 0.02 M NaOH + 0.02 M KCl
<i>m</i> -Cl-Ph-NO <sub>2</sub>	-0.40	90% water/methanol, 0.02 M NaOH + 0.02 M KCl
<i>p</i> -NH <sub>2</sub> -Ph-NO <sub>2</sub>	-0.59	90% water/methanol, 0.02 M NaOH + 0.02 M KCl
<i>p</i> -CH <sub>3</sub> -Ph-NO <sub>2</sub>	-0.49	90% water/methanol, 0.02 M NaOH + 0.02 M KCl
<i>p</i> -Cl-Ph-NO <sub>2</sub>	-0.44	90% water/methanol, 0.02 M NaOH + 0.02 M KCl

Ferry and Glaze[122] have studied the mechanism of the photocatalytic reduction of nitroaromatic compounds at illuminated TiO<sub>2</sub> particles in the presence of alcohols. They argued that under the employed experimental conditions (*i.e.*, absence of O<sub>2</sub> and excess of alcohol) two reducing agents will be present: (1) conduction band electrons (free or trapped as Ti(III)) and  $\alpha$ -hydroxyalkyl radicals formed as the one-electron oxidation products of the donors. In an irradiated TiO<sub>2</sub> slurry containing nitro organic compounds, these  $\alpha$ -hydroxyalkyl radicals may react with the photocatalyst surface (current doubling), or they may react with the nitro organic compounds directly. Although the  $\alpha$ -hydroxyalkyl radicals are known to be powerful reducing agents, with their reduction potentials being more negative than -1.0 V vs. the NHE[122], the results obtained by Ferry and Glaze indicated that the reduced surface sites were in fact the principal species responsible for the observed reduction reactions.

The influence of the solvent properties on the rate of the photocatalytic reduction of 4-nitrophenol to 4-aminophenol by TiO<sub>2</sub> suspended in different alcohols was investigated by Brezano et al.[67]. They reported that the photocatalytic reduction rate decreased by

increasing the viscosity of the employed alcohol whereas it increased with increasing the polarity of the solvent. Consequently, the ability of the solvent to stabilize the produced charged intermediate species was found to play an important role in the system.

The effect of the sacrificial electron donor on the selective reduction of *p*-chloronitrobenzene to the corresponding amino compound was reported by Zhang et al.[123]. Among the studied electron donors (methanol, ethanol, 2-propanol, and formic acid), the highest yield was obtained employing a mixture of 2-propanol and formic acid at a ratio of 9 to 1. Recently, the successful chemoselective photocatalytic reduction of various nitro compounds carrying also other reducible groups to the corresponding aminobenzenes by TiO<sub>2</sub> suspended in acetonitrile in the presence of oxalic acid as sacrificial reagent was reported[124]. The benefit of using oxalic acid is that carbon dioxide is the only product and no carbonyl compounds are formed in the reaction mixture. Applying the same holes scavenger (*i.e.*, oxalic acid) Imamura et al.[66] were able to achieve an almost quantitative conversion of aminonitrobenzenes to diaminobenzenes even in aqueous suspensions of TiO<sub>2</sub>.

#### **1.4.2.2 Effect of the modification of TiO<sub>2</sub> on the photocatalytic reduction of nitroaromatic compounds**

Tada et al.[125] have recently presented the concept of a “reasonable delivery photocatalytic reaction system” (RDPRS), in which the following three conditions must be satisfied to ensure highly efficient and selective photocatalytic reactions: (i) separation of the oxidation and the reduction sites; (ii) abundant and selective supply of oxidants and reductants to the reduction and the oxidation sites, respectively; and (iii) restriction of the product readsorption. The modification of the surface of TiO<sub>2</sub> with different noble metal nanoparticles such as Ag or Pt improves the charge separation efficiency (RDPRS condition i). Hence, both the activity and the product selectivity of the TiO<sub>2</sub> photocatalyzed reduction of nitrobenzene to aniline have been found to increase considerably upon loading a small amount of Ag clusters on the surface of TiO<sub>2</sub>. Moreover, the high activity and selectivity in

the Ag/TiO<sub>2</sub>-photocatalyzed reduction are rationalized not only in terms of the charge separation efficiency, but also because of the selective adsorption of the nitroaromatic compounds on the modified catalyst surfaces and the restriction of the product (aniline) readsorption[72, 73]. However, in the case of Pt modified TiO<sub>2</sub> suspended in alcohols, the reaction may not stop at the reduction step of the nitroaromatic compound to the corresponding aniline but further condensation with the photocatalytically generated carbonyl compounds may occur. Shiraishi et al.[126] have reported that loading a small amount of Pt (0.3 wt.%) on the surface of particulate TiO<sub>2</sub> promotes the formation of imines from alcohols and anilines upon irradiation. On the other hand, the presence of Pt islands on the surface of TiO<sub>2</sub> can also catalyze evolution of hydrogen gas which may result in the hydrogenation, under the catalytic property of Pt, of the formed imines thus producing *N*-alkylated products. Ohtani et al.[39, 114] have reported that secondary amines are produced from primary amines dissolved in alcohols employing platinized titanium dioxide as the photocatalyst[38-40]. However, among the primary amines used in their studies, aniline was *N*-alkylated most slowly reaching an efficiency of only 13.9% even after 20h of irradiation[39]. Ohtani and co-workers assumed that this lower efficiency of the *N*-alkylation of aniline can be attributed to the fact that *N*-ethylideneaniline is poorly reduced over Pt in ethanol under H<sub>2</sub> atmosphere. Shiraishi et al.[127] have also applied platinized titanium dioxide to synthesize benzimidazoles from 1,2-diaminobenzene under illumination of the respective alcoholic suspensions.

However, in order to decide whether the photocatalytic reduction of nitroaromatic compounds over TiO<sub>2</sub> as a useful synthetic method, a systematic study focusing on the factors that affect the selectivity of this reaction is of great importance.

## 1.5 Objectives of the study

In the literature review presented in the previous section, a general overview of the photocatalytic actions of semiconductor photocatalysts, especially  $\text{TiO}_2$ , and their related applications in oxidizing and/or reducing a desired organic molecule has been presented and described. In summary, titanium dioxide has been reported to be an active photocatalyst under UV(A) irradiation, a stable material against chemicals and light, and a nontoxic material with low production costs. Therefore,  $\text{TiO}_2$  is currently considered to be the most promising photocatalyst amongst the most extensively studied semiconductors. It has been reported that alcohols can be photocatalytically oxidized by the photogenerated holes at the surface of  $\text{TiO}_2$  particles to the corresponding carbonyl compounds. The efficiency of these reactions has been found to be considerably enhanced in the presence of electron acceptors. On the other hand, in the presence of an electron donor, the photogenerated conduction band electrons at irradiated  $\text{TiO}_2$  surfaces can reduce nitroaromatic compounds to the corresponding aminoaromatic compounds. Thus, the illumination of systems consisting of alcohols, nitroaromatic compounds, and  $\text{TiO}_2$  powders is expected to result in the simultaneous formation of carbonyl compounds and aminoaromatic compounds, respectively. These photocatalytically produced compounds are precursors for the synthesis of valuable products such as quinoline derivatives and *N*-alkylated aromatic compounds as can be seen in **Figure 1.9**

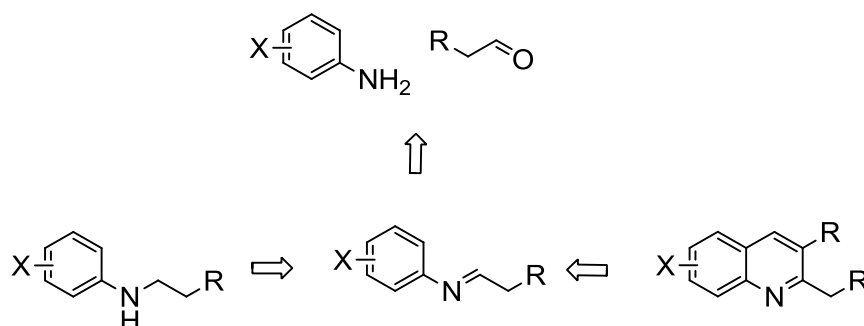


**Figure 1.9:** Schematic illustration of the synthesis of quinolines and *N*-alkylated compounds starting from the photocatalytically formed aminoaromatic compounds and aldehydes.

Quinolines and *N*-alkylated aromatic compounds are essential precursors for a variety of biologically active compounds and they are important intermediates in the production of polymers, pesticides, and dyes. However, the most frequently employed thermal routes to prepare these compounds[128-135] often suffer from the requirement of harsh reaction conditions (i.e., high temperature and/or pressure), the use of large amounts of hazardous acids or bases, and, in particular, expensive metal complexes. Therefore, the development of new strategies to obtain these compounds in a fast, clean, and efficient way is of great significance and still requires considerable efforts.

In this thesis, TiO<sub>2</sub>-based photocatalytic reactions have been chosen as an alternative method for the synthesis of aforementioned organic compounds, starting from inexpensive nitroaromatic compounds and alcohols. In the suggested system, several transformations during the preparation of these complex organic compounds (quinolines and *N*-alkylated aromatic compounds) should be performed in one sequence without the necessity of the isolation of the intermediates.

For this purpose, a systematic study focusing on the factors that affect the selectivity of the photocatalytic reactions to obtain the target compounds have been performed. Thus the following points have been investigated:

- Influence of the type of TiO<sub>2</sub> and its surface properties to the photocatalytic conversion of the nitroaromatic compounds in alcohols.
- Modification of TiO<sub>2</sub> with an acidic co-catalysts and its effect on the yield of the target compounds.
- The effect of depositing tiny islands of different precious metals as a co-catalysts on the surface of TiO<sub>2</sub> on the photocatalytic reaction pathway.
- Further investigations the concerning the optimization of the amount of metal loaded on the surface of TiO<sub>2</sub>, the loading method, and the light intensity, respectively.



---

The experimental work and the related discussion presented within this thesis should be useful as a tool to develop the understanding of the photocatalytic conversion of the studied organic molecules in order to consider the photocatalytic reduction of the nitroaromatic compounds over  $\text{TiO}_2$  as a useful and environmentally benign synthetic method.

## 2 Materials and experimental methods

### 2.1 Materials

Commercial titanium dioxide powders with different structures were obtained from different companies as follows: Hombikat UV 100 with anatase structure (Sachtleben, Germany), R34 with rutile structure (Cristal Global, KSA), Aeroxide P25 with mixed anatase and rutile structure (Evonik-Degussa, Germany). All TiO<sub>2</sub> powders were used as received from the respective companies. Mesoporous titania was prepared according to a procedure given in ref[136] yielding a photocatalyst materials with a hexagonal mesostructure. All nitroaromatic compounds were of analytical grade and used as received from Sigma-Aldrich except p-nitro phenol which was obtained from Fluka. Acetaldehyde was also from Fluka. Ethanol (99.8%) was obtained from Roth whereas all other alcohols were received from Sigma-Aldrich. Hexachloroplatinic acid hexahydrate, palladium chloride, tetrachloro auric acid and silver nitrate were obtained from Alfa-Aeser, Sigma-Aldrich, Merck, and Sigma-Aldrich, respectively. All other reagents and standards were used as received from the respective supplier.

### 2.2 Modification of the TiO<sub>2</sub> powders

#### 2.2.1 Modification of TiO<sub>2</sub> with arenesulfonic acid functionalized mesoporous SiO<sub>2</sub>

TiO<sub>2</sub>-arenesulfonic acid functionalized mesoporous silica materials were synthesized as follows: 4 g of Pluronic 123 (Aldrich) was dissolved by stirring in 125 g of 1.9 M HCl at room temperature until complete dissolution of the surfactant. Then 9.4 ml TEOS tetraethylorthosilicat (Aldrich) was added dropwise. After the addition of TEOS was completed, the amount of TiO<sub>2</sub> (Sachtleben Hombikat UV 100), needed to reach the desired TiO<sub>2</sub>:SiO<sub>2</sub> ratios, was added and the resulting suspension was kept at RT for 45 min under stirring to ensure pre-hydrolysis. Subsequently, the desired amount of 2-(4-chlorosulfonylphenyl)ethyltrimethoxysilane (CSPTMS) solution in methylene chloride (50%,

Gelest) was added dropwise (to prevent phase separation) into the mixture and stirred at RT for 20h, after which the mixture was aged at 100 °C for 24 h under static conditions. The template was removed from the as-synthesized material by washing with methanol and deionized water followed by refluxing in ethanol for 48 h and finally washing with deionized water for three times (to insure that the samples are free of residual HCl used during the preparation). The samples were labeled T(*n*)-S-Ar (*x*), where *n*:1:*x* is the molar ratio of TiO<sub>2</sub>:SiO<sub>2</sub>:Arenesulfonic acid.

## 2.2.2 Modification of TiO<sub>2</sub> with Pt nanoparticles

Two methods were used to prepare Pt/TiO<sub>2</sub>: The photocatalytic deposition method and the mixing of solids method, respectively.

### 2.2.2.1 Photocatalytic deposition method

Pt(*x*)/TiO<sub>2</sub> samples, containing different platinum loadings [*x* (wt%)=100\*m(Pt)/ m(TiO<sub>2</sub>); *x*=0.3, 0.5, 1.0], were prepared by a photodeposition method[137]: In a typical experiment, 0.5 g of the TiO<sub>2</sub> powder was suspended in 100 ml of deionized water and purged with argon for 30 min to remove dissolved O<sub>2</sub>. The desired ratio of H<sub>2</sub>PtCl<sub>6</sub> was added to the suspension and the mixture was irradiated from the top for 1h with UV(A) light by a Philips CLEO lamp (3 mW/cm<sup>2</sup>). Then 1 ml of methanol was added to the suspension which was kept under illumination over night. The reaction solution was removed by centrifugation, followed by repeated washing of the powder with distilled water, and finally by drying at 80 °C for 24 h yielding a gray solid.

### 2.2.2.2 Mixing of solids method using colloidal Pt suspensions

Colloidal Pt was prepared by reduction of H<sub>2</sub>PtCl<sub>6</sub> with sodium citrate[106]. Excess ions in the resulting colloidal suspension were removed with an ion exchange resin (Amberlite MBI) until a specific conductivity of ca. 3 μS cm<sup>-1</sup> was reached. Pt-loaded TiO<sub>2</sub> (0.5 wt%) was

prepared by suspending  $\text{TiO}_2$  in deionized water followed by the addition of the desired amount of the as-prepared colloidal Pt under continuous magnetic stirring over night. After evaporation under vacuum at room temperature a grayish powder was obtained. The obtained powder was dried at  $80\text{ }^\circ\text{C}$  overnight.

### **2.2.3 Modification of $\text{TiO}_2$ with other precious metal nanoparticles**

Other metals (Pd, Au, and Ag) were deposited on the surface of  $\text{TiO}_2$  using the procedure of the photocatalytic deposition method described above (2.2.2.1).  $\text{PdCl}_2$ ,  $\text{HAuCl}_4$ , and  $\text{AgNO}_3$  were used as precursors for Pd, Au, and Ag, respectively.

### **2.2.4 Modification of $\text{TiO}_2$ with bimetallic Ag-Pt nanoparticles**

Two series of catalysts were prepared using the procedure of the photocatalytic deposition method (see 2.2.2.1): In the first one,  $\text{Ag}_{(x)}$  [ $x = 0.1, 0.3, 0.5, \text{ and } 1.0\text{ wt. \%}$ ] were photocatalytically deposited on the surface of photocatalytically pre-prepared (0.5 wt.%) Pt/ $\text{TiO}_2$ . In the second one, (0.5 wt.%) Ag was first photocatalytically deposited on the surface of  $\text{TiO}_2$  followed by the photodeposition of different amounts of  $\text{Pt}_{(x)}$  [ $x = 0.1, 0.3, \text{ and } 0.5\text{ wt. \%}$ ].

## **2.3 Characterizations of the prepared materials**

### **2.3.1 Transmission electron microscopy**

Transmission electron microscopy (TEM) and the high-resolution transmission electron microscopy (HRTEM) measurements were carried out using a Field-Emission Transmission Electron Microscope of the type JEM-2100F-UHR (JEOL Ltd., Tokyo, Japan) equipped with a Gatan GIF 2001 energy filter and a 1k CCD camera. (HRTEM) was performed at 200 kV with an ultrahigh resolution pole piece ( $\text{CS} = 0.5\text{ mm}$ ) providing a point-resolution better than 0.19 nm. Energy dispersive X-ray spectroscopy (EDXS) were also carried out on the same device.

### 2.3.2 Specific surface area measurements

A Micromeritics AutoMate 23 instrument was used to determine the single-point standard BET surface area. A gas mixture of 30% nitrogen and 70% helium was used for the adsorption determinations. In order to clean the surface from adsorbed water, all TiO<sub>2</sub> samples were previously heated to 120 °C for approximately 1h.

### 2.3.3 Infrared spectroscopy

FTIR spectra were recorded on a Bruker FRA 106 instrument using KBr pressed powder discs. Each sample of TiO<sub>2</sub> powders (10 mg) was mixed with (190 mg) of spectroscopically pure dry KBr and pressed into disks before its spectrum was recorded.

In-situ ATR-FTIR spectra of 1 ml of pyridine dissolved in acetonitrile (100 mM) were recorded with a Bruker IFS 66 instrument equipped with horizontal ATR unit with a ZnSe crystal. A TiO<sub>2</sub> layer was firstly prepared by placing 400 µL of the suspension of TiO<sub>2</sub> in acetonitrile (4g L<sup>-1</sup> TiO<sub>2</sub>) on the crystal surface followed by evaporation of the solvent at room temperature by the mean of a N<sub>2</sub> flow. For each measurement 64 scans were recorded.

### 2.3.4 Diffuse reflectance spectroscopy

Diffuse reflectance spectra of TiO<sub>2</sub> powders were recorded on a Varian Cray 100 Scan UV-Vis spectrophotometer equipped with labsphere diffuse reflectance accessory. KBr was used as reflectance standard. Reflectance was converted by the instrument software to F(R) values.

### 2.3.5 Thermogravimetric measurements

Thermogravimetric measurements (TGA) were carried out on a Setaram Setsys evolution 1750 thermoanalyzer up to 900°C applying heating rates of 10 °C/min under oxygen.

### 2.3.6 X-ray diffraction

The small-angle XRD diffraction patterns were acquired on a Bruker-axs D8 device using Cu-K $\alpha$  radiation.

### 2.3.7 Acidic sites determination

The acidic sites of the surface of TiO<sub>2</sub> powders were investigated by FTIR spectroscopy of adsorbed pyridine. TiO<sub>2</sub> powders were heated to 120 °C for 24h. Afterwards, the samples were transferred to a desiccator saturated with pyridine vapor and stored in the dark for 24h at room temperature. At the end of the saturation process, the samples were flushed with a N<sub>2</sub> flow for 1h to remove the weakly adsorbed pyridine molecules.

### 2.3.8 Acidic capacity measurements

The ion-exchange capacities of the sulfonic mesoporous materials were determined using aqueous solutions of sodium chloride (NaCl, 2M) as exchange agents. In a typical experiment, 50 mg of the solid was added to 10 ml of aqueous NaCl solution. The resulting suspension was allowed to equilibrate for 24h and thereafter titrated potentiometrically by dropwise addition of 0.01 M aqueous KOH solution.

## 2.4 Photocatalytic reaction procedure

The photocatalytic reactions were carried out in a double jacket Duran glass reactor with a total volume of 40 cm<sup>3</sup> which was irradiated from the outside using an Osram XBO 1000 W Xenon lamp in a Mueller LAX 1000 lamp housing under magnetic stirring at 25 °C (see **Figure 2.1**). A 10 cm water bath and a WG 320 nm filter were used to cut off the IR and the short wavelengths UV light, respectively. In a typical experimental run the desired amount of the photocatalyst (equal to 25 mg of TiO<sub>2</sub>) was suspended in 10 cm<sup>3</sup> of an alcoholic solution containing 100  $\mu$ mol of the nitroaromatic compound. Before illumination, the reactor was

placed in a sonicator for 3 min and then purged with Ar until no N<sub>2</sub> and O<sub>2</sub> were detected by gas chromatography (Shimadzu 8A, TCD detector) in the headspace above the solution.

If the products were to be isolated, the double jacket Duran glass reactor was fed with 40 ml of the reaction mixture and irradiated from the outside by a 500-W mercury medium-pressure lamp (Heraeus TQ 718 Z4) with an UV(A) light intensity of 20 mW/cm<sup>2</sup>. After the complete consumption of the nitroaromatic compound, as detected by the GC, the catalyst was removed by filtration followed by evaporation of the solvent by a rotavapor. The products were purified by silica gel column chromatography with n-hexane: ethyl acetate 8:2 (v/v) as eluent. The structures of the isolated products were confirmed by both GC-MS analysis and <sup>1</sup>H NMR and <sup>13</sup>C NMR measurements recorded in CDCl<sub>3</sub>.

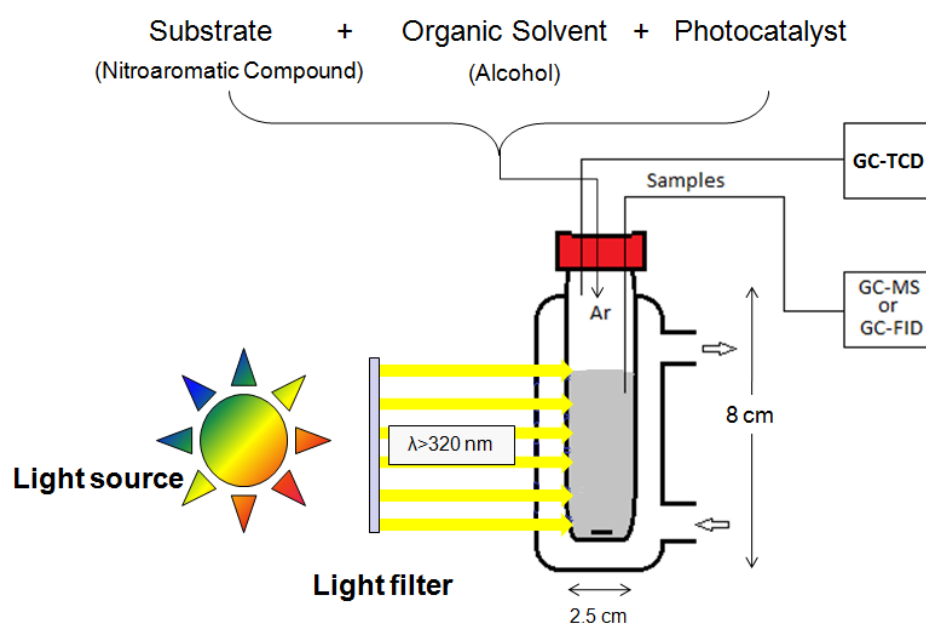


*Figure 2.1: Schematic view of the employed photocatalytic reaction system.*

## 2.5 Dark reaction procedure

The reaction was performed under continuous stirring in a glass snap-cap bottle (23 mm in diameter and 75 mm in length) covered with aluminum foil. The required amount (25 mg) of the catalyst (TiO<sub>2</sub> or modified TiO<sub>2</sub>) was suspended in an ethanolic solution (10 cm<sup>3</sup>)

containing (100  $\mu\text{mol}$ ) of the nitroaromatic compound (or the corresponding aminoaromatic compound). The reaction mixtures were purged with Ar (or  $\text{H}_2$  if needed) for 30 min. For the dark *N*-alkylation reaction tests, the required amounts of the ethanolic solution of acetaldehyde (100 mM) were added to the reaction mixture after the purging step. Samples were also analyzed by GC-FID after filtration.

## 2.6 Analysis of the reaction mixture

### 2.6.1 Gas chromatography-mass spectroscopy measurements

The products were analyzed qualitatively at different illumination times, after removing the semiconductor particles through filtration (0.20  $\mu\text{m}$  filter) from the irradiated mixture, by Gas chromatography-mass spectroscopy measurements (GC-MS). A Shimadzu gas chromatograph and mass spectrometer (Shimadzu GC/MS-QP 5000) equipped with a 30 m Rxi-5ms ( $d = 0.32$  mm) capillary column was used. Operating temperature programmed: injection temperature 305  $^{\circ}\text{C}$ , oven temperature 120  $^{\circ}\text{C}$  (hold 2 min), from 120  $^{\circ}\text{C}$  to 280  $^{\circ}\text{C}$  at the rate of 10  $^{\circ}\text{C}/\text{min}$ , 280  $^{\circ}\text{C}$  (hold 15 min) in splitless mode, injection volume (3.0  $\mu\text{l}$ ) with helium as a carrier gas.

### 2.6.2 Gas chromatography-flame ionization detector measurements

The concentrations of the substrates as well as of the products were determined by gas chromatography equipped with a flame ionization detector (GC-FID). A Shimadzu GC 2010 equipped with a Rtx-5 ( $d = 0.25$  mm) capillary column and an FID detector were used for this purpose. Operating temperature programmed: injection temperature 250  $^{\circ}\text{C}$ , oven temperature 70  $^{\circ}\text{C}$  (hold 2 min), from 70  $^{\circ}\text{C}$  to 280  $^{\circ}\text{C}$  at the rate of 10  $^{\circ}\text{C}/\text{min}$ , in splitless mode. Injection volume: 2.0  $\mu\text{l}$  with nitrogen as the carrier gas. The concentrations of the substrate as well as of the products were determined based on calibration curves prepared with authentic standards (m-toluidine; Aldrich 99%, *N*-ethyl-m-toluidine; Fluka 98%, *N,N*-diethyl-m-toluidine; Acros 99%, and 2,7-dimethylquinoline; Aldrich 99%)



---

### 2.6.3 Gas chromatography- thermal conductivity detector measurements

The produced H<sub>2</sub> gas was analyzed in the headspace above the reaction mixture during the illumination using gas chromatography (Shimadzu 8A) equipped with Molecular Sieve 5A column, TCD detector, and Ar as carrier gas. Column and detection temperature were 60 °C and 150 °C, respectively.

### 2.6.4 Nuclear magnetic resonance spectroscopy

The structures of the isolated products were analyzed using a Bruker DPX 200 MHz NMR spectrometer equipped with 5 mm DUL <sup>13</sup>C-<sup>1</sup>H and BACS sample changer. CCl<sub>3</sub>D was used as solvent.

### 3 Results

#### 3.1 General reaction sequence for the photocatalytic conversion of nitroaromatic compounds (NACs)

**Figure 3.1** shows the general reaction sequence of the photocatalytic conversion of nitroaromatic compounds in alcohols based upon the reaction products identified by the GC-MS analyses. The products were found to be strongly affected by the employed photocatalyst and the reaction conditions.

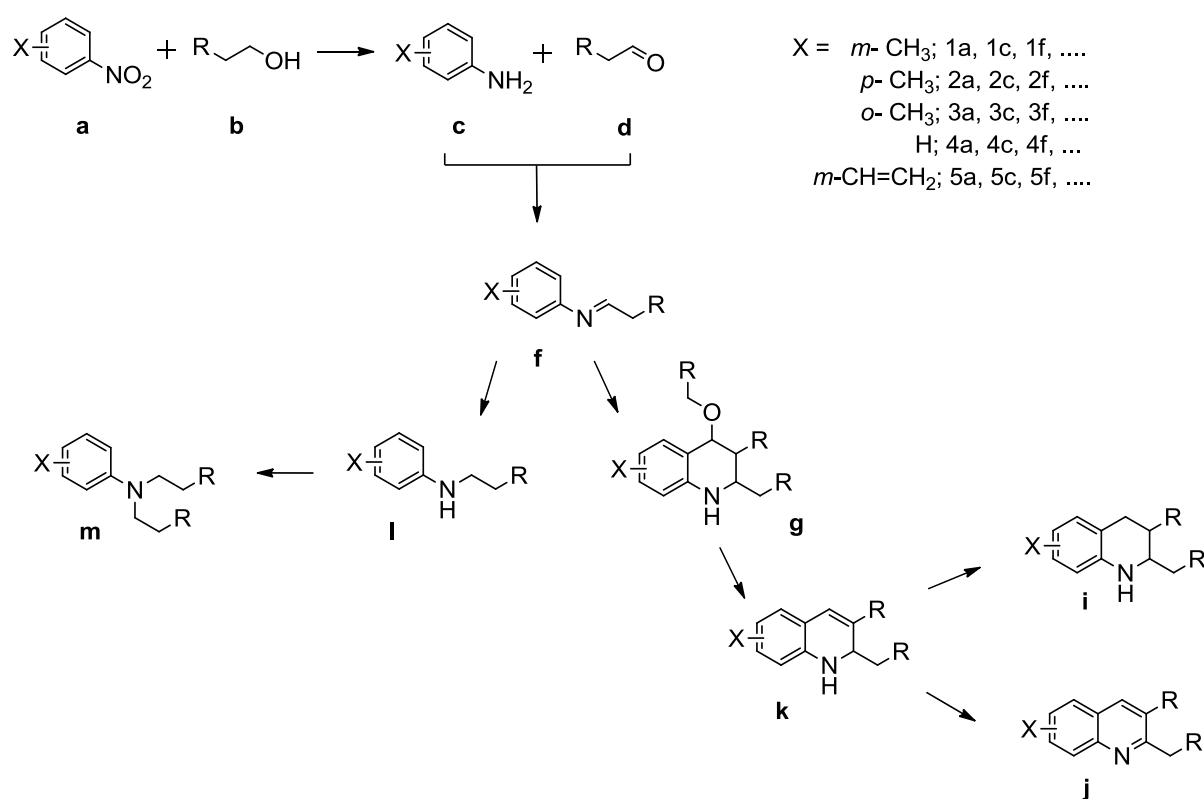


**Figure 3.1:** General reaction sequence for the photocatalytic conversion of the nitroaromatic compounds. A list of compounds with their names and corresponding symbols is provided in the Appendix. (e and h are not used in the symbols because they are usually used for the electron and the hole, respectively, in the discussion).

The conversion of m-nitrotoluene (**1a**) dissolved in ethanol was used as a model reaction in order to investigate the fate of the nitroaromatic compounds dissolved in non-aqueous media upon illumination in the presence of TiO<sub>2</sub> or modified TiO<sub>2</sub> as the photocatalyst.

### 3.2 Photocatalytic conversion of the nitroaromatic compounds over bare TiO<sub>2</sub>

The GC chromatograms obtained at different irradiation ( $\lambda > 320$  nm) times of *m*-nitrotoluene (**1a**) dissolved in ethanol under Ar atmosphere at 25 °C in the presence of Sachtleben Hombikat UV100 as a photocatalyst are shown in **Figure 3.2**.

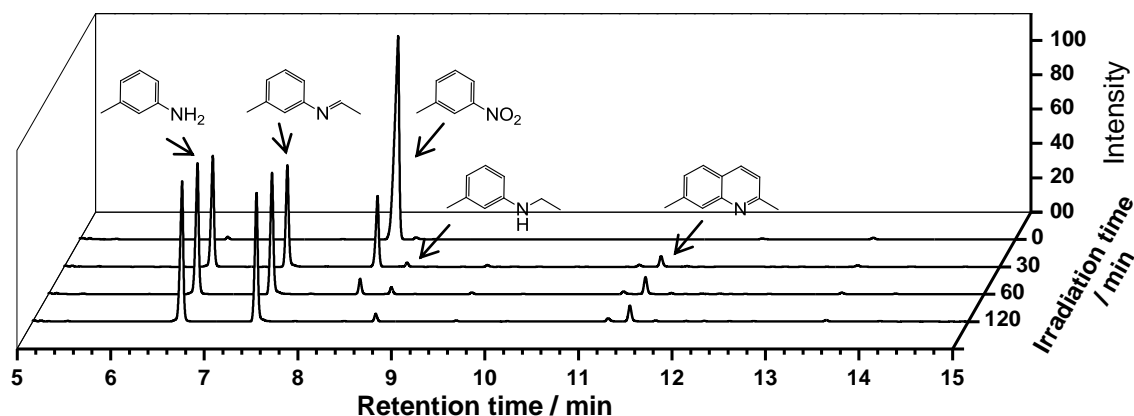


**Figure 3.2:** GC chromatograms obtained at different irradiation times of the reaction mixture (reaction conditions: 100  $\mu$ mol *m*-nitrotoluene (**1a**) and 25 mg TiO<sub>2</sub> in 10 ml EtOH, 60 mW UV(A)/cm<sup>2</sup>, 25 °C, under Ar atmosphere).

It is clearly seen from these chromatograms (**Figure 3.2**) that the peak attributed to (**1a**) (RT: 8.37 min) completely disappeared after 2h of illumination and new peaks appeared at retention times of 6.59, 7.42, and 11.38 min attributed to *m*-toluidine (**1c**), *N*-ethylidene-3-methylaniline (**1f**), and 2,7-dimethylquinoline (**1j**); respectively. A trace of *N*-ethyl-3-methylaniline (**1l**) was also detected as a small peak at 8.81 min. The products were identified using standards and/or GC-MS by comparing the molecular ion and mass fragmentation pattern with those reported in the GC-MS library.

After stirring the reaction mixtures in the dark for several hours as well as after irradiation of the ethanolic solution of the nitroaromatic compound in the absence of TiO<sub>2</sub> no conversion of the nitroaromatic compound was detected clearly indicating that both, the presence of TiO<sub>2</sub> and UV(A) light are essential for the reaction.

**Figure 3.3** shows the time course of the m-nitrotoluene (**1a**) conversion and the products formation under UV(A) irradiation of a reaction mixture containing TiO<sub>2</sub>, (**1a**), and ethanol. The time course of the summation of the amounts of nitrotoluene (**1a**), aminoaromatic compound (**1c**), imine derivative (**1f**), and quinoline derivative (**1j**) is also shown in **Figure 3.3**. A satisfactory material balance (with experimental error of  $\pm 0.5\%$ ) is apparently kept during the reaction so no degradation reaction of the nitroaromatic compound occurs in the present system.

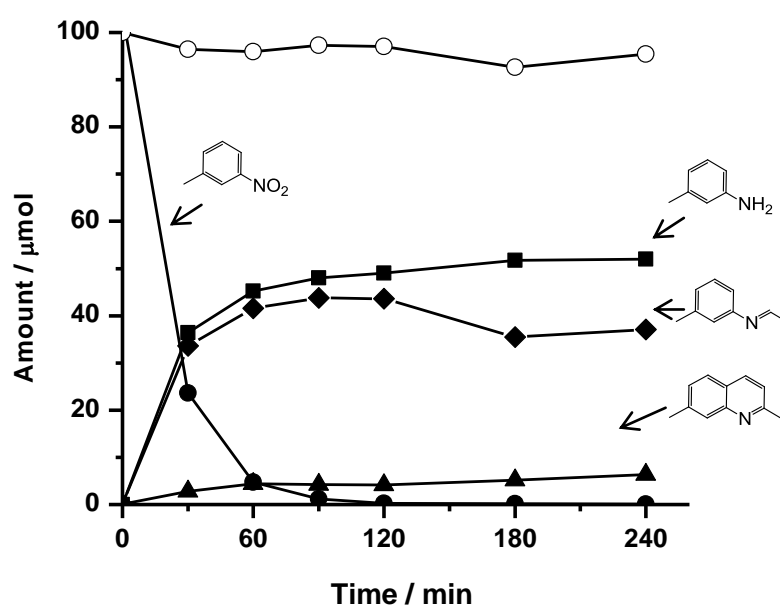


**Figure 3.3:** Time course of: photocatalytic conversion of (**1a**) ( $\bullet$ ); photocatalytic formation of: (**1c**) ( $\blacksquare$ ), (**1f**) ( $\blacklozenge$ ), (**1j**) ( $\blacktriangle$ ); and ( $\circ$ ) summation (reaction conditions: 100  $\mu\text{mol}$  (**1a**) and 25 mg TiO<sub>2</sub> in 10 ml EtOH, 60 mW UV(A)/cm<sup>2</sup>, 25 °C, under Ar atmosphere). Experimental error of the analysis is calculated to be 0.5%.

Under the experimental conditions employed here the complete consumption of the substrate required 2h of UV(A) irradiation. At this time the colour of the suspension changed from white to blue due to the trapping of the photogenerated electrons by Ti(IV) to form Ti(III), indicating the complete conversion of the electron acceptor (**1a**) and the fact that no new electron acceptor was introduced into the system.

### 3.2.1 Effect of TiO<sub>2</sub> type on the photocatalytic conversion of the nitroaromatic compounds

The effect of the type of TiO<sub>2</sub> employed as photocatalyst in the system alcohol - nitroaromatic compound - TiO<sub>2</sub> - light on the reaction products was studied employing several kinds of TiO<sub>2</sub> including anatase, rutile, anatase-rutile mixture, and mesoporous anatase. **Table 3.1** summarizes the physical properties of the employed photocatalysts' powders. The BET surface areas of the TiO<sub>2</sub> materials were determined using nitrogen adsorption-desorption. The crystallite particle sizes of these photocatalysts were obtained from XRD analysis.

*Table 3.1: Physical properties of the employed photocatalysts.*

Entry	Photocatalyst	Phase composition		Notation	S <sub>BET</sub> <sup>[a]</sup> / (m <sup>2</sup> g <sup>-1</sup> )	Particle crystallite size /nm
		Anatase	Rutile			
1	Cristal Global (R34)	-	100	R	58	34
2	Sachtleben Hombikat (UV100)	100	-	A	265	10
3	Evonik-Degussa Aeroxide (P25)	80	20	P25	77	25
4	Home-made mesoporous sample	100	-	MA	174	13

[a] S<sub>BET</sub> surface area

**Figure 3.4.(A-D)** shows the time courses of the consumed amounts of the nitroaromatic compound (**1a**) and the produced amounts of the reaction products - the aminoaromatic compound (**1c**), the imine (**1f**), and the quinoline (**1j**) - respectively, obtained during the photoirradiation of the reaction mixtures employing different kinds of TiO<sub>2</sub>.

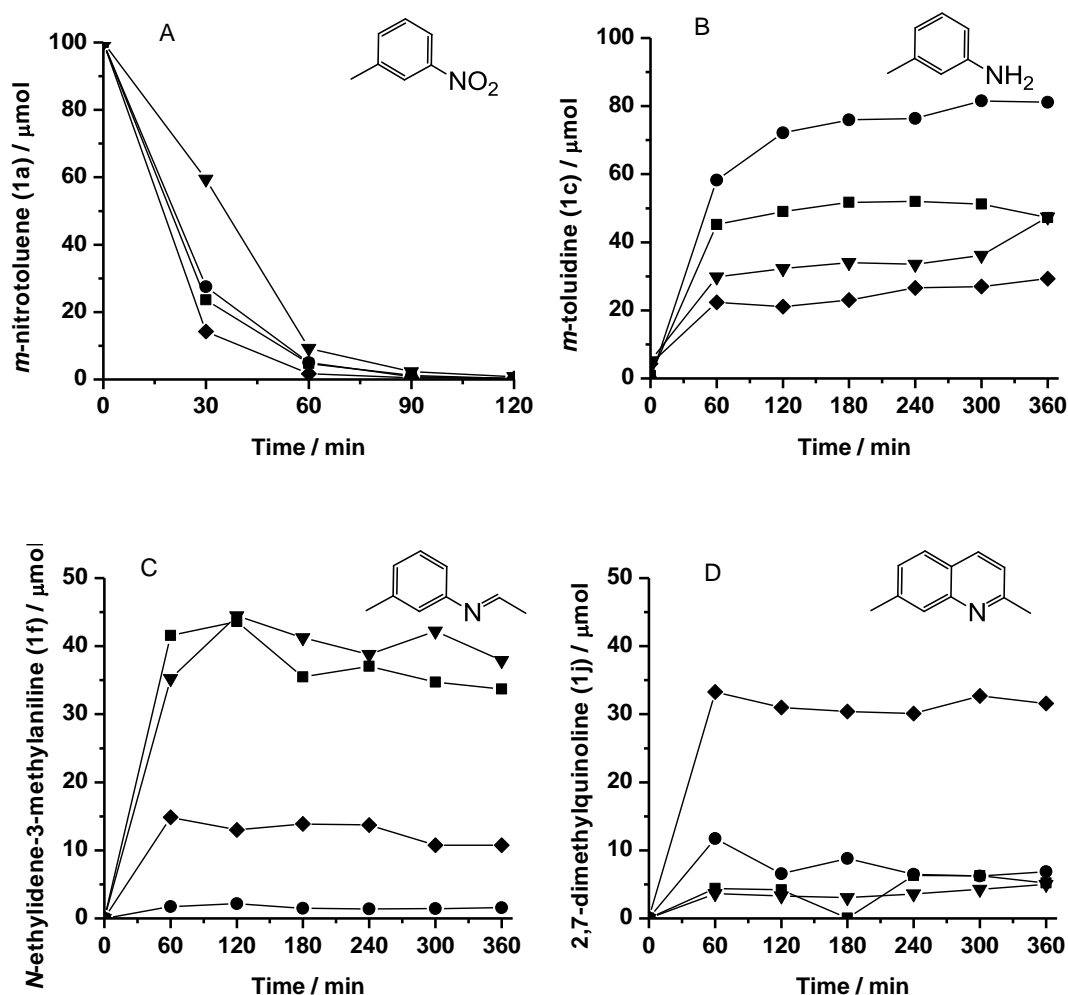


**Figure 3.4:** Time courses of the: (A) consumption of *m*-nitrotoluene (**1a**), (B) production of the aminoaromatic compound (**1c**), (C) production of the imine (**1f**), and (D) production of the quinoline (**1j**); employing: UV100 ( $\blacksquare$ ), rutile ( $\bullet$ ), P25 ( $\blacklozenge$ ), and mesoporous anatase ( $\blacktriangledown$ ). (reaction conditions: 100  $\mu\text{mol}$  (**1a**) and 25 mg  $\text{TiO}_2$  in 10 ml EtOH, 60 mW UV(A)/ $\text{cm}^2$ , 25  $^\circ\text{C}$ , under Ar atmosphere).

As can be seen from **Figure 3.4.A**, all the employed photocatalysts are efficient to convert the nitroaromatic compound (**1a**) by ca. 100% within the first 2h of illumination. However, the data illustrated in **Figure 3.4(B-D)** show that the type of  $\text{TiO}_2$  strongly affects the distribution of the reaction products.

The highest amount of the aminoaromatic compound (**1c**) (ca. 80  $\mu\text{mol}$ ) was obtained employing pure rutile as the photocatalyst (*cf.* **Figure 3.4.B**) whereas this photocatalyst was less efficient than other photocatalysts to produce the imine (**1f**) or its cyclization product the quinoline (**1j**). On the other hand, pure anatase photocatalysts promote the formation of the

imine (**1f**) (ca. 44  $\mu\text{mol}$ ) (cf. **Figure 3.4.C**).  $\text{TiO}_2$  P25, which is a mixture of anatase (80%) and rutile (20%), catalyses the cyclization of the imine (**1f**) to produce the corresponding quinoline (**1j**) (ca. 31%  $\mu\text{mol}$ ) (cf. **Figure 3.4.D**) while employing either pure anatase or pure rutile was not sufficient to improve the amount of the quinoline (**1j**) over 10  $\mu\text{mol}$  even after 6h of irradiation as can be seen from **Figure 3.4.D**.

The photonic efficiencies  $\zeta$  (%) of the photocatalytic reduction of the nitroaromatic compounds (NACs) were calculated as the ratio of the initial reduction rate of NACs and the incident photon flux ( $I_0$ ) according to equations (3.1) and (3.2), where  $k$  is the first order rate constant obtained from the slope of the curve  $\ln(C_0/C)$  vs. time (s). The incident photon flux per volumetric unit has been calculated based upon the UV(A) light meter measurements and assuming an average illumination wavelength  $\lambda = 350$  nm; the irradiated surface area was  $7.85 \text{ cm}^2$ , and the volume of the suspension was 0.01 l.

$$\zeta (\%) = \frac{k \cdot C_0 \cdot V}{I_0 \cdot A} 100 \quad (\text{Eq. 3.1})$$

$$I_0 = \frac{I \cdot \lambda}{N_A \cdot h \cdot c} \quad (\text{Eq. 3.2})$$

with  $I_0$ , being the photon flux;  $I$ , the light intensity;  $N_A$ , Avogadro's number;  $h$ , the Planck constant;  $c$ , the light velocity;  $k$ , the initial rate constant;  $A$ , the illuminated area;  $C_0$ , the initial NAC concentration;  $\lambda$ , the illumination wavelength; and  $V$ , the reactor volume. The calculated  $\zeta$  (%) were found to be 5.8, 6.8, 7.0 and 4.7 for rutile, UV100, P25, and home-made anatase, respectively.

The chemical features of the surface of the employed photocatalysts were investigated by FTIR spectroscopy of adsorbed pyridine, being one of the more selective reagents for studying the acidic sites of the solid acids[138-141]. The FTIR absorption spectra of the pure  $\text{TiO}_2$  materials, as well as of  $\text{TiO}_2$  powders treated with pyridine vapor are shown in **Figure 3.5** and in **Figure 3.6**, respectively.

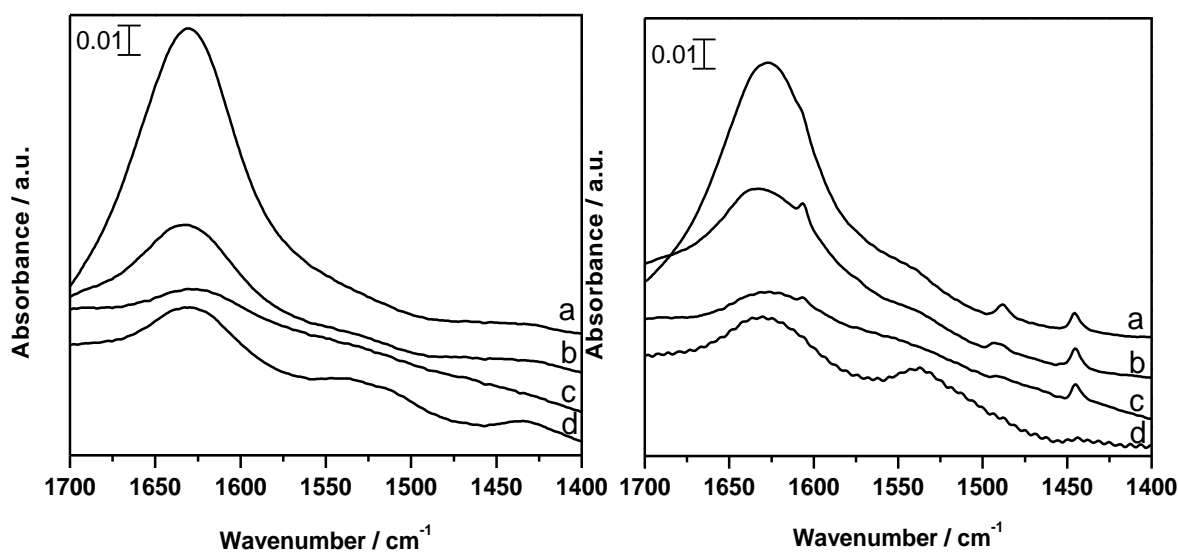


**Figure 3.5:** Infrared spectra of bare  $\text{TiO}_2$ ; (a) UV100, (b) P25, (c) mesoporous anatase, and (d) rutile

**Figure 3.6:** Infrared spectra of  $\text{TiO}_2$  powders treated with pyridine vapor; (a) UV100, (b) P25, (c) mesoporous anatase, and (d) rutile.

The wide absorbance peak at  $1640\text{ cm}^{-1}$  (**Figure 3.5** and **Figure 3.6**) is attributed to vibrations of the surface-adsorbed  $\text{H}_2\text{O}$  and to Ti-OH bonds. As shown in (**Figure 3.6**), several significant new peaks at  $1445$ ,  $1489$ ,  $1540$ ,  $1607$ , and  $1639\text{ cm}^{-1}$  appeared upon adsorption of pyridine on some of the  $\text{TiO}_2$  samples. These peaks have been assigned to the chemisorption of molecular pyridine at different types of surface acidic sites[142]. The peaks at  $1445$  and  $1607\text{ cm}^{-1}$  are due to the interaction of pyridine with Lewis acid sites (exposed  $\text{Ti}^{4+}$  cations), while the peaks at  $1540$  and  $1639\text{ cm}^{-1}$  result from the protonation of the pyridine molecule by the Brönsted acid sites (surface-bound hydroxyl groups). However, under our experimental conditions, the peak at  $1639\text{ cm}^{-1}$  overlapped with vibrations of the surface adsorbed water while the peak at  $1540\text{ cm}^{-1}$  was very broad and weak. The band at  $1489\text{ cm}^{-1}$  reflects pyridine interactions with active centers of both acidic types. For the rutile



sample no clear new peaks appeared after its treatment with pyridine vapor confirming the poor acidity of this TiO<sub>2</sub> type[143].

### 3.2.2 Effect of the addition of an acid as a co-catalyst

#### 3.2.2.1 Photocatalytic conversion of the nitroaromatic compound in ethanol

Bearing in mind that the traditional methods to prepare quinolines usually require large amounts of acids[144], it is conceived that, in a photocatalytic system, the addition of a small amount of an external acid as a co-catalyst to the reaction mixture could be effective to increase the yield of the produced quinoline. For this reason, prior to illumination, varying amounts (5, 10, 20, or 40 mol%) of *p*-toluenesulfonic acid (*p*-TsOH) were added to the *m*-nitrotoluene ethanolic solution in the presence of Hombikat UV100 being the photocatalyst. The yields of the quinoline (**1j**) obtained after 2h photoirradiation are illustrated in **Figure 3.7**.

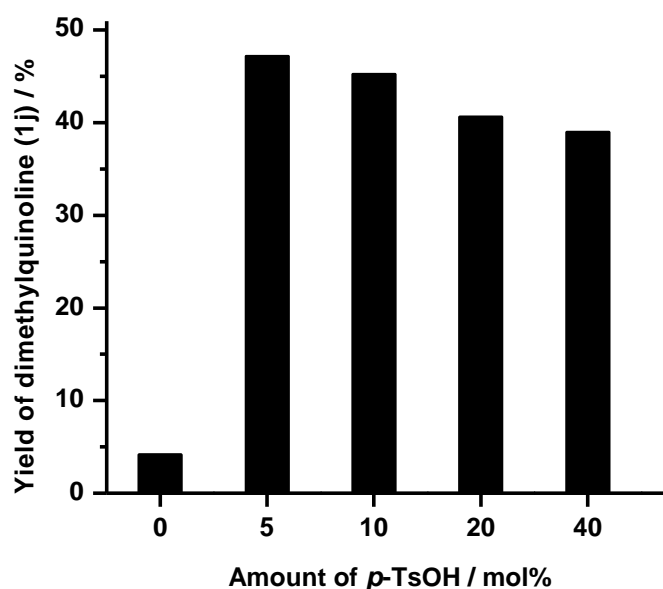


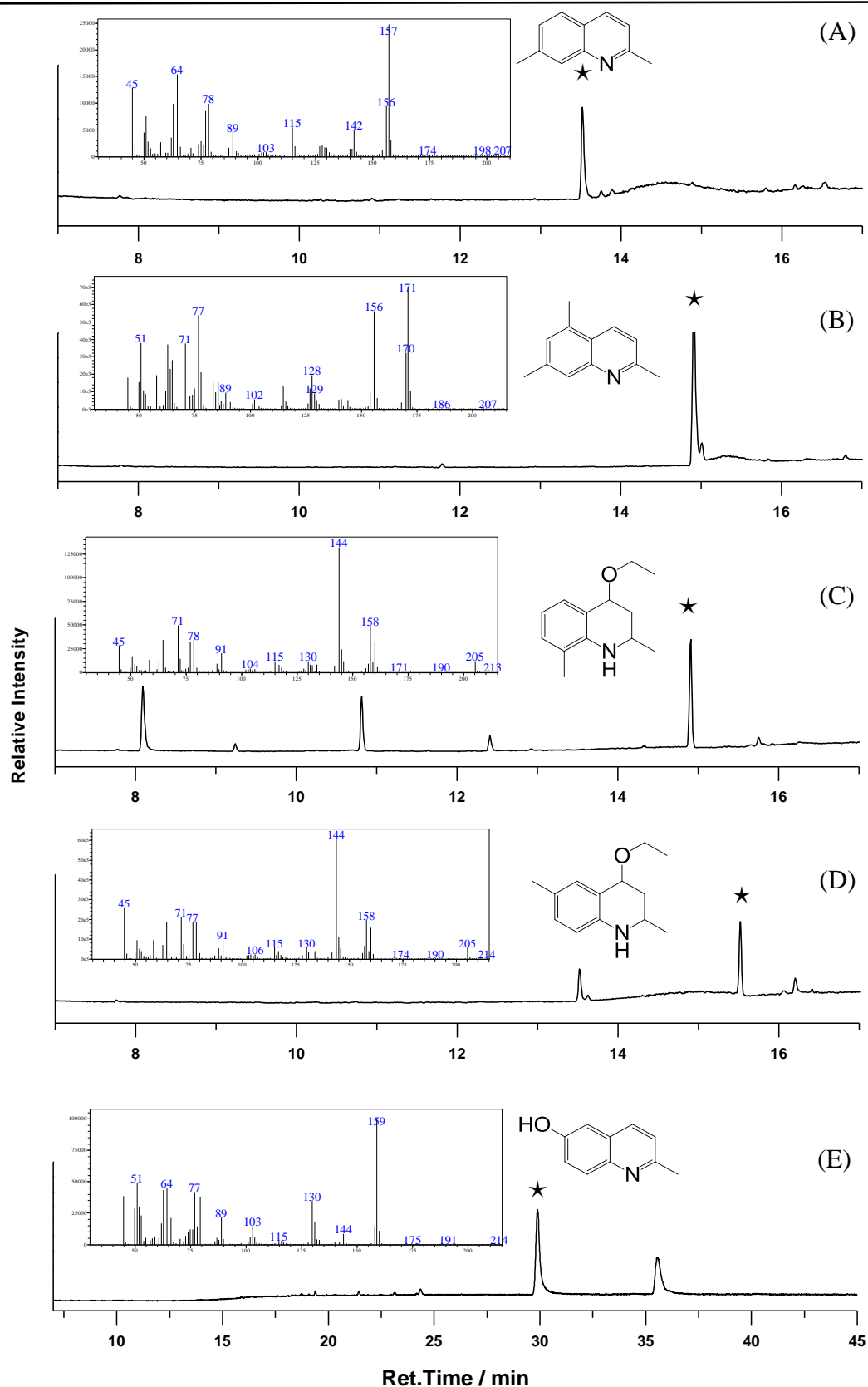
**Figure 3.7:** Yield of the photocatalytically produced quinoline (**1j**) at: different *p*-TsOH concentrations (reaction conditions: 100  $\mu$ mol (**1a**), 25 mg TiO<sub>2</sub>, and the required amounts of *p*-TsOH in 10 ml EtOH, 60 mW UV(A)/cm<sup>2</sup>, 25 °C, under Ar atmosphere).

It can be seen from **Figure 3.7** that the yield of the quinoline (**1j**) increased significantly, i.e., from 4% upto 47%, upon the addition of only a small amount of *p*-TsOH (5mol%). However, increasing the added amount of *p*-TsOH does not help to increase the yield of the produced quinoline any further but rather decreases it a little.

### 3.2.2.2 Photocatalytic conversion of different nitroaromatic compounds and different alcohols

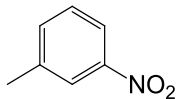
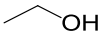
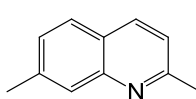
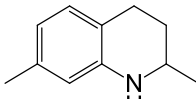
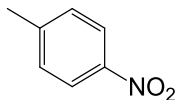
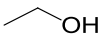
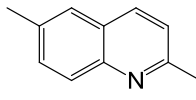
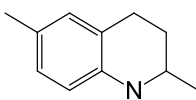
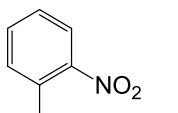
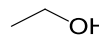
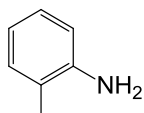
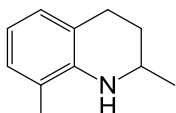
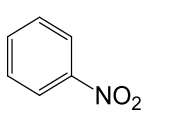
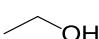
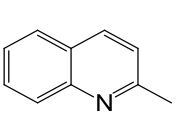
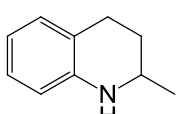
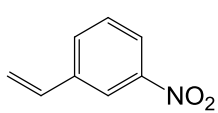
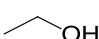
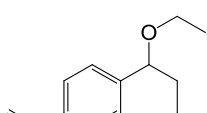
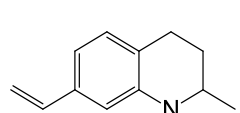
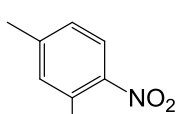
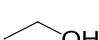
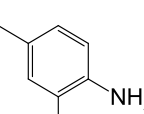
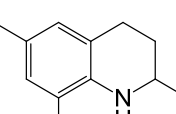
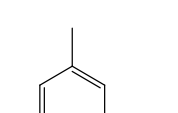
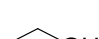
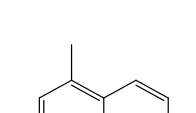
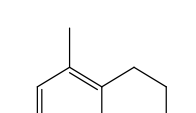
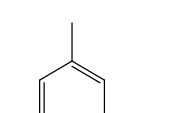
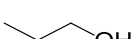
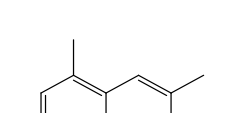
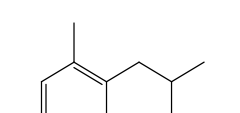
The combination of the solid photocatalyst (TiO<sub>2</sub>) and the acidic co-catalyst (*p*-toluenesulfonic acid) can also be successfully applied for the light-induced conversion of other derivatives of nitrobenzene (*p*-nitrotoluene (**2a**), *o*-nitrotoluene (**3a**), 3-vinyl-1-nitrobenzene (**5a**), 3,5-dimethyl-1-nitrobenzene (**6a**), 2,4-dimethyl-1-nitrobenzene (**7a**), and *p*-nitrophenol (*p*-NPh)) in O<sub>2</sub>-free ethanolic suspensions yielding substituted quinolines and tetrahydro-quinolines.

The GC-MS analysis of the respective irradiated mixtures, containing (5mol%) *p*-TsOH, are shown in **Figure 3.8**. These analyses show the formation of substituted quinolines as the main products when (**1a**), (**6a**), or *p*-NPh were employed as substrates, while ethoxy-tetrahydro-quinolines are the main products when (**2a**) or (**3a**) were used. However, by increasing the amount of the co-catalyst (*p*-TsOH) to 40mol%, quinoline and tetrahydroquinoline derivatives were obtained as main products in all cases. Using toluene as internal standard in the GC-MS analysis the concentrations of the produced cyclic compounds were determined. Thus, the yields of the products were calculated on the basis of the consumption of the corresponding nitroaromatic compounds. The respective results are summarised in **Table 3.2**.



**Figure 3.8:** GC-MS chromatograms obtained after 4 hours irradiation of the reaction mixtures: (A) **1a**, (B) **6a**, (C) **3a**, (D) **2a**, and (E) *p*-NPh. The MS spectra refer to the peaks labeled with (★). (reaction conditions: 100  $\mu$ mol of nitroaromatic compound, 25 mg  $\text{TiO}_2$ , and (5mol%) *p*-TsOH in 10 ml EtOH, 20 mW UV(A)/ $\text{cm}^2$ , 25  $^\circ\text{C}$ , under Ar atmosphere)

**Table 3.2:** Photocatalytic conversion of different NACs in different alcohols in the presence of  $\text{TiO}_2$  and *p*-TsOH as co-catalyst.

Entry <sup>[a]</sup>	Substrate	Alcohol	Products (Yields [%]) <sup>[b]</sup>	
1			 (45)	 (55)
2			 (50)	 (49)
3			 (46)	 (16)
4			 (59)	 (41)
5			 (35)	 (14)
6			 (8)	 (34)
7			 (51)	 (46)
8			 (64)	 (33)

**Table 3.2(continued):** Photocatalytic conversion of different NACs in different alcohols in the presence of  $\text{TiO}_2$  and *p*-TsOH as co-catalyst



[a] Reaction conditions: 200  $\mu\text{mol}$  of the nitroaromatic compound, 50 mg  $\text{TiO}_2$ , and 40mol% of *p*-TsOH in 20 ml EtOH, 20 mW  $\text{UV(A)/cm}^2$  for 4 hours, 25 °C, under Ar atmosphere.

[b] GC yield using toluene as internal standard.

### 3.3 Photocatalytic conversion of the nitroaromatic compounds over modified $\text{TiO}_2$

#### 3.3.1 $\text{TiO}_2$ Modified with acid functionalized $\text{SiO}_2$

The previous results (*c.f.* 3.2.2) showed that substituted quinolines can be successfully prepared by the combination of a solid photocatalyst ( $\text{TiO}_2$ ) and an acidic co-catalyst (*p*-toluenesulfonic acid). However, the subsequent isolation of the homogeneously distributed co-catalyst is still a problematic reaction step. In order to overcome this problem,  $\text{TiO}_2$  and the acid were embedded on one heterogeneous bifunctional catalyst. For this purpose, hybrid organic–inorganic materials in which the organic acid is stabilized into the pores of mesoporous silica-titania composites were prepared. Acid modified mesoporous  $\text{SiO}_2$  decorated with  $\text{TiO}_2$  was prepared via the co-condensation of 2-(4-chlorosulfonylphenyl)ethyltrimethoxysilane (CSPTMS) and tetraethyl orthosilicate (TEOS) in the presence of commercially available Hombikat UV100  $\text{TiO}_2$  particles. The resulting bifunctional catalysts were tested for the one-pot photocatalytic conversion of nitroaromatic compounds into quinolines in  $\text{O}_2$ -free alcoholic solutions.

$\text{SiO}_2$  has been chosen for several aspects: Firstly, for its ability to connect easily and strongly to  $\text{TiO}_2$ , thus, stable  $\text{TiO}_2$ - $\text{SiO}_2$  composites can be obtained[145-147]. Secondly, the preparation of well-ordered mesoporous silica structures with uniform pore sizes is well known and such materials can be easily synthesized[148]. Finally, the possibility to

functionalize the mesoporous silica with organic acid groups to produce promising solid acid catalysts will avoid the use of traditional homogeneous acid catalytic systems and hence their serious drawbacks such as hazards in handling, corrosiveness, toxic wastes and difficulties in their separation[149]. Such a solid acid catalyst has been successfully tested for a large number of thermal acid-catalysed reactions such as esterification[150-152], alkylation[153], condensation[154-156] and different rearrangement processes[153, 157]. On the other hand, any additional problems induced by the difficulty to fabricate a TiO<sub>2</sub> photocatalyst with sufficient activity (*i.e.*, comparable to that of commercially available TiO<sub>2</sub>) was omitted per se by employing the commercially available TiO<sub>2</sub> powder Sachtleben Hombikat UV100 which already exhibits a sufficient photocatalytic performance for the reduction of the nitroaromatic compounds as was shown in the previous sections.

### 3.3.1.1 Characterization of the prepared catalysts

TiO<sub>2</sub>-SiO<sub>2</sub>-ArSO<sub>3</sub>H samples containing different TiO<sub>2</sub> and -ArSO<sub>3</sub>H loadings were prepared using a conventional preparation method[148]. The physical and chemical properties of the obtained catalysts are summarized in **Table 3.3**.

*Table 3.3: Physical and chemical properties of the prepared catalysts.*

Sample	<u>Molar composition</u>			S <sub>BET</sub> /m <sup>2</sup> g <sup>-1</sup>	Acid capacity (mmol/g)	Theoretical Ar-SO <sub>3</sub> H content (mmol/g)
	TiO <sub>2</sub>	SiO <sub>2</sub>	Ar-SO <sub>3</sub> H			
TiO <sub>2</sub>	1	0	0	265	0.02	0
SiO <sub>2</sub>	0	1	0	757	0.02	0
T <sub>0.1</sub> S <sub>1</sub>	0.1	1	0	608	nd.	0
T <sub>0.5</sub> S <sub>1</sub>	0.5	1	0	480	nd.	0
T <sub>1</sub> S <sub>1</sub>	1	1	0	581	0.03	0
T <sub>5</sub> S <sub>1</sub>	5	1	0	263	nd.	0
T <sub>10</sub> S <sub>1</sub>	10	1	0	179	nd.	0
T <sub>1</sub> S <sub>1</sub> Ar <sub>0.03</sub>	1	1	0.03	424	0.20	0.20
T <sub>1</sub> S <sub>1</sub> Ar <sub>0.06</sub>	1	1	0.06	345	0.32	0.39
T <sub>1</sub> S <sub>1</sub> Ar <sub>0.1</sub>	1	1	0.10	323	0.50	0.60

nd.: Not detected

The transformation of the chlorosulfonyl moieties into sulfonic groups mediated by acid-catalysed hydrolysis during the preparation of the mixed catalyst powders was confirmed by measuring the acid capacity of the sulfonic-modified materials. The acid capacity was measured by means of acid–base potentiometric titration using  $\text{Na}^+$  as an ion-exchange agent. The respective results are also shown in **Table 3.3**. The close agreement between the ion-exchange capacities measured using sodium as exchange ion with the calculated  $\text{SO}_3\text{H}$  content based upon the employed concentration of CSPTMS can be taken as clear evidence that most of the arenesulfonic groups are effectively incorporated in the silica network and are accessible and useful for the catalytic reaction processes. Moreover, the decrease of the BET surface area by increasing the loaded amount of the organic acid (*cf.* **Table 3.3**) clearly indicates that the acid is located on the pore wall of the mesoporous support.

**Figure 3.9** shows the FT-IR spectra of the bare oxides and of the arenesulfonic modified  $\text{SiO}_2\text{-TiO}_2$  samples with different Ar- $\text{SO}_3\text{H}$  molar ratios. For all the samples which contain  $\text{SiO}_2$ , the typical Si-O-Si stretching and bending vibrations bands of the condensed silica network are present around 1210, 1080, and 794  $\text{cm}^{-1}$  while the peak at 956  $\text{cm}^{-1}$  corresponds to the Si-OH group[158]. The peak at 1630  $\text{cm}^{-1}$  is due to adsorbed  $\text{H}_2\text{O}$ [158]. From the enlarged parts of the FT-IR spectra of the bare  $\text{SiO}_2\text{-TiO}_2$  and of the arenesulfonic modified  $\text{SiO}_2\text{-TiO}_2$  samples with different Ar- $\text{SO}_3\text{H}$  molar ratios (*cf.* I and II in **Figure 3.9**) it can be clearly seen that new bands at 1010  $\text{cm}^{-1}$ , 1122  $\text{cm}^{-1}$ , 1409  $\text{cm}^{-1}$ , and 1498  $\text{cm}^{-1}$  appear only in the samples which were synthesized in the presence of CSPTMS. The intensity of these bands increases as the CSPTMS / (CSPTMS + TEOS) molar ratio in the initial mixture is increased. The two peaks at 1409 and 1498  $\text{cm}^{-1}$  are assigned to CC stretching vibrations in the aromatic ring of the embedded organic acid whereas a weak vibration appears as a shoulder at 1600  $\text{cm}^{-1}$  corresponding also to the aromatic ring [159]. On the other hand, the two peaks at 1010 and 1122  $\text{cm}^{-1}$  are close to those of the C-H aromatic in-plan bending vibrations[159]. However, Pejov et al. [160] have reported that the bands, which are usually assigned to the C-

H aromatic in-plane bending vibrations, may also be attributed to the antisymmetric  $\text{SO}_3$  stretching modes and to the symmetric  $\text{SO}_3$  stretching mode, respectively.

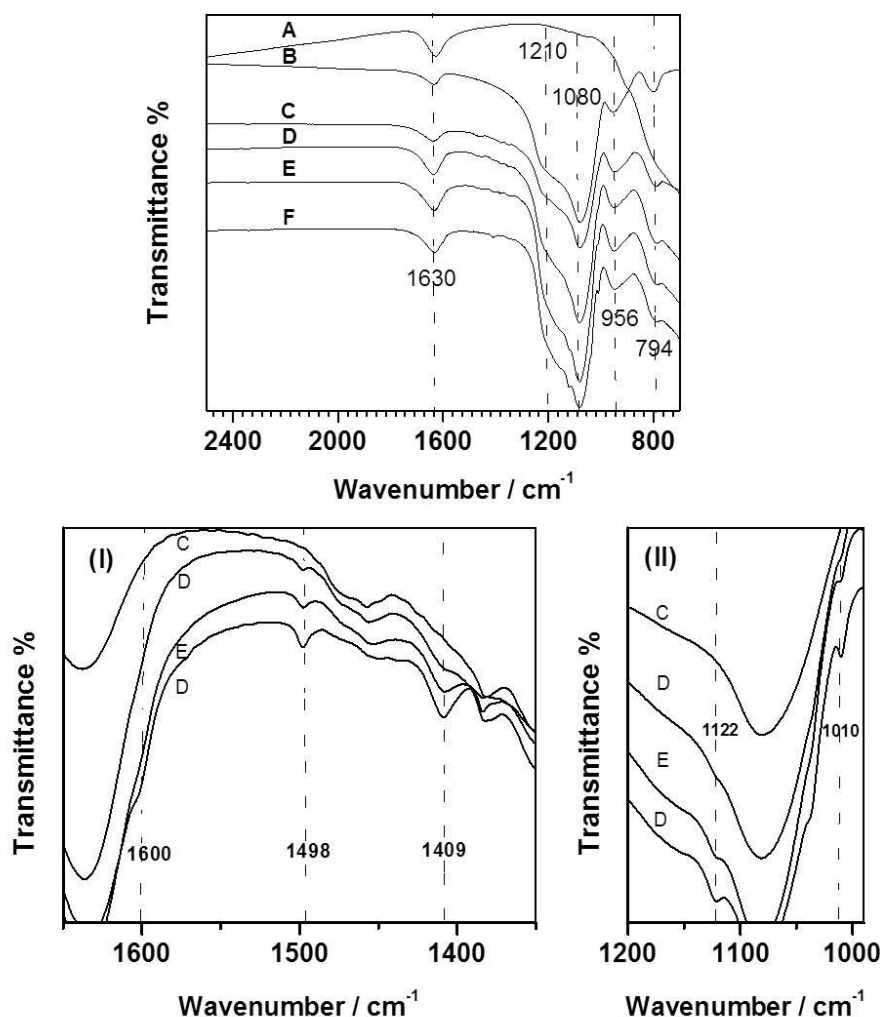


**Figure 3.9:** FT-IR spectra of  $\text{TiO}_2$  (A),  $\text{SiO}_2$  (B), and extracted arenesulfonic modified  $\text{SiO}_2$ - $\text{TiO}_2$  samples with different  $\text{Ar-SO}_3\text{H}$  molar ratios: 0 (C), 0.03 (D), 0.06 (E), 0.1 (F). (I) enlarged region from 1350-1650  $\text{cm}^{-1}$ , and (II) enlarged region from 990-1200 $\text{cm}^{-1}$ .

TGA measurements (**Figure 3.10**) also confirm the presence of the arenesulfonic acid group on the inner mesopore surfaces of the functionalized silica. A continuous mass loss with various rates is observed which can be better interpreted in combination with the DTA results. Three well resolved regions of mass loss can be distinguished: i) below 200  $^\circ\text{C}$ , ii) between 200  $^\circ\text{C}$  and 380  $^\circ\text{C}$ , and iii) above 380  $^\circ\text{C}$ . The first peak for each sample is associated with the desorption of physisorbed water or ethanol[151, 161, 162]. A peak around



280 °C is observed in both extracted samples (a,b) but not in the sample which was calcined at 450 °C for 4h (c). Consequently, this peak can be attributed to the presence of residual surfactant. The decomposition of the organic acid groups was observed as two peaks in the region above 380 °C, hence, the thermal decomposition of ethylphenylsulfonic acid groups occurs in two steps starting at 418 °C and being completed at 580 °C.

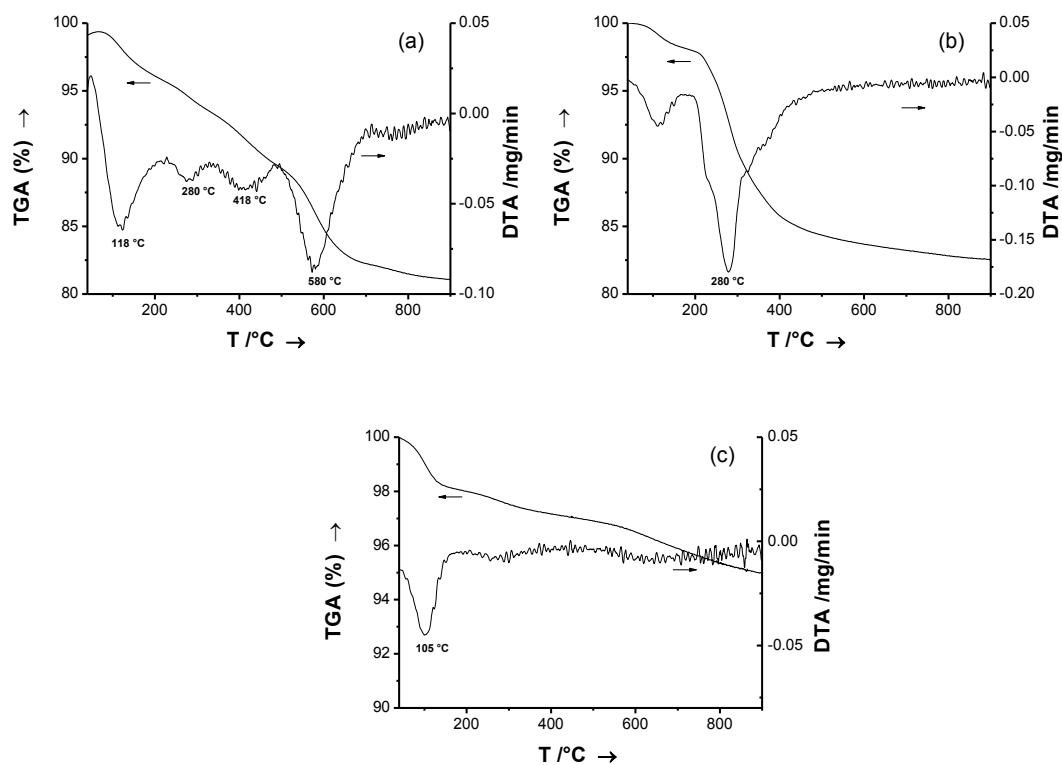


**Figure 3.10:** TGA and DTA measurements of: (a) the extracted arenesulfonic modified  $\text{SiO}_2\text{-TiO}_2$  sample  $T_1S_1Ar_{0.1}$ , (b) extracted  $\text{TiO}_2$  modified with mesoporous silica, and (c)  $\text{TiO}_2$  modified with mesoporous silica calcined at 450 °C for 4h.

EDXS imaging was used to determine the localization of each component of the prepared composite material. As can be seen from **Figure 3.11** (a, b) the particles consist of a network of  $\text{SiO}_2$  whereas the  $\text{TiO}_2$  was located as islands of agglomerates on the surface of the  $\text{SiO}_2$  particle. Furthermore, EDXS imaging (**Figure 3.11** c) shows a statistical distribution of the sulfur over the whole particle evincing that the organic acid is not localized just on one side of the material but is distributed over the entire  $\text{SiO}_2$  matrix. The transmission electron microscopy (TEM) images (**Figure 3.11** d, e, and f) provide clear evidence of a well ordered

hexagonal structure of the porous  $\text{SiO}_2$  network which is decorated with agglomerates of small (5nm)  $\text{TiO}_2$  nanoparticles (as is evidenced by the interlattice diffraction fringes clearly observed in the HRTEM images in **Figure 3.11 f**).

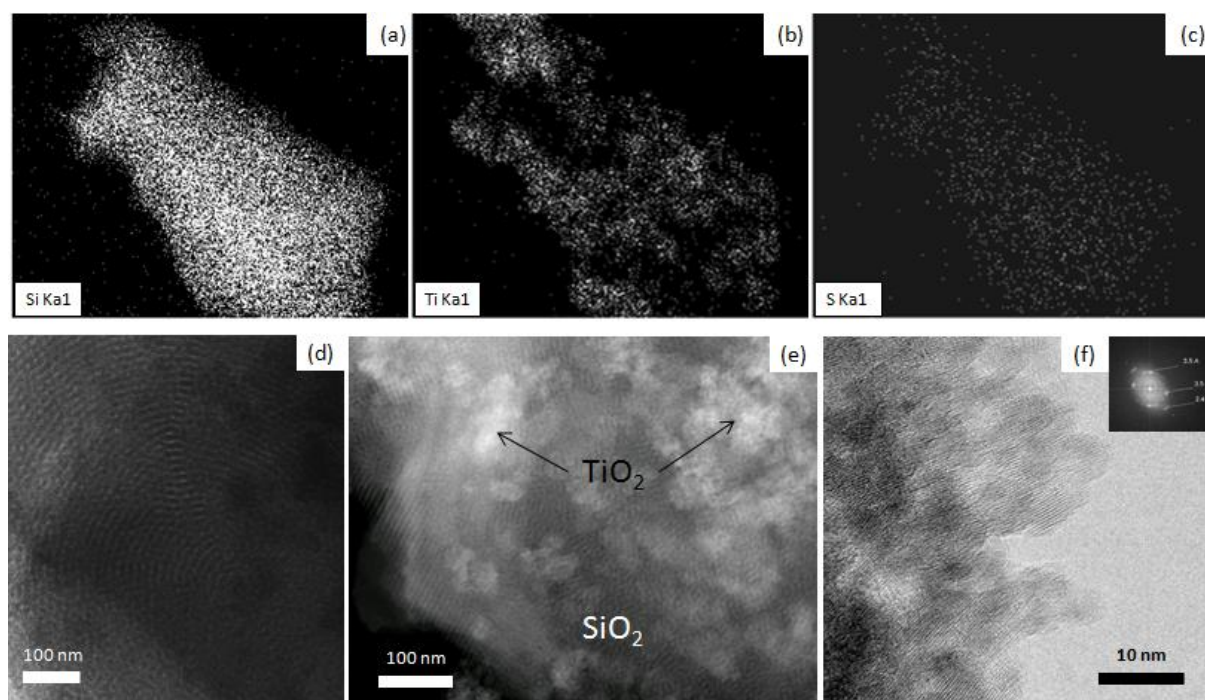


**Figure 3.11:** EDXS elemental map of: (a) silicon, (b) titanium, and (c) sulfur in the extracted arenesulfonic modified  $\text{SiO}_2\text{-TiO}_2$  (sample  $\text{T}_1\text{S}_1\text{Ar}_{0.1}$ ); (d) TEM image of the porous  $\text{SiO}_2$  matrix in the same sample (e) Dark-field TEM micrograph showing the nanocrystalline  $\text{TiO}_2$  deposited on the  $\text{SiO}_2$  matrix; (f) HRTEM image of the sample showing the anatase polycrystallites on the surface of the sample  $\text{T}_1\text{S}_1\text{Ar}_{0.1}$ . The Fourier transformation (FFT) is shown as inset.

In order to confirm the highly ordered hexagonal structure of the prepared materials, small-angle XRD analyses were carried out (**Figure 3.12**). As can be seen in **Figure 3.12** both bare  $\text{SiO}_2$  and  $\text{T}_1\text{S}_1$  samples exhibit four well resolved peaks that are indexable as (100), (110), (200) and (210) reflections associated with the  $p6mm$  hexagonal symmetry. The intensities of the XRD peaks of the arenesulfonic modified sample were too low to be recognized. Such a feature which has also been reported by other research groups [157, 163] can be explained by the presence of arenesulfonic groups inside the channels of the mesoporous  $\text{SiO}_2$  structure

resulting in a substantial loss in scattering contrast between the channel and the wall and, therefore, in a poor XRD pattern.

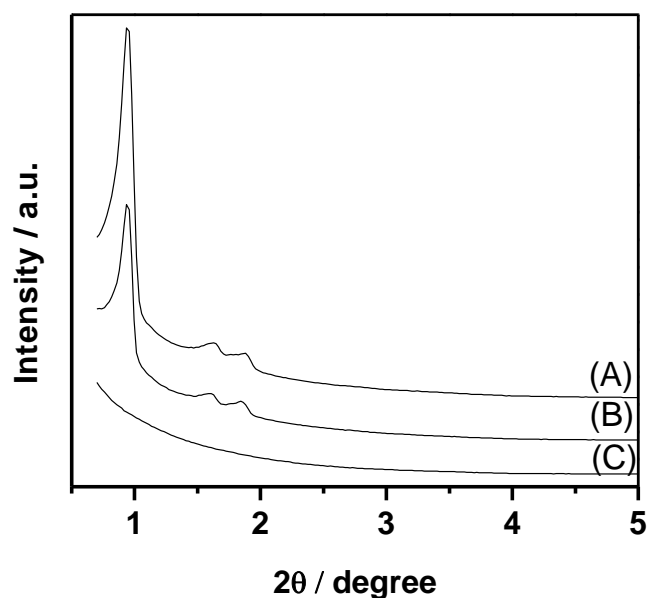


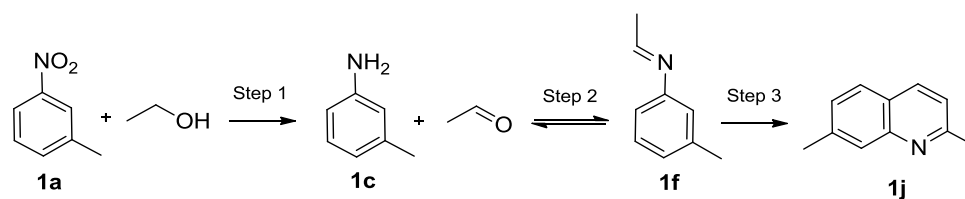
**Figure 3.12:** XRD patterns of: (A) pure  $\text{SiO}_2$ , (B)  $\text{SiO}_2\text{-TiO}_2$  (sample  $T_1S_1$ ), and (C) arenesulfonic modified  $\text{SiO}_2\text{-TiO}_2$  sample  $T_1S_1Ar_{0.03}$ .

### 3.3.1.2 Photocatalytic activity of the newly prepared photocatalysts for the conversion of nitroaromatic compounds

The conversion of *m*-nitrotoluene (**1a**) dissolved in ethanol was investigated as a model reaction to identify the potential of the prepared  $\text{TiO}_2\text{-SiO}_2\text{-ArSO}_3\text{H}$  catalysts. Irradiation ( $\lambda > 320$  nm) of the reaction mixture under Ar at 25 °C in the presence of the acid modified mesoporous  $\text{TiO}_2\text{-SiO}_2$  particles resulted in the formation of 2,7-dimethylquinoline (**1j**).

**Table 3.4** presents the results of the quinoline (**1j**) synthesis upon irradiation of the nitroaromatic compound (**1a**) in EtOH with the different catalysts.

**Table 3.4:** Conversion of *m*-nitrotoluene (**1a**) and yields of *m*-toluidine and 2,7-dimethylquinoline (**1j**) obtained upon the illumination of EtOH solutions containing *m*-nitrotoluene and the corresponding catalyst.



Entry <sup>[a]</sup>	Catalyst <sup>[b]</sup>	Conversion [%]	Yield [%]	
			<b>1c</b>	<b>1j</b>
1	Bare TiO <sub>2</sub>	100	52	6
2	T <sub>1</sub> S <sub>1</sub>	98	58	18
3	T <sub>0.5</sub> S <sub>1</sub>	92	38	11
4	T <sub>5</sub> S <sub>1</sub>	83	41	12
5	T <sub>1</sub> S <sub>1</sub> Ar <sub>0.03</sub>	98	3	53
6	T <sub>1</sub> S <sub>1</sub> Ar <sub>0.03(r2)</sub>	99	2	54
7	T <sub>1</sub> S <sub>1</sub> Ar <sub>0.03(r3)</sub>	99	3	53
8	T <sub>1</sub> S <sub>1</sub> Ar <sub>0.06</sub>	98	8	51
9	T <sub>1</sub> S <sub>1</sub> Ar <sub>0.1</sub>	98	7	45

[a] Reaction conditions: catalyst (equal to 25 mg TiO<sub>2</sub>), (**1a**) (100 μmol), EtOH (10 mL), 20 mW UV(A)/cm<sup>2</sup> for 4h, 25 °C, under Ar atmosphere., [b] for notation see **Table 3.3**.

In all cases the catalysts achieve almost total conversion of the starting nitroaromatic compound within 4 hours of UV(A) irradiation. However, as have been previously observed (*c.f.* **3.2**), bare TiO<sub>2</sub> (Sachtleben Hombikat UV100) exhibits considerably lower activity for the subsequent cyclization reaction yielding the quinoline (**1j**) (*cf.* entry 1 in **Table 3.4**). Modifying the titania with bare SiO<sub>2</sub> was also not really sufficient to promote the yield of (**1j**) (*cf.* entries 2-4 in **Table 3.4**). Higher yields of (**1j**) were obtained, however, employing arenesulfonic acid modified SiO<sub>2</sub>-TiO<sub>2</sub> as catalysts (*cf.* entries 5-9 in **Table 3.4**).

### 3.3.2 TiO<sub>2</sub> modified with precious metals nanoparticles

#### 3.3.2.1 Comparison of different precious metals loaded on the surface of TiO<sub>2</sub>

The surface of the TiO<sub>2</sub> powder Sachtleben Hombikat UV100 was modified with different precious metals (Pt, Pd, Au, and Ag). For this purpose, the photocatalytic deposition method of the metals from the aqueous solutions of the corresponding salts in the presence of methanol as sacrificial reagent was used. A comparative study of the obtained catalysts for the photocatalytic conversion of the nitroaromatic compounds in alcohols has been performed using again the photocatalytic conversion of *m*-nitrotoluene (**1a**) in ethanol as the model reaction.

Irradiation ( $\lambda > 320$  nm) of Pt<sub>0.5</sub>/TiO<sub>2</sub> particles suspended in an ethanolic solution of *m*-nitrotoluene (**1a**) under Ar atmosphere at 25 °C led to the *N*-alkylation and the *N,N*-dialkylation of the nitroaromatic compound as indicated by the GC/MS chromatograms recorded at different times of the photocatalytic reaction (*cf.* **Figure 3.1**). **Figure 3.13** shows the time course of the (**1a**) consumption and of the products formation under UV irradiation of a reaction mixture containing Pt<sub>0.5</sub>/TiO<sub>2</sub>. Two hours photoirradiation were sufficient to achieve the complete consumption of (**1a**). About 70% yield of the mono *N*-alkylated product, *N*-ethyl-*m*-toluidine (**1l**), was achieved when Pt<sub>0.5</sub>/TiO<sub>2</sub> was used as the photocatalyst, while only traces of (**1l**) were detected in the case of bare TiO<sub>2</sub> (*cf.* **Figure 3.2**). On the other hand, prolonged illumination converts the initially produced (**1l**) gradually into *N,N*-diethyl-*m*-toluidine (**1m**) in the presence of Pt on the surface of TiO<sub>2</sub>.

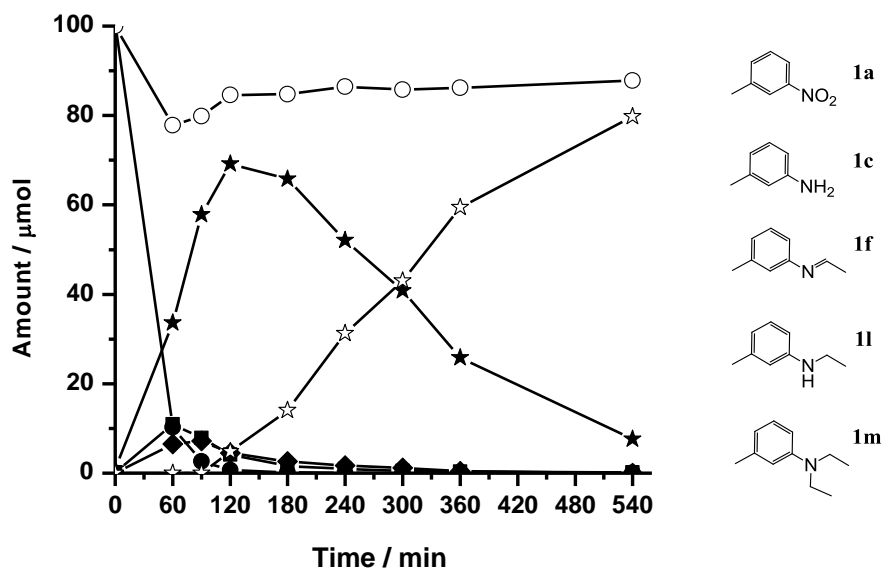


**Figure 3.13:** Time-dependent change in the amounts of substrate and products during the photoirradiation of (**1a**) in EtOH: (**1a**) (●), (**1c**) (■), (**1f**) (◆), (**1l**) (★), (**1m**) (☆), and (○) summation (reaction conditions: 100 μmol (**1a**) and 25 mg Pt<sub>0.5</sub>/TiO<sub>2</sub> in 10 ml EtOH, 60 mW UV(A)/cm<sup>2</sup>, 25 °C, under Ar atmosphere).

**Table 3.5** presents the selectivity of the reaction products after 2 and 6 h of illumination of an ethanolic solution of (**1a**) in the presence of TiO<sub>2</sub> modified with different precious metals. A complete conversion of the substrate (**1a**) was achieved in all cases. However, the type of the deposited metal plays an important role for the selectivity of the products especially for the mono *N*-alkylated compound (**1l**). The highest selectivity (69%) of (**1l**) was obtained after 2h of irradiation employing Pt<sub>0.5</sub>/TiO<sub>2</sub> as the photocatalyst.

**Table 3.5:** Photocatalytic conversion of *m*-nitrotoluene with EtOH employing different metal loaded on TiO<sub>2</sub> UV100.

Entry <sup>[a]</sup>	Photocatalyst	t [h]	Conv. <sup>[b]</sup> [%]	Selectivity [%] <sup>[c]</sup>				
				1c	1f	1j	1l	1m
1	TiO <sub>2</sub> UV100	2	> 99	49	44	4	2	<1
2		6		47	34	6	<1	<1
3	Pt <sub>0.5</sub> /TiO <sub>2</sub> UV100	2	> 99	4	14	1	69	5
4		6		<1	2	<1	26	59
5	Pd <sub>0.5</sub> /TiO <sub>2</sub> UV100	2	> 99	<1	0	9	43	25
6		6		<1	0	8	6	58
7	Ag <sub>0.5</sub> /TiO <sub>2</sub> UV100	2	> 99	31	23	3	21	<1
8		6		29	15	3	28	<1
9	Au <sub>0.5</sub> /TiO <sub>2</sub> UV100	2	> 99	<1	0	10	54	2
10		6		<1	0	9	45	18

[a] Reaction conditions: catalyst (25 mg), *m*-nitrotoluene (**1a**) (100 μmol), EtOH (10 mL), *I*>320 nm, 25 °C, under Ar atmosphere.

[b] Conversions were determined by GC on the basis of (**1a**) consumption.

[c] Determined by GC.

As Pt/TiO<sub>2</sub> has shown the highest selectivity towards the mono-*N*-alkylated product, further investigations concerning the mechanism of the enhancement of the reaction yield and of the selectivity by optimizing the type of TiO<sub>2</sub> that supports Pt particles, the Pt/TiO<sub>2</sub> preparation method, the amount of platinum loaded on the TiO<sub>2</sub> surface, and the light intensity, respectively, have been carried out.

### 3.3.2.2 Effect of the type of TiO<sub>2</sub> supporting the Pt particles

The selectivity of the products obtained after the photocatalytic conversion of (**1a**) using different types of TiO<sub>2</sub> modified with Pt is shown in **Table 3.6**. The results obtained using Pt<sub>0.5</sub>/TiO<sub>2</sub> UV100 prepared by the solids mixture method are also included in **Table 3.6**:

**Table 3.6:** Photocatalytic conversion of *m*-nitrotoluene with EtOH employing different Pt loaded TiO<sub>2</sub>.

Entry <sup>[a]</sup>	Photocatalyst	t [h]	Conv. <sup>[c]</sup> [%]	Selectivity [%] <sup>[d]</sup>				
				1c	1f	1j	1l	1m
1	Pt <sub>0.5</sub> /TiO <sub>2</sub> UV100	2	100	4	4	1	69	5
2		6	100	<1	1	<1	26	59
3	Pt <sub>0.5</sub> /TiO <sub>2</sub> rutile	2	100	13	8	7	50	7
4		6	100	3	1	4	36	43
5	Pt <sub>0.5</sub> /TiO <sub>2</sub> P25	2	100	10	1	2	68	4
6		6	100	0	0	<1	43	57
7	Pt <sub>0.5</sub> /TiO <sub>2</sub> meso.	2	100	22	14	5	41	3
8		6	100	3	2	1	53	36
9	mix Pt <sub>0.5</sub> /TiO <sub>2</sub> UV100	2	100	68	0	7	9	<1
10		6	100	48	0	12	22	<1
11 <sup>[b]</sup>	Pt <sub>0.5</sub> /TiO <sub>2</sub> UV100	2	100	21	14	6	26	2
12		6	100	7	3	3	51	28

[a] Reaction conditions: catalyst (25 mg), *m*-nitrotoluene (**1a**) (100 μmol), EtOH (10 mL), *I*>320 nm, 25 °C, under Ar atmosphere.

[b] Ar was purged during the irradiation.

[c] Conversions were determined by GC on the basis of (**1a**) consumption.

[d] Determined by GC.

As can be seen from **Table 3.6** a complete conversion of (**1a**) was achieved in all cases. However, the type of TiO<sub>2</sub> plays an important role for the selectivity of the products especially for the mono *N*-alkylated one (**1l**). Both Pt<sub>0.5</sub>/TiO<sub>2</sub> UV100 and Pt<sub>0.5</sub>/TiO<sub>2</sub> P25 exhibit a higher selectivity towards (**1l**) after 2h of illumination (*cf.* entries 1 and 5 in **Table 3.6**) than all other employed photocatalysts. The selectivity of the reaction was also affected



by the preparation method of the catalyst. As can be seen from the data presented in **Table 3.6** (entries 9 and 10), colloidal Pt loaded onto Hombikat UV-100 by physical mixing is not as selective towards the *N*-alkylation reaction as that prepared by the photodeposition method. Although a complete conversion of (**1a**) occurred within 120 min in both cases, less than 10% selectivity for (**1l**) was obtained employing the catalysts prepared by the mixed solid method. Obviously, the type of interaction between Pt and TiO<sub>2</sub> also plays an important role for the activity of the catalyst towards the mono *N*-alkylation reaction.

### 3.3.2.3 Effect of the loaded amount of Pt

The data obtained after UV(A) illumination of an ethanolic solution of (**1a**) in the presence of Sachtleben Hombikat UV100 loaded with 0.3, 0.5, and 1.0 wt% Pt, respectively, are illustrated in **Figure 3.14**. It is obvious from this bar graph that the amount of platinum plays an important role for the selectivity of the products especially for the mono *N*-alkylated compound.

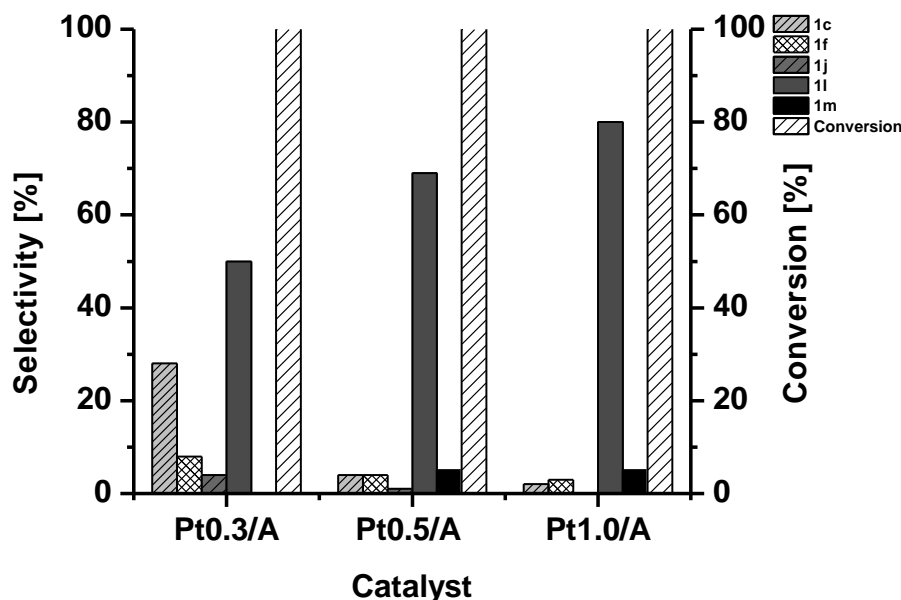


**Figure 3.14:** Selectivity of the reaction products obtained upon illumination of the ethanolic solutions of *m*-nitrotoluene (**1a**) in the presence of Sachtleben Hombikat UV100 loaded with different amounts of Pt.

The selectivity toward the formation of (**II**) after 2 hours of illumination increases from 50% to 80% when the Pt loading increases from 0.3% to 1.0%. The Pt sites significantly influence the condensation reaction of the aminoaromatic compound (**1c**) with the photocatalytically generated acetaldehyde as is reflected in the decrease of the selectivity for the formation of the aminoaromatic compound (**1c**) by increasing the loaded amount of Pt.

In order to investigate the influence of the particle size of the platinum particles loaded on the surface of TiO<sub>2</sub> on the selectivity of the catalysts towards the mono *N*-alkylation reaction transmission electron microscopy (TEM) images of the TiO<sub>2</sub> powders loaded with different amounts of Pt were recorded. Dark-field TEM images of Pt<sub>0.5</sub>/TiO<sub>2</sub> UV100 (**Figure 3.15**) clearly show that the Pt nanoparticles are well dispersed exhibiting particle diameters between 3 and 10nm. However, no clear change in the particle size can be observed upon changing the loaded amount of platinum. This is consistent with a previous report by Ohtani and co-workers who demonstrated that increasing the loaded amount of Pt on the surface of TiO<sub>2</sub> only results in an increase of the number of the Pt islands but not in their size[119].

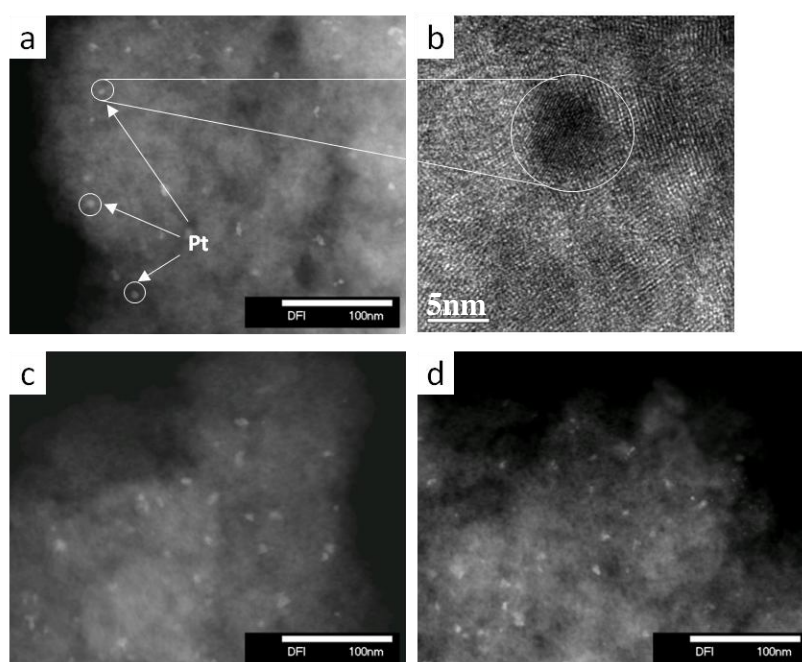


**Figure 3.15:** TEM images of Hombikat UV100 samples containing different amounts of Pt: (a) Pt<sub>0.3</sub>/TiO<sub>2</sub> (c) Pt<sub>0.5</sub>/TiO<sub>2</sub>, and (d) Pt<sub>1.0</sub>/TiO<sub>2</sub>. (b) HRTEM image of Pt<sub>0.3</sub>/TiO<sub>2</sub>.

### 3.3.2.4 Influence of the light intensity

**Figure 3.16** demonstrates the changes in the concentrations of the substrate (**1a**) and the product (**1l**) as a function of the employed light intensity.

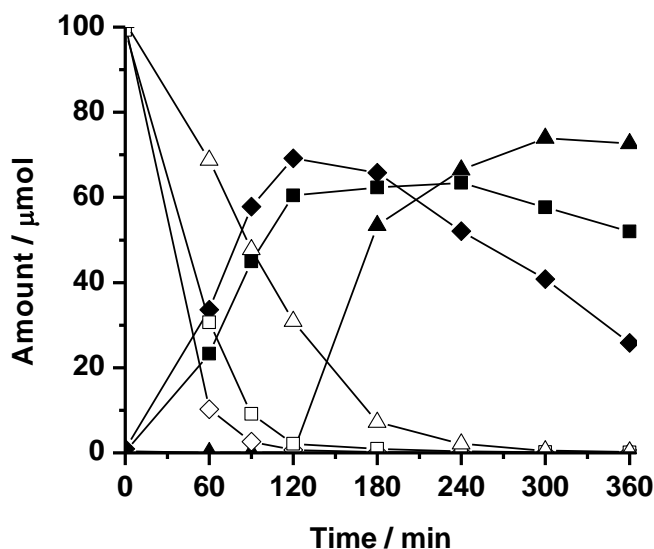


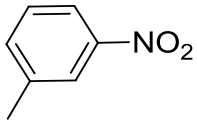
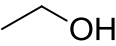
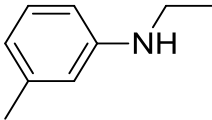
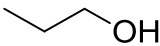
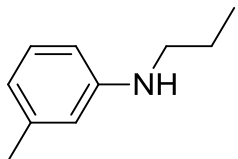
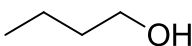
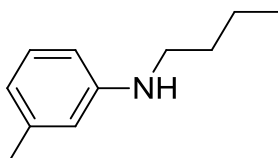
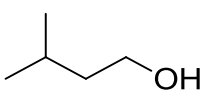
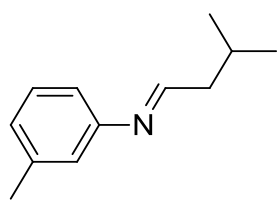
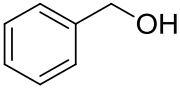
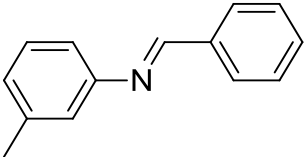
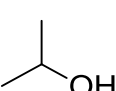
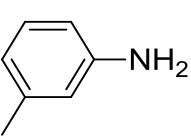
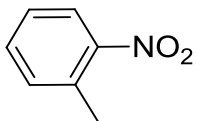
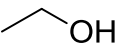
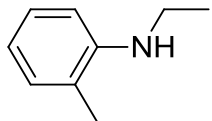
**Figure 3.16:** Time-dependent change in the concentrations of **1a** (empty symbols) and **1l** (filled symbols) in the presence of  $Pt_{0.5}/TiO_2$  UV100 at different light intensities:  $60\text{ mW/cm}^2$  ( $\blacklozenge$ ),  $30\text{ mW/cm}^2$  ( $\blacksquare$ ), and  $15\text{ mW/cm}^2$  ( $\blacktriangle$ ). (reaction conditions:  $100\ \mu\text{mol}$  (**1a**) and  $25\text{ mg}$   $Pt_{0.5}/TiO_2$  UV100 in  $10\text{ ml EtOH}$ ,  $25\text{ }^\circ\text{C}$ , under Ar atmosphere).

It can be seen from **Figure 3.16** that the photocatalytic conversion of *m*-nitrotoluene (**1a**), using  $Pt_{0.5}/TiO_2$ UV100, is still highly selective towards the formation of the mono *N*-alkylated amine even when lower light intensities are used. It is obvious from the data shown in **Figure 3.16** that decreasing the light intensity leads to a reduced reduction rate of the nitro compound. However, the maximum yield of the mono *N*-alkylated product (**1l**) is not significantly affected by the employed light intensity. On the other hand, at lower light intensities the further conversion of (**1l**) to (**1m**) is also slowed down as can be seen from the slope of the amount of (**1l**) =  $f(t)$  after reaching its maximum (**Figure 3.16**). Hence, it seems to be possible to control the conversion towards the mono *N*-alkylated product by suppressing its further *N*-alkylation by employing “milder” reaction conditions, i.e., by working at lower illumination intensities.

### 3.3.2.5 *N*-alkylation reactions of nitroaromatic compounds in different alcohols

In order to evaluate the general applicability of this newly developed photocatalytic *N*-alkylation method, various types of nitroaromatic compounds as well as different alcohols have been studied. The respective results are summarized in **Table 3.7**:

**Table 3.7:** Photocatalytic *N*-alkylation of different nitroaromatic compounds in different alcohols employing 1%Pt/TiO<sub>2</sub>UV100.

Entry <sup>[a]</sup>	Nitroaromatic compound	Alcohol	Product	t (min) <sup>[b]</sup>	Yield [%] <sup>[c]</sup>	
					GC	is
1				150	90	85
2				180	100	91
3				240	83	80
4				360	91	[e]
5 <sup>[d]</sup>				480	94	92
6				180	99	[e]
7				150	93	84

8				120	90	75
9				120	83	80
10				300	72	53
11				150	79	54

[a] Reaction conditions: 0.4 mmol nitroaromatic compound, 40 ml alcohol, 0.1 g 1%Pt/TiO<sub>2</sub>, 25 °C, under Ar. [b] Illumination time needed to achieve 100 % conversion of the nitroaromatic compound. [c] Yields are based on 100% nitroaromatic compound consumption. [d] 4 mmol of benzyl alcohol was dissolved in 40 ml MeCN. [e] Not isolated.

As can be seen from **Table 3.7**, the photocatalytic *N*-alkylation has been successfully achieved in most cases with a moderate to very good yield. However, the time required to achieve the complete conversion of *m*-nitrotoluene (**1a**) increases by increasing the length of the aliphatic chain of the alcohol.

It is interesting to note that only trace amounts of the mono *N*-alkylated products are produced when branched or aromatic alcohols are used, whereas the main products in these cases are the imines in the case of 3-methyl-butanol or benzyl alcohol or even the anilines in case of iso-propanol (entries 4-6 in **Table 3.7**). Obviously, the structure of the employed alcohol plays an important role in the photocatalytic *N*-alkylation reaction. On the other hand, it can be seen from **Table 3.7** that the position as well as the number of the methyl group in the nitroaromatic compound does not affect the reaction sequence and, in all cases, the mono *N*-alkylated products are obtained in very good yields (entries 7-10 in **Table 3.7**). Interestingly, *N*-ethyl-*m*-ethyl-benzene is obtained when *m*-nitrostyrene is used as the substrate (entry 10), thus, Pt/TiO<sub>2</sub>UV100 is also able to photocatalytically hydrogenate the C=C double bond. The GC-MS analyses of the reaction mixture at different reaction times indicate that a competitive photocatalytic reduction between the nitro group and the styrene C=C double bond takes place.

### 3.3.2.6 Modification of the surface of TiO<sub>2</sub> with bimetallic platinum-silver nanoparticles

In order to enhance the selectivity of the photocatalytic conversion reaction of the nitroaromatic compounds towards mono *N*-alkylated products, bimetallic (Pt-Ag) deposits on TiO<sub>2</sub> (Sachtleben Hombikat UV100) were prepared and tested. Silver was chosen due to its relatively low price, thus, it should be particularly suitable for industrial applications. For this purpose, two series of catalysts were prepared: In the first one, various amounts of Ag (0.1, 0.3, 0.5 and 1.0 wt.%) were photocatalytically deposited on pre-prepared (0.5 wt.%)Pt/TiO<sub>2</sub>. In the second one, (0.5 wt.%) Ag was first deposited photocatalytically on the surface of TiO<sub>2</sub> followed by the photodeposition of different amounts of Pt (0.1, 0.3, and 0.5 wt.%). The activities of the obtained photocatalysts were tested using the same model reaction, i.e., the photocatalytic conversion of (**1a**) in O<sub>2</sub>-free ethanolic solutions.

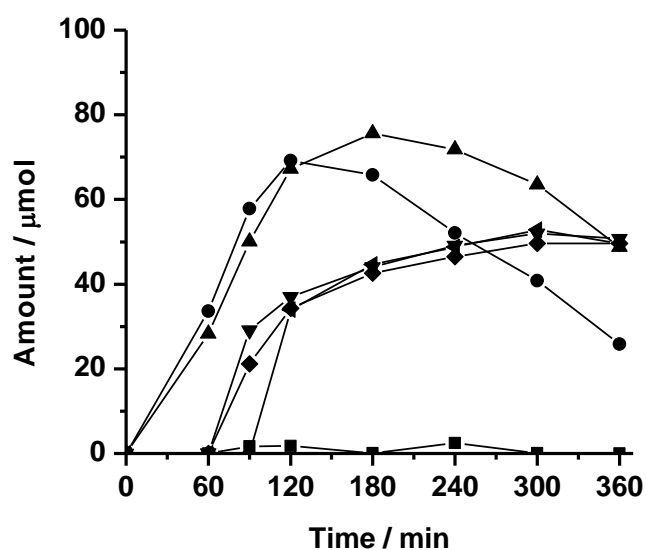


**Figure 3.17:** Time-dependent change in the amount of *N*-ethyl-*m*-toluidine (**II**) during the photoirradiation of (**1a**) in EtOH in the presence of Ag<sub>*n*</sub>/Pt<sub>*m*</sub>/TiO<sub>2</sub>: bare TiO<sub>2</sub> (■), Pt<sub>0.5</sub>/TiO<sub>2</sub> (●), Ag<sub>0.1</sub>/Pt<sub>0.5</sub>/TiO<sub>2</sub> (▲), Ag<sub>0.3</sub>/Pt<sub>0.5</sub>/TiO<sub>2</sub> (▼), Ag<sub>0.5</sub>/Pt<sub>0.5</sub>/TiO<sub>2</sub> (◆), Ag<sub>1.0</sub>/Pt<sub>0.5</sub>/TiO<sub>2</sub> (◄), (reaction conditions: 100 μmol (**1a**) and 25 mg Ag<sub>*n*</sub>/Pt<sub>*m*</sub>/TiO<sub>2</sub> in 10 ml EtOH, 60 mW UV(A)/cm<sup>2</sup>, 25 °C, under Ar atmosphere).

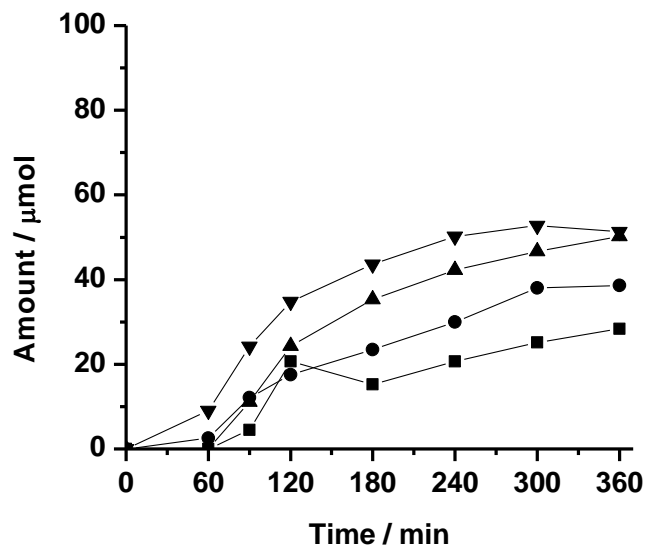


**Figure 3.18:** Time-dependent change in the amount of the *N*-ethyl-*m*-toluidine (**II**) during the photoirradiation of (**1a**) in EtOH in the presence of Pt<sub>*m*</sub>/Ag<sub>*n*</sub>/TiO<sub>2</sub>: Ag<sub>0.5</sub>/TiO<sub>2</sub> (■), Pt<sub>0.1</sub>/Ag<sub>0.5</sub>/TiO<sub>2</sub> (●), Pt<sub>0.3</sub>/Ag<sub>0.5</sub>/TiO<sub>2</sub> (▲), Pt<sub>0.5</sub>/Ag<sub>0.5</sub>/TiO<sub>2</sub> (▼), (reaction conditions: 100 μmol (**1a**) and 25 mg Pt<sub>*m*</sub>/Ag<sub>*n*</sub>/TiO<sub>2</sub> in 10 ml EtOH, 60 mW UV(A)/cm<sup>2</sup>, 25 °C, under Ar atmosphere).

The produced amounts of the mono *N*-alkylated product (**II**) in the (Pt-Ag)/TiO<sub>2</sub> photocatalyzed system upon different illumination times are shown in **Figure 3.17** and **Figure 3.18**. Whatever the employed catalyst was, 100% conversion of the nitroaromatic compound (**1a**) in the (Pt-Ag)/TiO<sub>2</sub> photocatalyzed reaction was achieved after 2h of illumination. However, the selectivity for the formation of the mono *N*-alkylated product differs considerably upon variation of the ratio of the metals as can be seen from **Figure 3.17** and **Figure 3.18**. Loading of (0.1 wt.%) Ag over (0.5 wt.%) Pt/TiO<sub>2</sub> increases the selectivity of (**II**) from 66% to 76% after 3h photoirradiation (*cf.* **Figure 3.17**), while the selectivity of (**II**) decreases by increasing the loaded amount of Ag above (0.1 wt.%). Moreover, only 37% yield of *N,N*-diethyl-*m*-toluidine was produced after 6h of illumination of the reaction mixture in the presence of Ag<sub>0.1</sub>/Pt<sub>0.5</sub>/TiO<sub>2</sub> while 59% yield of the same product was recorded employing Pt<sub>0.5</sub>/TiO<sub>2</sub> as the photocatalyst instead.

On the other hand, the data illustrated in **Figure 3.18** show that modification of Ag<sub>0.5</sub>/TiO<sub>2</sub> with increasing amounts of Pt increases the selectivity towards the mono *N*-alkylated product.

However, Pt<sub>0.5</sub>/Ag<sub>0.5</sub>/TiO<sub>2</sub> was not as selective for this reaction as bare Pt<sub>0.5</sub>/TiO<sub>2</sub>, hence, the pre-existence of Ag particles apparently suppresses the activity of Pt towards the *N*-alkylation reaction of the photocatalytically produced *m*-toluidine (**1c**) into *N*-ethyl-*m*-toluidine (**1l**). Interestingly, both Pt<sub>0.5</sub>/Ag<sub>0.5</sub>/TiO<sub>2</sub> and Ag<sub>0.5</sub>/Pt<sub>0.5</sub>/TiO<sub>2</sub> show the same behavior in this system.

To understand these differences in the selectivity of the employed (Pt-Ag)/TiO<sub>2</sub> photocatalysts, the photocatalytically produced H<sub>2</sub> in the system during the illumination time was measured and the recorded amounts are presented in **Table 3.8**.

**Table 3.8:** Amount of the photocatalytically generated hydrogen during the photocatalytic reduction of *m*-nitrotoluene employing different (Ag<sub>*m*</sub>-Pt<sub>*n*</sub>)/TiO<sub>2</sub> photocatalysts.

Entry <sup>[a]</sup>	Photocatalyst	H <sub>2</sub> / μmol	
		2h	6h
<b>1</b>	Pt <sub>0.5</sub> /TiO <sub>2</sub>	393	739
<b>2</b>	Ag <sub>0.1</sub> /Pt <sub>0.5</sub> /TiO <sub>2</sub>	218	553
<b>3</b>	Ag <sub>0.3</sub> /Pt <sub>0.5</sub> /TiO <sub>2</sub>	190	460
<b>4</b>	Ag <sub>0.5</sub> /Pt <sub>0.5</sub> /TiO <sub>2</sub>	80	291
<b>5</b>	Ag <sub>1</sub> /Pt <sub>0.5</sub> /TiO <sub>2</sub>	52	287
<b>6</b>	Ag <sub>0.5</sub> /TiO <sub>2</sub>	25	115
<b>7</b>	Pt <sub>0.5</sub> /Ag <sub>0.5</sub> /TiO <sub>2</sub>	95	324

[a] Reaction conditions: catalyst (25 mg), *m*-nitrotoluene (**1a**) (100 μmol), EtOH (10 mL), *I*>320 nm, 25 °C, under Ar atmosphere.

As expected, the amount of the photocatalytically generated H<sub>2</sub> increases with increasing illumination time in all cases. However, bare Pt<sub>0.5</sub>/TiO<sub>2</sub> produces the highest amount of H<sub>2</sub>. Modification of this photocatalyst with an increased loading of Ag results in a reduced photocatalytic H<sub>2</sub> formation efficiency (entries 1-5 in **Table 3.8**). On the other hand, Ag<sub>0.5</sub>/TiO<sub>2</sub> exhibits the lowest activity for the photocatalytic production of H<sub>2</sub> (entry 6 in **Table 3.8**). Moreover, Pt<sub>0.5</sub>/Ag<sub>0.5</sub>/TiO<sub>2</sub> exhibits less activity for the formation of H<sub>2</sub> than



Pt<sub>0.5</sub>/TiO<sub>2</sub>, hence, the pre-modification of TiO<sub>2</sub> with Ag particles apparently decreases the efficiency of Pt for the photocatalytic formation of H<sub>2</sub> (entries 1 and 7 in **Table 3.8**).

The optical absorption spectra of Ag<sub>m</sub>/Pt<sub>n</sub>/TiO<sub>2</sub> were recorded in order to investigate the electronic properties of these photocatalysts. The obtained spectra are shown in **Figure 3.19**.

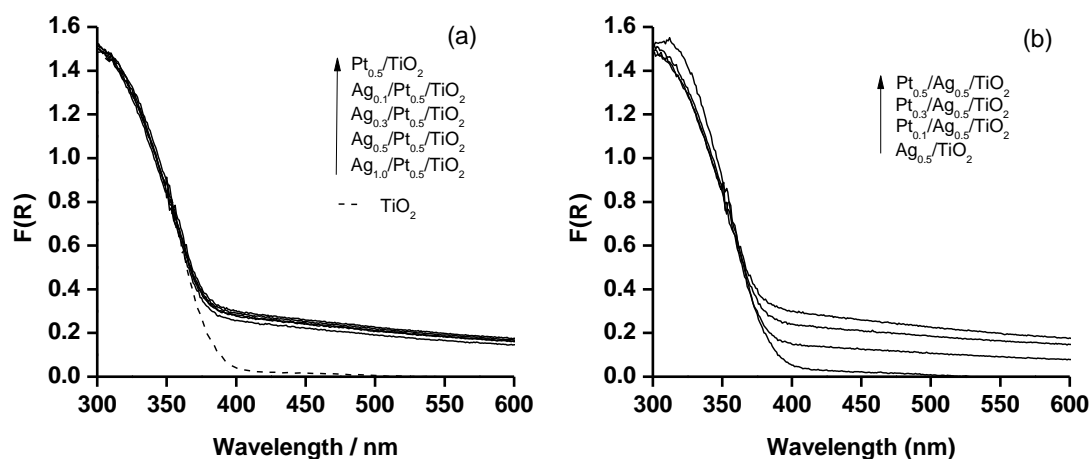


**Figure 3.19:** Diffuse reflectance spectra of bare TiO<sub>2</sub> (Schachtleben Hombikat UV100) and of TiO<sub>2</sub> (Schachtleben Hombikat UV100) photocatalytically modified with bimetallic (Pt-Ag) nanoparticles: (a) Ag<sub>m(m=0-1.0)</sub>/Pt<sub>0.5</sub>/TiO<sub>2</sub> and (b) Pt<sub>n(n=0-0.5)</sub>/Ag<sub>0.5</sub>/TiO<sub>2</sub>.

Although the surface plasmon absorption of Pt nanoparticles is known to have a peak at 215 nm, which is covered by the strong optical absorption of TiO<sub>2</sub> in this region, the materials exhibit increasing absorption in the wavelengths range between 400-600 nm by increasing the loaded Pt amount. However, no significant change in the absorption is observed upon loading of Ag on bare or Pt modified TiO<sub>2</sub> although Ag should exhibit a surface plasmon absorption in the wavelength range between 420-500 nm. This can most likely be explained by the small level of Ag loading. Dark-field TEM images of Ag<sub>0.5</sub>/Pt<sub>0.5</sub>/TiO<sub>2</sub> (**Figure 3.20**) clearly show that the metal nanoparticles are well dispersed exhibiting particle diameters between 5 and 10 nm. However, because of the similarity between the metal particle size and the crystallite size of TiO<sub>2</sub> it was not possible to obtain energy-dispersive X-ray (EDX) data for a single metal nanoparticle in order to confirm its bimetallic structure.

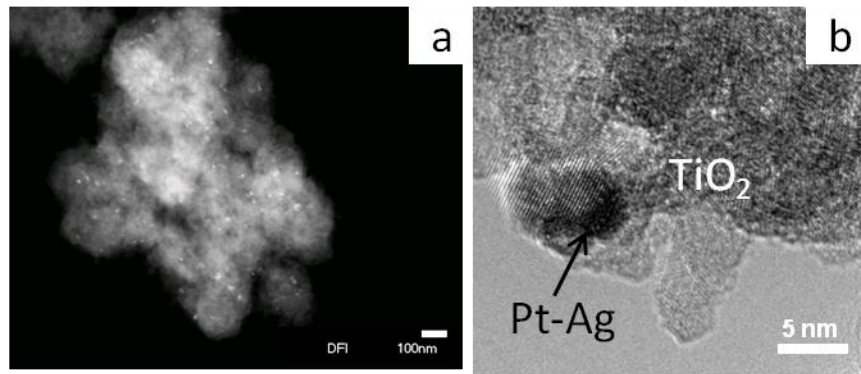


**Figure 3.20:** Dark Field-TEM image of  $Ag_{0.5}/Pt_{0.5}/TiO_2$  sample (a) and HRTEM image of the same sample (b).

## 4 Discussion

### 4.1 Reduction of the nitroaromatic compounds

The chromatograms presented in **Figure 3.2** show that the UV(A) irradiation ( $\lambda > 320$  nm) of TiO<sub>2</sub> particles suspended in an ethanolic solution of *m*-nitrotoluene (**1a**) under Ar atmosphere at 25°C, leads to complete conversion of the nitroaromatic compound to the following reaction products: *m*-toluidine (**1c**), *N*-ethylidene-3-methylaniline (**1f**), and 2,7-dimethylquinoline (**1j**) in addition to a trace of *N*-ethyl-3-methylaniline (**1l**). The time course of the summation of the amounts of the substrate and the products, **Figure 3.3**, indicates that a material balance is almost kept during the reaction and no significant degradation reaction of the nitroaromatic compound or hydrogenation of the aromatic ring seems to occur in the present system. It is suggested that the reaction occurs in the following sequence: i) reduction of the nitroaromatic compound and simultaneous oxidation of the alcohol; ii) imine formation; and, iii) imine cyclization and/or hydrogenation as illustrated in **Figure 4.1**.

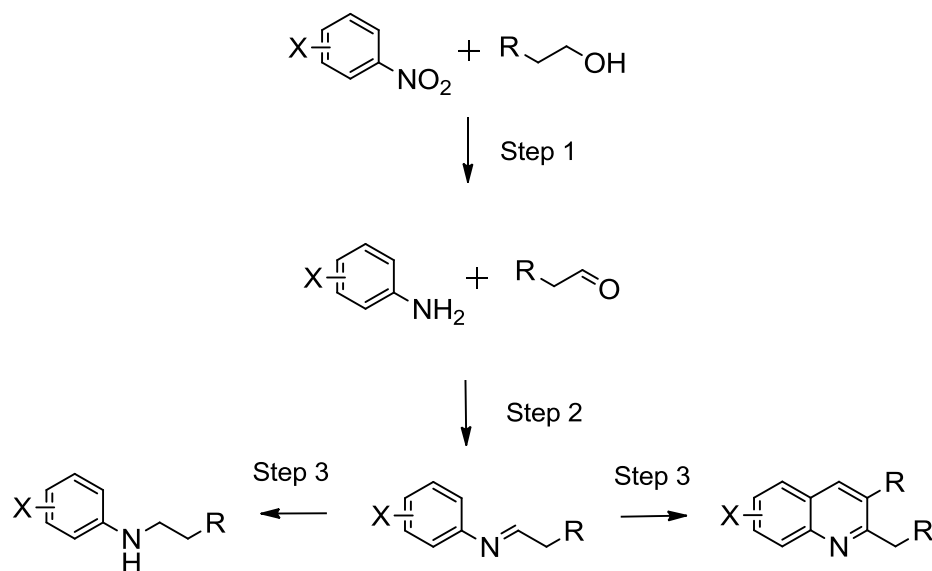


**Figure 4.1:** Suggested overall reaction steps of the photocatalytic conversion of the NACs.

In the following discussion, each step of the reaction will be discussed in detail. The influence of different parameters on these steps will also be discussed and clarified.

**Step 1 (reduction of the NACs and oxidation of the alcohol, i.e., the photocatalytic reactions)**

Under the employed reaction conditions, NACs are reduced to the corresponding aminoaromatic compounds via the reactions that are illustrated in **Figure 4.2**. Upon irradiation of TiO<sub>2</sub> with a photon of equal or higher energy than its band gap, an electron (e<sup>-</sup>)/ hole (h<sup>+</sup>) pair is generated. The formed electrons and holes can either migrate to the TiO<sub>2</sub> surface on which they will react with the adsorbed reactants, i.e., the nitroaromatic compound and the alcohol, respectively, or they can undergo an undesired recombination reaction.

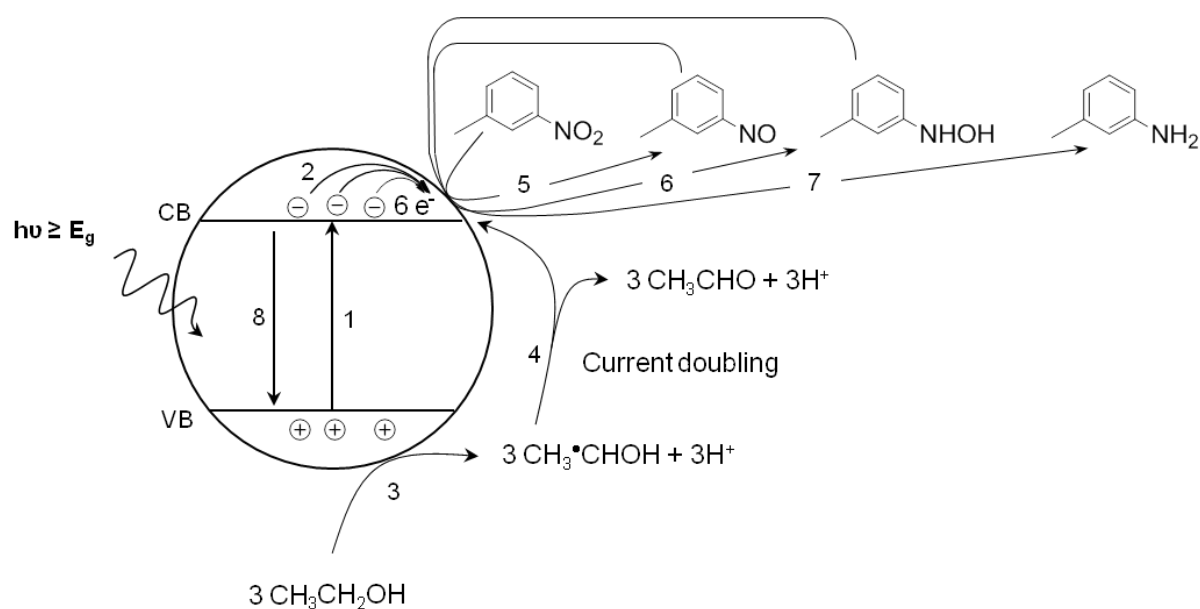


**Figure 4.2:** Schematic representation of the proposed steps for the photocatalytic reduction of *m*-nitrotoluene dissolved in ethanol at an irradiated TiO<sub>2</sub> particle, (1) photogeneration of charge carriers, e<sup>-</sup> and h<sup>+</sup>; (2) trapping of e<sup>-</sup>; (3) first oxidation step of EtOH by trapped hole; (4) formation of acetaldehyde through electron injection into the conduction band of TiO<sub>2</sub> (current-doubling); (5) reduction of *m*-nitrotoluene to *m*-nitrosotoluene by two of the CB electrons; (6) reduction of *m*-nitrosotoluene to *m*-(hydroxyamino)toluene by two of the CB electrons; (7) reduction of *m*-(hydroxyamino)toluene to *m*-toluidine by two of the CB electrons; (8) recombination channel. Note: For simplicity, the electrons (trapped and injected) required for total reduction of the nitro group to the amino group is presented as 6e<sup>-</sup> in the CB.

According to the literature[65, 120, 122], the aforementioned process consists of a series of two-electron additions, proceeding through nitroso and hydroxylamino intermediates (*c.f.* processes 5-7 in **Figure 4.5**). For example, Mahdavi and co-workers have detected hydroxylamine formation during the photocatalytic reduction of *p*-nitroacetophenone in neat 2-propanolic suspensions of TiO<sub>2</sub> (using HPLC techniques)[120]. On the other hand, an accumulation of the nitroso compound is rarely found in practice, and special techniques are necessary to obtain direct evidence for its formation[164]. However, the nitroso- and the hydroxylamine intermediates were not detected by our analytical techniques (GCs) with the employed experimental conditions.

The total reduction of one nitro group in the nitroaromatic compound to one amino group requires six electrons as well as the same number of protons. These electrons and protons are supplied by the simultaneous oxidation of the alcohol, *i.e.*, the solvent, which is induced by the photogenerated valence band holes of the TiO<sub>2</sub>. Prolonged illumination time, beyond that, which is necessary for the complete consumption of the nitroaromatic compound, results in colour change of the TiO<sub>2</sub> suspension from white to blue. This phenomenon is due to the trapping of the photogenerated electrons near the surface by Ti(IV) forming tri-valent titanium Ti(III)[106], indicating that no other electron acceptor which could trap these photogenerated electrons is present in the reaction mixture. The formation of the tri-valent titanium Ti(III), which occurs only upon the total reduction of the nitroaromatic compound, confirms the hypothesis that the conduction band electrons are directly involved in the reduction of NACs.

However, under the employed reaction conditions the photogenerated conduction band electrons are not the only reducing agents present in the reaction media. In an irradiated deaerated TiO<sub>2</sub> slurry containing an alcohol and a nitroaromatic compound,  $\alpha$ -hydroxyalkyl radicals are produced (*cf.* Eq. 4.2). These radicals are formed by hydrogen abstraction from the  $\alpha$ -carbon atom of the alcohol as expressed in equation eq. 4.2. These radicals are known to

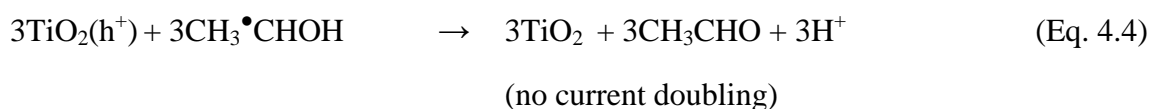
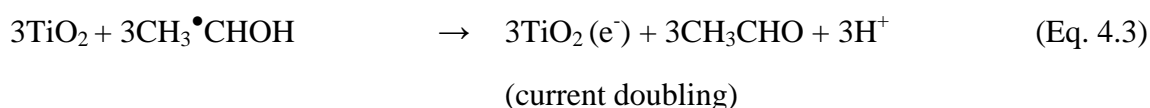
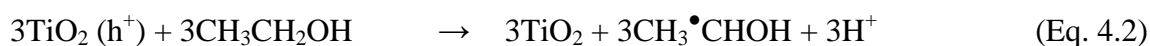
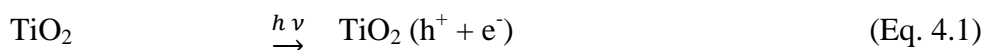
be powerful reducing agents with reduction potentials lower than  $-1.25$  V vs. the NHE [165]. Thus, in the absence of  $O_2$  and the presence of the nitroaromatic compound,  $CH_3^{\bullet}CHOH$  may undergo one of the following reactions: (i) It may inject an electron into the conduction band of  $TiO_2$  forming acetaldehyde and proton (see Eq. 4.3). This process is referred to as “current-doubling” in photoelectrochemistry and has been observed in many related systems including the photoanodic oxidation of alcohols on  $TiO_2$  [105], (ii) it may be reoxidized by the trapped photogenerated holes forming, again, acetaldehyde and a proton (see Eq. 4.4), or (iii) they may directly react with the nitro group to form acetaldehyde, a proton, and a nitroaromatic radical anion [166] (see Eq. 4.8); the latter may trap an electron from the conduction band forming the corresponding nitroso compound (see Eq. 4.9). However, Ferry and Glaze[122] assumed that the conduction band electrons are the principal species driving the photocatalytic reduction of nitroaromatic compounds to aminoaromatic compounds. They have shown that the reduction rates of the nitroaromatic compounds in illuminated  $TiO_2$  slurries containing MeOH or *i*-PrOH are almost unchanged while these reduction rates measured using pulse radiolysis techniques employing isopropoxyl radicals were more than 16 times higher than that obtained for methoxyl radicals in absence of  $TiO_2$ . Nevertheless, the possibility remains that the reduction process involves a combination of agents, *i.e.*, the photocatalyst surface and reducing radicals derived from the primary or secondary alcohols as electron donors. It is worth mentioning that the irradiation of *m*-aminotoluene, instead of *m*-nitrotoluene, dissolved in ethanol in the presence of  $TiO_2$  (Schactleben Hombikat UV100) for 2 hours does not result in any significant change in its amount, and no acetaldehyde was detected. This indicates that the oxidation of ethanol to acetaldehyde is stopped after the complete reduction of the nitroaromatic compound.

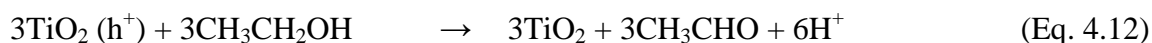
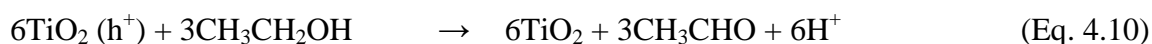
Regardless of which reduction pathway is more likely, the reduction of one molecule of nitroaromatic compound to the corresponding aminoaromatic compound is accompanied with the simultaneous formation of three acetaldehyde molecules that are produced by the

oxidation of three alcohol molecules by the photogenerated holes. However, the number of required photons is different according to the reduction pathway.

If the nitroaromatic compound is reduced only by the photogenerated conduction band electrons (no current doubling and no direct reduction with the  $\alpha$ -hydroxyalkyl radicals, see Eqs. 4.5-4.7), six photons are required to photogenerate these six electrons (see Eqs. 4.10 and 4.11). On the other hand, only three photons are required in case of the contribution of the  $\alpha$ -hydroxyalkyl radicals via either direct reduction of the nitroaromatic compound or injection of the electron in the conduction band of  $\text{TiO}_2$  (current doubling) (see Eqs. 4.12 and 4.13; in Eq. 4.13,  $(3e^-)$  refers to the electrons coming from  $\text{CH}_3^\bullet\text{CHOH}$  either via direct reaction with the nitroaromatic compound or via injection of its electron into the conduction band, *i.e.*, the current doubling).

The individual photocatalytic reaction steps as well as the overall photocatalytic reactions are summarized in the following equations:





According to the concluded overall photocatalytic reactions, the molar ratio between the photocatalytically generated acetaldehyde and the photocatalytically reduced nitroaromatic compound would be expected to be 3. However, no acetaldehyde has been detected after the total consumption of the nitroaromatic compound, *i.e.*, 2 hours of irradiation. In further reactions, the photocatalytically generated acetaldehyde may be consumed, partially or totally, so that any remaining acetaldehyde is present, in quantities less than the detection limit of the analytical method (GC) employed in this work. The fate of the photocatalytically produced acetaldehyde and aminoaromatic compound is discussed in steps 2 and 3.

The photonic efficiencies of the photocatalytic reduction of *m*-nitrotoluene (**1a**) in the presence of ethanol employing different types of TiO<sub>2</sub> (anatase, rutile, and anatase-rutile mixture) photocatalysts have been calculated and summarized in **Table 4.1**.

**Table 4.1:** Photonic efficiencies  $\xi$  (%) of the photocatalytic reduction of *m*-nitrotoluene in ethanol over different type of TiO<sub>2</sub> powders with their respective BET surface area .

Entry <sup>[a]</sup>	Photocatalyst <sup>[b]</sup>	S <sub>BET</sub> / (m <sup>2</sup> g <sup>-1</sup> )	$\xi$ / %
1	rutile (R)	58	5.8
2	anatase (A)	265	6.8
3	antase-rutile (P25)	77	7.0
4	anatase (MA)	174	4.7

[a] Reaction conditions: photocatalyst (25 mg), (**1a**) (100  $\mu$ mol), EtOH (10 mL),  $I > 320$  nm, 2h, 25 °C, under Ar atmosphere.

[b] For notation see Table 3.1.



From the photonic efficiency values of the photocatalytic reduction of (**1a**) which are summarized in **Table 4.1**, it can be seen that both TiO<sub>2</sub> UV100 and TiO<sub>2</sub> P25 exhibit the highest photocatalytic activities. The photocatalytic activity of rutile is less than that of UV100 or TiO<sub>2</sub> P25 but it is still higher than that of anatase (MA). Although rutile has been typically considered less active than anatase or anatase-rutile mixtures for the photocatalytic degradation of organic molecules, several reports have shown a good activity of this TiO<sub>2</sub> phase for the oxidation of alcohols to the corresponding carbonyl compounds[45, 98, 167].

The photocatalytic activities of TiO<sub>2</sub> UV100 and TiO<sub>2</sub> P25 photocatalysts are almost similar even though the BET surface area of TiO<sub>2</sub> UV100 is ca. 3.5 times higher than that of TiO<sub>2</sub> P25. In contrast, anatase (MA) shows the lowest photocatalytic activity although it has a relatively high BET surface area. Thus, the differences in the photocatalytic activity of the different types of TiO<sub>2</sub> for the reduction of the nitroaromatic compounds cannot be explained by the differences in the BET surface area of these photocatalysts. On the other hand, it has been reported that the potential of the conduction band edge of TiO<sub>2</sub>, dependent on the crystalline forms, is positioned at -0.16 and 0.04 V vs. NHE at pH=0 for anatase and rutile, respectively[168]. Thus the difference in  $E_{CB}$  of 0.2 V between these two phases might account for the higher photocatalytic activity of the anatase containing photocatalysts, *i.e.* TiO<sub>2</sub> UV100 and TiO<sub>2</sub> P25, than that of rutile. In the latter case, the driving force for the nitroaromatic compound reduction will be smaller than in the former. The relatively low photocatalytic activity of anatase (MA) may also be attributed to the low crystallinity of this material which is calcined at only 450 °C for 4h. The dependence of the photocatalytic activity for the photocatalytic oxidation of alcohols on the crystallinity of the photocatalyst has been reported [136].

### ***Step 2 (the condensation reaction)***

As can be seen from **Figures 3.1** and **3.2**, imines are also produced under the reaction conditions employed here. The reaction of aldehydes (or ketones) with amines is perhaps the

most common method for the preparation of imines as was first discovered by Schiff[169]. This reaction is generally carried out by refluxing the carbonyl compound and amine in the presence of Lewis acid as the catalyst[170]. The success of this transformation under the reaction conditions employed here may be attributed to the action of Lewis acid sites present on the surface of the employed  $\text{TiO}_2$ . The presence of these Lewis acid sites on the surface of  $\text{TiO}_2$  (Schactleben Hombikat UV100, Evonik P25, and mesoporous anatase powdes) is confirmed by the FTIR investigations of the adsorption of pyridine on the surface of these  $\text{TiO}_2$  powders, being one of the most selective reagents for studying the acidic sites of the solid acids[138-141] (see **Figure 3.5** and **Figure 3.6**). The appearance of new peaks at 1445, 1489, and 1639  $\text{cm}^{-1}$  upon the adsorption of pyridine at the surface of these  $\text{TiO}_2$  powders is due to the interaction between pyridine molecules and Lewis acid sites, *i.e.*, the electrophilic  $\text{Ti}_{5c}$  cations, present at the surface of anatase containing  $\text{TiO}_2$  powders.

The coordination of the  $\text{Ti}_{5c}$  cation, *i.e.*, the Lewis acid site, with the O-atom of the carbonyl group (see **Figure 4.3**) will activate the carbonyl group for the attack by the photocatalytically generated amioaromatic compound.

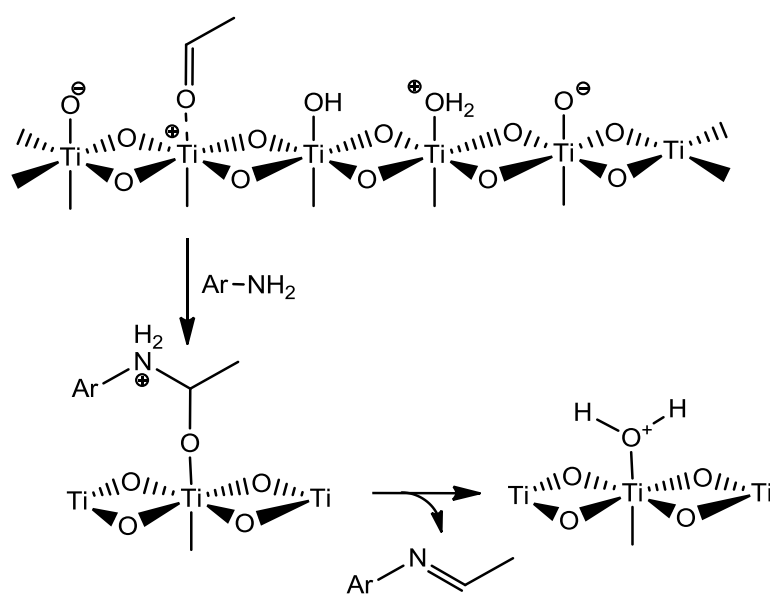


**Figure 4.3:** Proposed reaction mechanism for the Lewis acid-catalyzed formation of the imine on the surface of  $\text{TiO}_2$ .

### Step 3 (the cyclization reaction)

Besides the formation of the aminoaromatic compound and its imine, a small amount of the cyclization product (**1j**) is also produced upon illumination of the reaction mixture as can be seen from **Figure 3.2**. The formation of the cyclization product may involve the condensation of the enamine of the produced imine with the imine itself (*cf.* **Figure 4.9**), according to the interpretation reported by Forrest et al.[171] concerning the mechanism of the Doebner-Miller reaction. The mechanism of this cyclization reaction and the effect of different reaction conditions on it will be discussed in more detail in the following sections.

## 4.2 Effect of TiO<sub>2</sub> type on the photocatalytic conversion of the nitroaromatic compounds

The results illustrated in **Figure 3.4** show that almost complete conversion of the substrate (**1a**) was achieved after 2h of illumination employing any of the studied TiO<sub>2</sub> types (anatase, rutile, anatase-rutile mixture, and mesoporous anatase). However, the distribution of the reaction products differs depending on the employed TiO<sub>2</sub> type. **Table 4.2** summarizes the selectivity for the formation of the products obtained after 2 hours of UV(A) irradiation of *m*-nitrotoluene (**1a**) dissolved in ethanol in the presence of different types of TiO<sub>2</sub>.

**Table 4.2:** Selectivity of the photocatalytic conversion of *m*-nitrotoluene employing different TiO<sub>2</sub> photocatalysts under UV(A) irradiation.

Entry <sup>[a]</sup>	Photocatalyst <sup>[b]</sup>	S <sub>BET</sub> / (m <sup>2</sup> g <sup>-1</sup> )	Selectivity / [%] <sup>[c]</sup>		
			<b>1c</b>	<b>1f</b>	<b>1j</b>
1	R	58	72	2	7
2	A	265	49	44	4
3	P25	77	21	13	31
4	MA	174	32	44	3
5	A+R	nc.	48	47	5

[a] Reaction conditions: photocatalyst (25 mg), (**1a**) (100 μmol), EtOH (10 mL), *I*>320 nm, 2h, 25 °C, under Ar atmosphere.

[b] For notation see Table 3.1.

[c] Determined by GC according to calibration curves using corresponding authentic compounds.

nc.: Not calculated.

In the case of pure rutile the main product is the corresponding aminoaromatic compound (**1c**) with a selectivity of 72% (*cf.* entry 1 in **Table 4.2**). On the other hand, pure anatase promotes the condensation of the aminoaromatic compound (**1c**) with the photocatalytically generated acetaldehyde to produce the imine (**1f**) with a selectivity of (44%) (*cf.* entries 2 and 4 in **Table 4.2**). TiO<sub>2</sub> P25 which is a mixture of anatase (80%) and rutile (20%), exhibits a moderate selectivity (31%) for the formation of the quinoline (**1j**) (*cf.* entry 3 in **Table 4.2**). Physical mixing of anatase (A) and rutile (R) in the same ratio of that of P25 (*cf.* entry 5 in **Table 4.2**) showed a similar distribution of that of pure anatase indicating that the effect of P25 is not due to a simple rutile-anatase mixture property.

In an attempt to understand these differences between the employed TiO<sub>2</sub> photocatalysts the BET surface areas of the different TiO<sub>2</sub> samples were measured and are also included in **Table 4.2**. It can be seen from the data summarized in **Table 4.2** that the highest selectivity for the formation of the imine (**1f**) is obtained employing anatase (UV100 and MA) powders which exhibit BET surface area higher than that of rutile or P25 powders, while the latter powders show poor selectivity for the formation of this imine.

Another factor which may play a role for the selectivity of a photocatalytic reaction is the acidic properties of the applied photocatalysts. As discussed above, the FTIR investigations of the adsorption of pyridine on the surface of the studied TiO<sub>2</sub> powders can be used to evaluate the nature of the acidic sites at the surfaces of the employed photocatalysts. No clear new peaks appeared when the rutile sample was treated with pyridine vapor. However, new peaks appeared at 1445 and 1607 cm<sup>-1</sup> in case of the anatase containing samples (A, P25, and MA) indicating that pyridine is adsorbed at the TiO<sub>2</sub> surface most likely by the interaction between its nitrogen lone-pair and the TiO<sub>2</sub> Lewis acid sites. Thus, negligible amounts of Lewis acid sites present on the surface of the rutile photocatalyst employed here whereas anatase containing samples do exhibit these acidic sites. As mentioned previously, Lewis acid sites (Ti<sub>5c</sub>) are suggested to be the catalyst of the condensation reaction between the

photocatalytically produced aldehydes and amines to produce the corresponding imines. The poorness of rutile sample with Lewis acid sites might thus explain the high selectivity of this photocatalyst towards the formation of aminoaromatic compound (**1c**) in comparison with other employed photocatalysts. On the other hand, the presence of the Lewis acid sites in the anatase samples could explain the increase in the amount of the imine produced upon using these photocatalysts. When employing P25 as the photocatalyst, higher amount of the quinoline (**1j**) was produced than with UV100 or rutile. This is perhaps due to the presence of two kinds of acid sites at the surface of this photocatalyst, *i.e.* Lewis acid and Brönsted acid sites. It has been reported that P25 has both Lewis and Brönsted acid sites on its surface[142]. It is well known that Brönsted acids can catalyze the cyclization reaction of imine into the corresponding quinoline[78, 172].

However, when P25 has been tested as a thermal catalyst (*i.e.* in the dark) for the reaction of *m*-aminotoluene with acetaldehyde at room temperature, only 4% yield from 2,7-dimethylquinoline has been obtained. Thus, the activity of this photocatalyst for the formation of the quinoline compound is enhanced by irradiation. This may be due to the increase in the amount of Brönsted acid sites at the surface of this photocatalyst upon irradiation.

The acidic properties of TiO<sub>2</sub> P25, TiO<sub>2</sub> UV100, and TiO<sub>2</sub> rutile, before and after UV(A) irradiation, were also verified by monitoring the pyridine adsorption by ATR-FTIR (**Figure 4.4**). Again the adsorption bands at 1445, 1489, and 1604 cm<sup>-1</sup>, which correspond to pyridine interaction with Lewis acid sites, are more intensive in anatase containing TiO<sub>2</sub> samples than in the rutile sample. On the other hand, the weak peak at 1640 cm<sup>-1</sup>, which confirms the interaction between the pyridine molecule and the Brönsted acid sites, becomes more intense after the UV(A) irradiation of P25.

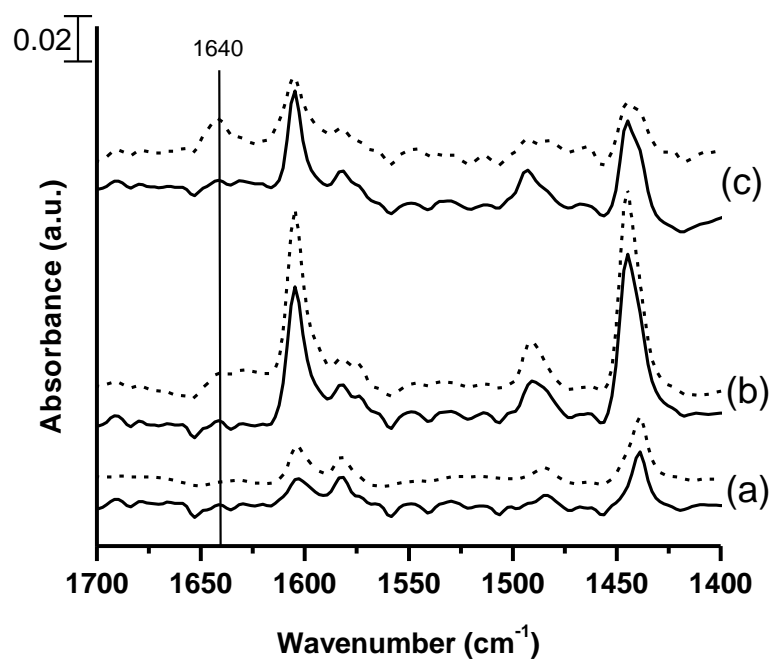


**Figure 4.4:** ATR-FTIR spectra of  $\text{TiO}_2$  layers in contact with pyridine in acetonitrile solution (100 mM). Solid lines and dotted lines refer to non irradiated and UV(A) irradiated samples, respectively. (a)  $\text{TiO}_2$  rutile, (b)  $\text{TiO}_2$  UV100, and (c)  $\text{TiO}_2$  P25.

### 4.3 Effect of the addition of an acid as a co-catalyst

The importance of the Brönsted acid sites for the cyclization reactions is supported by the direct addition of a Brönsted acid into the reaction dispersions containing Sachtleben Hombikat UV100 as the photocatalyst. It can be seen from **Figure 3.7** that the yield of the produced quinoline (**1j**) is significantly increased from ca. 6% up to ca. 47% when only a small amount of *p*-toluenesulfonic acid (*p*-TsOH) (5mol%) is added. By increasing the amount of *p*-TsOH a small drop in the yield is apparent.

The presence of a Brönsted acid in the reaction mixture will catalyze the reaction of the photocatalytically produced aldehyde with its alcohol to produce the corresponding acetal. It is well known that acetals are formed by treating aldehydes with alcohols in the presence of Brönsted acid catalyst. If the original aldehyde has an  $\alpha$ -hydrogen, as in the case of acetaldehyde, a vinyl ether can be produced (see **Figure 4.5**). As reported by Povarov[173], this vinyl ether suffers a condensation reaction with Schiff bases to produce

tetrahydroquinoline and quinoline derivatives. Cyclization of the imine with the enol ether will lead to the formation of 4-ethoxy-2,7-dimethyl-1,2,3,4-tetrahydroquinoline which can be converted to 2,7-dimethyl-1,2-dihydroquinoline upon splitting of an alcohol molecule (see **Figure 4.5**). Oxidation of this dihydroquinoline will, consequently, lead to the formation of 2,7-dimethyl-quinoline[174].

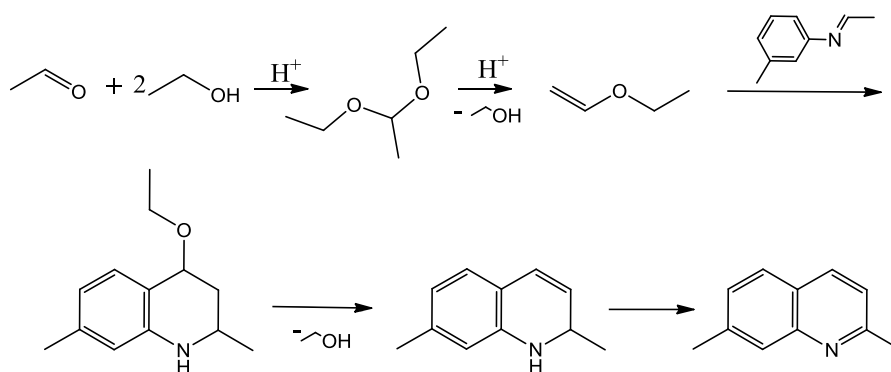


**Figure 4.5:** Schematic presentation of the formation of the vinyl ether and its addition to the imine to form the quinoline compound.

As can be seen from **Figure 3.8**, the ability of splitting of the alcohol from the thus formed ethoxy-1,2,3,4-tetrahydroquinoline strongly depends on the position as well as on the type of the substituent on the aromatic ring in the starting nitroaromatic compound. In the case of *m*-nitrotoluene or *p*-nitrophenol the corresponding ethoxy-1,2,3,4-tetrahydroquinoline will be less stable, therefore, the main product in both cases is the corresponding quinoline. In the case of *o*- or *p*-nitro toluene, the main products are the corresponding ethoxy-1,2,3,4-tetrahydroquinolines. These differences can be explained by the difference in the basicity of the aminoaromatic compounds ( $pK_a = 5.08$  and  $4.71$  for *p*- and *m*-toluidine, respectively). The inductive effect of the methyl group in case of the *o*- and the *p*-substituent would turn the corresponding ethoxy-1,2,3,4-tetrahydroquinoline into stronger bases thus decreasing the rate of the alcohol splitting due to an increased ability of the nitrogen atom to be protonated. This behavior is in good agreement with a mechanism involving resonance stabilization of the intermediate carbonium ion by the lone electron pair of the heterocyclic nitrogen (**Figure 4.6**)

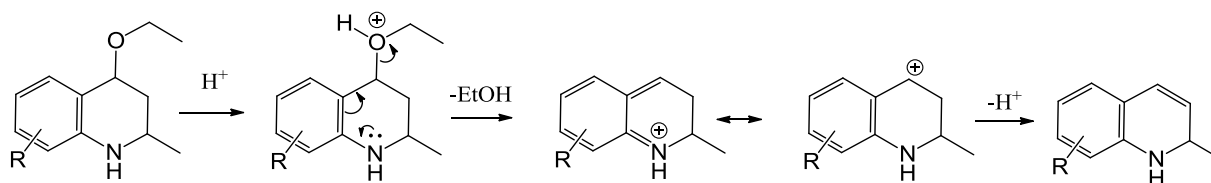


**Figure 4.6:** Splitting of alcohol from the ethoxy-1,2,3,4-tetrahydroquinoline molecule to form the dihydroquinoline derivative.

However, as can be seen from the results presented in **Table 3.2**, increasing the amount of *p*-TsOH up to 40 mol% results in the conversion of the ethoxy-1,2,3,4-tetrahydroquinolines to the corresponding quinolines and tetrahydroquinolines in almost all cases.

#### 4.4 Immobilization of Brønsted acid and TiO<sub>2</sub> into one heterogeneous photocatalyst

To overcome the separation problem of the added acid at the end of the reaction, hybrid organic–inorganic materials in which the organic acid is fixed into the pores of mesoporous silica-titania composites have been prepared. The newly synthesized catalysts were characterized by SEM, BET, FT-IR, TGA, and acid-base titration measurements.

As explained in the results section (3.3.1.1) acid modified mesoporous SiO<sub>2</sub> decorated with TiO<sub>2</sub> (T-S-ArSO<sub>3</sub>H) was successfully prepared. The amount of the fixed organic acid can be controlled and it is accessible and located inside the SiO<sub>2</sub> pores.

As shown in **Table 3.4** the newly prepared photocatalysts have been successfully applied to catalyze the photocatalytic synthesis of quinolines starting from the NACs. The yields of the quinoline obtained employing Sachtleben Hombikat UV100 modified with different amounts of bare SiO<sub>2</sub> were slightly increased from 6% in the case of pure TiO<sub>2</sub> to 18% in the case of T<sub>1</sub>S<sub>1</sub> (*cf.* entries 2-4 in **Table 3.4**). However, the yield of the target product (**1j**) was successfully increased up to 53% when small amounts of the arenesulfonic acid were imbedded inside the pores of T<sub>1</sub>S<sub>1</sub> (*cf.* entries 5-9 in **Table 3.4**). In particular, T<sub>1</sub>S<sub>1</sub>Ar<sub>0.03</sub> exhibits the highest yield (53%) while increasing the organic acid amount does not result in



an increased yield (see **Table 3.4**, entries 5,8, and 9), although more accessible acid centers are formed by increasing the amount of Ar-SO<sub>3</sub>H during the preparation as confirmed from the ion-exchange capacity and the BET measurements, respectively (see **Table 3.3**). The same behavior was noticed previously when the organic acid (*p*-TsOH) was added as homogeneous co-catalyst to the bare TiO<sub>2</sub> (*cf.* **Figure 3.7**). Moreover, the prepared heterogeneous catalysts demonstrate an excellent stability and reusability even after three catalytic runs (see **Table 3.4**, entries 5-7).

New strong Brönsted acid centers different from the weak Lewis-acid centers are apparently created by the modification of the silica-titania composite with arenesulfonic acid. The formation of these Brönsted acid centers on the silica has also been confirmed by Melero et al.,[157]. As described previously the presence of the Brönsted acid is essential to catalyze the cyclization reaction of the in situ produced imine.

To clarify the role of the light in the formation of the quinoline from the nitroaromatic compound and alcohol, the direct conversion of the aminoaromatic compound (**1c**) and acetaldehyde at RT over T<sub>1</sub>S<sub>1</sub>Ar<sub>0.03</sub> has been investigated. For this study the concentration of acetaldehyde was chosen to be 6 times higher than that of the aminoaromatic compound (**1c**) assuming, in the photocatalytic reaction, six electrons and six protons are required to complete the reduction of one nitro group to one amino group, thus, three molecules of alcohol will be oxidized to the equal number of acetaldehyde molecules. After 4h of stirring the reaction mixture in the dark (51% yield) of the quinoline (**1j**) was obtained. This result confirms that the photocatalytic reaction steps are only the initial reduction of the nitrotoluene and the oxidation of the alcohol while the cyclization reactions are catalyzed by the supported organic acid even in the dark.

## 4.5 Discussion of the reaction mechanism

Careful analyses for the reaction mixture at different reaction times have been performed in order to understand the reaction mechanism. The GC-MS analysis of the reaction mixtures, using *m*-nitrotoluene as substrate, indicates the formation of several products and intermediates including *m*-toluidine (**1c**), *N*-ethylidene-3-methylaniline (**1f**), 4-ethoxy-2,7-dimethyl-1,2,3,4-tetrahydroquinoline (**1g**), 2,7-dimethyl-1,2-dihydroquinoline (**1i**), 2,7-dimethyl-1,2,3,4-tetrahydroquinoline (**1k**), and 2,7-dimethyl-quinoline(**1j**).

The first steps in the reaction, which are necessary for all following reaction steps, are the photocatalytic reduction of the nitro group of the nitroaromatic compound and the photocatalytic oxidation of the alcohol (these steps have been previously discussed in detail). The further conversion of the photocatalytically produced species to the corresponding cyclization products as schematically presented in **Figure 4.7** has many possible pathways which will be discussed in detail below.

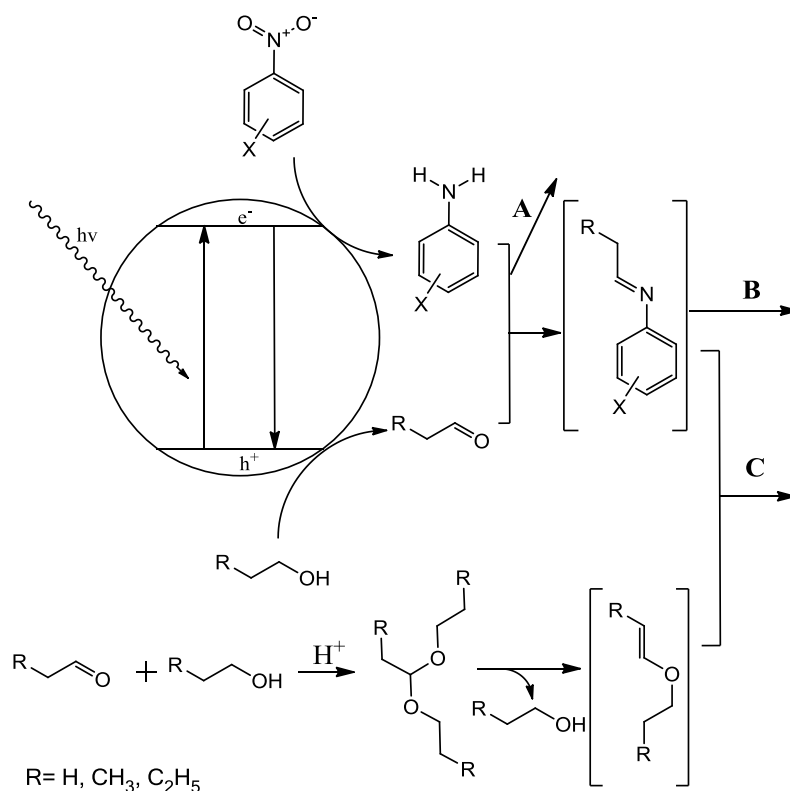


**Figure 4.7:** Pathways of the photocatalytic formation of the quinoline compounds from NACs and alcohols.

Pathway A (*c.f.* **Figure 4.8**): The acid-catalyzed Michael addition of the aminoaromatic compound to the self aldol condensation product of the acetaldehyde might occur, followed by ring closure with dehydration to form dihydroquinoline, which would be finally dehydrogenated to afford the quinoline products. Such a mechanism has been suggested by He et al.[175] for the thermal synthesis of quinolines from NACs and alcohols over titania-supported iridium nanoclusters. The aldol condensation of acetaldehyde to form crotonaldehyde over  $\text{TiO}_2$  has been reported [176-178]. However, the intermediate 4-hydroxy-1,2,3,4-tetrahydroquinolines were not detected in our case. In addition, Schiff bases, which are not involved in this mechanism, are always produced as intermediates under the employed reaction conditions thus reducing the likelihood of this mechanism.

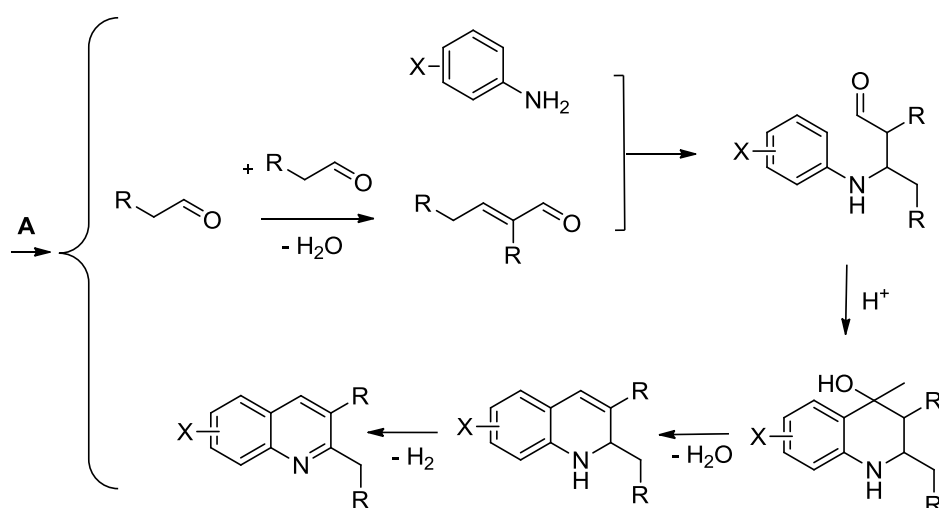


**Figure 4.8:** Pathway A in **Figure 4.7**.

Pathways B (see **Figure 4.9**) and C (see **Figure 4.10**) suggest the formation of the Schiff base upon the condensation of the photocatalytically generated aminoaromatic compounds and aldehydes. A competition between the Döbner-Miller and the Povarov reaction mechanisms may occur[133]. The reactions of imines with the corresponding tautomeric enamines are traditionally considered as one stage of the Döbner-Miller quinoline synthesis [171, 179]. Concerning this mechanism 4-arylamino-1,2,3,4-tetrahydroquinolines must be an intermediate stable enough to be isolated[180]. However, we were not able to detect such compounds,

therefore, the Povarov reaction mechanism (pathway C) appears to be preferred under our reaction conditions.

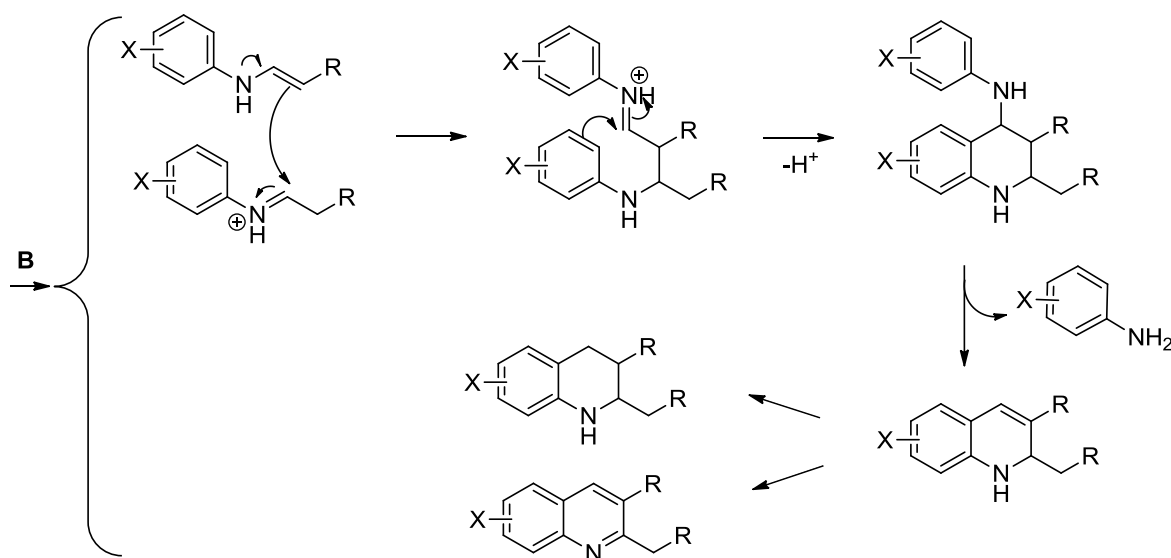


**Figure 4.9:** Pathway B in Figure 4.7

Povarov and Grigos[173] showed that the condensation of ethyl-vinyl-ether with Schiff bases in benzene in the presence of catalytic amounts of boron trifluoride etherate produces substituted 4-ethoxy-1,2,3,4-tetrahydro-quinolines in moderate yields (up to 60%). Upon treatment of the reaction mixture with *p*-toluenesulfonic acid or suitable oxidants [atmospheric oxygen or KMnO<sub>4</sub>], these compounds eliminate ethanol yielding the corresponding quinolines. Recently, it is reported that the mechanism of the Povarov reaction is stepwise and can be regarded as a sequential Mannich process, arising from the nucleophilic attack of the ethyl-vinyl-ether upon the acid activated imine to furnish a cationic intermediate, which subsequently undergoes an intramolecular electrophilic aromatic substitution to yield the ethoxy-1,2,3,4-tetrahydroquinoline. Under the employed photocatalytic reaction conditions both the Brønsted acid and oxidizing environment (originating from the holes generated in the photocatalytic process) are available which are needed to convert the 4-ethoxy-1,2,3,4-tetrahydro-quinoline to the corresponding dihydroquinolines upon the loss of an alcohol molecule (see **Figure 4.5**). The disproportionation of

this dihydroquinoline will, consequently, lead to the formation of the quinoline (**1j**) and the tetrahydroquinoline (**1k**).

Therefore, based upon the intermediates which have been detected here by the GC-MS analysis the Povarov reaction mechanism appears to be the most acceptable mechanism to explain the overall photocatalytic reaction system studied in this work.

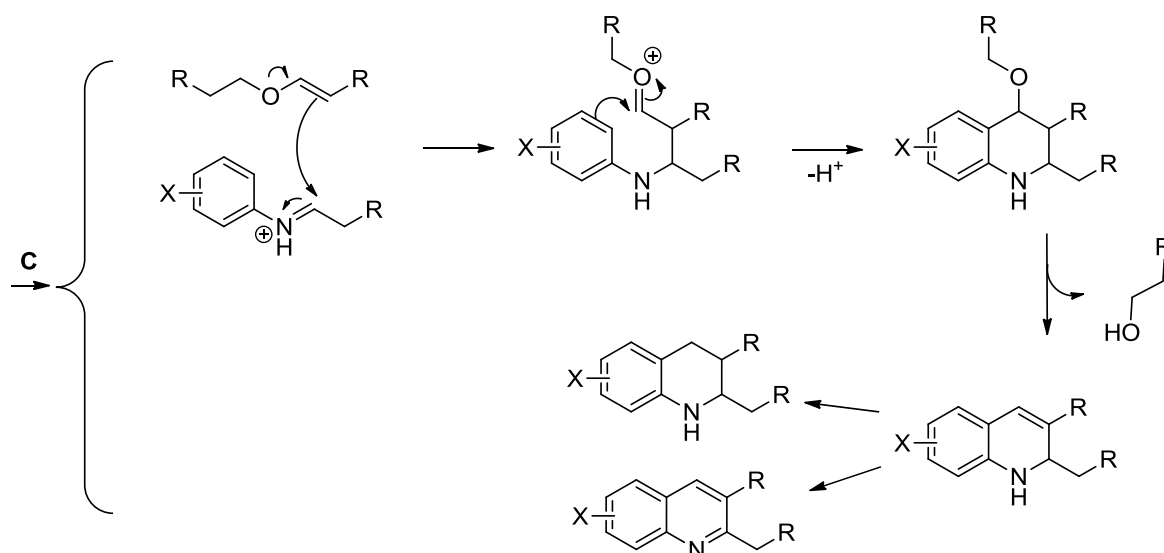


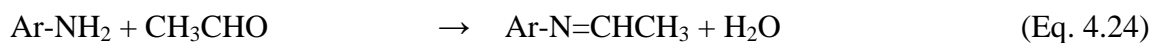
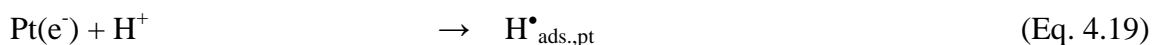
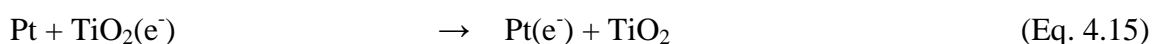
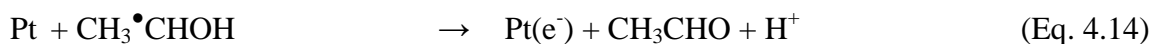
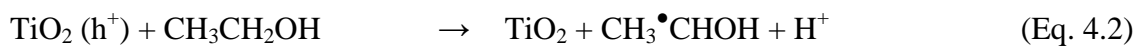
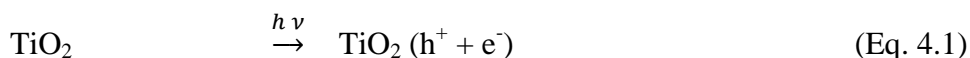
**Figure 4.10:** Pathway C in **Figure 4.7**

#### 4.6 Effect of the deposition of metal nanoparticles on the surface of $\text{TiO}_2$ on the photocatalytic reaction of the nitroaromatic compounds

It can be clearly seen from **Figure 3.13** that the presence of the co-catalyst, *i.e.*, Pt, directs the photocatalytic reaction towards *N*-alkylation and *N,N*-dialkylation of the nitroaromatic compound. Bearing in mind the reaction sequence illustrated in **Figure 4.1**, it can be concluded that steps 1 and 2 in **Figure 4.1** have not changed by the presence or absence of Pt while step 3 has changed to the hydrogenation of the in situ produced imine.

However, in case of the presence of Pt nanoparticles on the surface of  $\text{TiO}_2$ , the reducing agents present in the photocatalytic system may be different from that present employing bare

TiO<sub>2</sub>. Besides the photocatalytic reaction steps described in Eqs. 4.1-4.9, new reaction steps will take place when employing Pt/TiO<sub>2</sub> as the photocatalyst as summarized in Eqs. 4.14-4.26:



The photogenerated electrons will be trapped at the Pt nanoparticles presented at the surface of TiO<sub>2</sub> (Eq. 4.15). These trapped electrons may either reduce the nitroaromatic compound via a sequence of electron transfer, protonation and dehydration (Eqs. 4.16-4.18) or reduce the protons, generated from the oxidation of ethanol by the photogenerated holes, forming adsorbed H<sup>•</sup> radicals. The latter may also reduce the nitroaromatic compound to the aminoaromatic compound otherwise they will combine producing molecular hydrogen

(Eqs.4.20-4.23). However, the present study does not enable any differentiation between these pathways. When the photonic efficiency of the photocatalytic reduction of the nitroaromatic compound (**1a**) employing Pt<sub>0.5</sub>/TiO<sub>2</sub>(UV100) compared with that obtained employing bare TiO<sub>2</sub>(UV100), a decrease in the photonic efficiency is observed (see **Table 4.3**). It is usually known that the modification of the TiO<sub>2</sub> surface with Pt will enhance the photocatalytic activity due to the trapping of the photogenerated e<sup>-</sup> by Pt nanoparticles enhancing the e<sup>-</sup>/h<sup>+</sup> charge separation[96]. This will result in higher yields of the oxidation of the alcohol and thus also of the simultaneous reduction of the electron acceptor. However, under the employed reaction conditions, this decrease of the photonic efficiency of the reduction of *m*-nitrotoluene can be explained by the competition between the *m*-nitrotoluene and the protons (H<sup>+</sup>), which are produced by the photocatalytic oxidation of the alcohol, for the electrons trapped by the Pt nanoparticles. Upon illumination of an ethanolic solution of *m*-aminotoluene in the presence of Pt<sub>0.5</sub>/TiO<sub>2</sub> UV100 about 700 μmol H<sub>2</sub> is produced within 120 min of illumination, while only 400 μmol H<sub>2</sub> is produced using *m*-nitrotoluene as the substrate during the same time of irradiation. Hence, an excess of about 300 μmol H<sub>2</sub> is observed starting from the aminotoluene as the substrate instead of the *m*-nitrotoluene. This is exactly the amount of H<sub>2</sub> required to reduce the initially present amount (100 μmol) of the nitroaromatic compound to the aminoaromatic compound.

In a reference experiment, *m*-nitrotoluene was totally reduced to the *m*-aminotoluene when H<sub>2</sub> was purged in a reaction mixture containing Pt<sub>0.5</sub>/TiO<sub>2</sub> UV100 in the dark. No reduction of *m*-nitrotoluene was observed under the same conditions in the dark in the presence of bare TiO<sub>2</sub>. Thus, in the presence of Pt as a co-catalyst, the produced H<sub>2</sub> may act as the reducing agent of the nitro group instead of the direct reduction by the valence band electrons as in case of bare TiO<sub>2</sub>. On the other hand, it is worth mentioning that no reduction of *m*-nitrotoluene occurs in the reaction mixture containing Pt<sub>0.5</sub>/TiO<sub>2</sub> UV100 in the dark under Ar thus

confirming that this catalyst is not able to catalyze the dark hydrogen transfer reaction from the alcohol to the nitroaromatic compound.

**Table 4.3:** Photonic efficiencies  $\xi$  (%) of the photocatalytic reduction of *m*-nitrotoluene (**1a**) and the photocatalytic H<sub>2</sub> evolution in ethanol over bare TiO<sub>2</sub> UV100 or Pt<sub>0.5</sub>/TiO<sub>2</sub> UV100.

Entry <sup>[a]</sup>	Photocatalyst <sup>[b]</sup>	$\xi$ / %	
		reduction of <i>m</i> -nitrotoluene	H <sub>2</sub>
1	Bare TiO <sub>2</sub> UV100	6.8	0
2	Pt <sub>0.5</sub> /TiO <sub>2</sub> UV100	5.1	1.45

[a] Reaction conditions: photocatalyst (25 mg), (**1a**) (100  $\mu$ mol), EtOH (10 mL),  $\lambda > 320$  nm, 2h, 25 °C, under Ar atmosphere.

Condensation reaction between the photocatalytically generated acetaldehyde and aminoaromatic compound will produce the imine which will be further hydrogenated to the corresponding *N*-alkylated compound by the hydrogen atoms adsorbed on Pt islands (see Eqs. 4.24-4.26).

## 4.7 Effect of different parameters on the selectivity of the photocatalytic *N*-alkylation reaction

### 4.7.1 Effect of the type of TiO<sub>2</sub>

As can be seen from **Table 3.6**, the type of TiO<sub>2</sub> plays an important role on the selectivity for the formation of the mono *N*-alkylated product (**11**) upon the photocatalytic conversion of the nitroaromatic compound (**1a**). The best selectivity towards the formation of (**11**) (*c.f.* **Table 3.6** entries 1,3,5, and 7) obtained when Pt<sub>0.5</sub>/TiO<sub>2</sub> UV100 or Pt<sub>0.5</sub>/TiO<sub>2</sub> P25 were employed. As previously discussed, the yield of the imine (**1f**) is higher employing anatase as the photocatalyst. This is explained by the activated condensation of the photocatalytically produced acetaldehyde and the aminoaromatic compound on the Lewis acid sites presented at the surface of anatase TiO<sub>2</sub>. The mono *N*-alkylated product (**11**) is formed upon the hydrogenation of the produced imine, thus, increasing the amount of the imine will increase



the yield of (**11**). In the case of Pt<sub>0.5</sub>/TiO<sub>2</sub> P25, the presence of the co-catalyst, *i.e.* Pt nanoparticles, changes the reaction pathway from the cyclization of the imine (**1f**) to its hydrogenation to form *N*-alkylated product (**11**) instead of the quinoline (**1j**). Consequently, the imine (**1f**) is hydrogenated before it undergoes the cyclization reaction.

#### 4.7.2 Effect of the platinization method

The selectivity of the products obtained when Pt<sub>0.5</sub>/TiO<sub>2</sub> UV100 prepared by solids mixing method was used as a catalyst is also shown in **Table 3.6** (entries 9 and 10). The preparation method of the catalyst also influences the selectivity of the reaction, *i. e.*, colloidal Pt loaded onto Hombikat UV100 is not as selective as the same catalyst prepared by the photodeposition method. Although a complete conversion of the nitroaromatic compound (**1a**) occurs within 120 min employing the former photocatalyst, less than 10% selectivity for the formation of the *N*-alkylated product (**11**) is obtained. Obviously, the type of interaction between Pt and TiO<sub>2</sub> has an important role in the activity of Pt as a hydrogenation catalyst. One explanation may be that the bare surface of the photodeposited platinum is larger than that of the Pt<sub>0.5</sub>/TiO<sub>2</sub> obtained by the mixing solids method. In Pt<sub>0.5</sub>/TiO<sub>2</sub> prepared by mixing of colloidal Pt with TiO<sub>2</sub>, the Pt particles should rather be surrounded by TiO<sub>2</sub> particles resulting in reducing the available surface of Pt particles. It should be noted that, Wang et al.[96] have also reported that Pt/TiO<sub>2</sub> photocatalyst prepared by colloidal mixing method is poorer electrocatalyst for H<sub>2</sub> evolution, upon the photocatalytic oxidation of methanol in water under deaerated conditions, than the photocatalytically prepared one. This is in agreement with the results of the photocatalytic *N*-alkylation reactions obtained here.

#### 4.7.3 Effect of the loaded amount of Pt

The data obtained from UV(A) illumination of an ethanolic solution of the nitroaromatic compound (**1a**) in the presence of Sachtleben Hombikat UV100 loaded with 0.3, 0.5, and 1.0 wt.% Pt are presented in **Figure 3.14**. These data confirms that the amount of platinum has a

major role for the selectivity of the products especially for the mono *N*-alkylated compound (**II**). As expected, the higher the Pt loaded amount the higher the selectivity of the photocatalytic reaction for the formation of the mono *N*-alkylated compound (**II**). Similar effect of the amount of Pt loaded on the surface of TiO<sub>2</sub> has also been reported by Ohtani and co-workers in their study on the photocatalytic conversion of Lysine to pipercolinic acid[119]. This enhancement in the selectivity may be due to the increase of the total surface area of Pt on which the generated imine is being hydrogenated to the mono *N*-alkylated compound. Increasing the loaded amount of the Pt will result either in an enlargement of the deposited metal islands or in an increase of their number. However, in both cases the total surface area of the metal will increase.

In order to investigate the influence of the loaded amount of platinum on the size of the deposited particles, TEM of the TiO<sub>2</sub> powders loaded with different Pt amount were measured. Dark-field TEM images of Pt/TiO<sub>2</sub>UV100 powders (**Figure 3.15**) clearly show that the Pt nanoparticles are well dispersed exhibiting particles diameters between 3 and 10 nm. However, it is difficult to evaluate the Pt particles size precisely and thus to determine the change in the Pt particles size upon changing the loaded amounts of platinum. The theoretical calculation (assuming that Pt nanoparticles are semi-sphere-like, and considering the mass densities of platinum and TiO<sub>2</sub> are 21.4 and 3.894 g cm<sup>-3</sup>, respectively) of the change in the particle size resulted upon changing the loaded amount of Pt predicts that when the amount of Pt is decreased from 1.0% via 0.5% to 0.3%, the particle size should change from 5nm via 3.9nm to 3.3nm. However, these small changes cannot be clearly recognized from the obtained TEM images.

Shiraishi et al.[181] suggested that TiO<sub>2</sub> with higher Pt loading produce a larger amount of protons upon photocatalytic oxidation of benzyl alcohol in the presence of aromatic amines. They assumed that these protons are not only reduced at the Pt surface but also react with the surface –OH groups at TiO<sub>2</sub>, producing (Ti–OH<sub>2</sub><sup>+</sup>), *i.e.*, Brönsted acid site. Thus, one will expect an enhancement in the yield of the quinoline (**1j**) by increasing the loaded amount of Pt due to the effect of Brönsted acid site on the cyclization reaction of (**1f**) (see 4.3). However, that is not the case here; the selectivity towards the quinoline (**1j**) decreases while the selectivity towards the formation of *N*-alkylated product (**1l**) enhances by increasing the Pt amount. Thus, the imine (**1f**) is hydrogenated over Pt sites before it undergoes cyclization over the formed Brönsted acid sites. It is worth mentioning that purging of Ar during the illumination of the reaction mixture (entries 11 and 12 in **Table 3.6**) to remove the liberated H<sub>2</sub> during the reaction was not efficient to switch the reaction pathway from hydrogenation to cyclization. This indicates that the hydrogenation of the imine (**1f**) occurs with the photocatalytically formed H<sup>•</sup><sub>ads, Pt</sub> radicals (see Eq. 4.25) rather than with molecular H<sub>2</sub> via (Eq. 4.26) thus no higher pressure of H<sub>2</sub> gas is needed.

#### 4.7.4 Effect of the light intensity

The effect of the light intensity on both the conversion of the nitroaromatic compound and the selectivity of the products is illustrated in **Figure 3.16**. It can be seen from this Figure that the selectivity of photocatalytic conversion of the nitroaromatic compound (**1a**) to the *N*-alkylated product (**1l**), using Pt<sub>0.5</sub>/TiO<sub>2</sub> UV100, is not affected by the employed light intensities. However, the reduction rate of the nitro compound declines by decreasing the light intensity. Consequently, it is just more time needed to get the same maximum yields of the *N*-alkylated product (**1l**) employing lower light intensities.

#### 4.7.5 Effect of the type of the loaded metal

The activities of other metals (Pd, Ag, and Au) loaded on the surface of TiO<sub>2</sub> UV100 have also been investigated and compared with that of Pt<sub>0.5</sub>/TiO<sub>2</sub>UV100. As can be seen from **Table 3.6**, the selectivity of the reaction depends strongly on the type of the metal deposited on the surface of the photocatalyst. In the case of Pt or Pd loaded nanoparticles, almost the entire amount of initially (photocatalytically) formed aminoaromatic compound (**1c**) is converted within the first 2h of the illumination with the yield of *N*-alkylated products being higher than that obtained when employing Au<sub>0.5</sub>/TiO<sub>2</sub>UV100 or Ag<sub>0.5</sub>/TiO<sub>2</sub>UV100. Moreover, a clear superiority of platinum over all other metals for the selectivity towards the formation of the mono *N*-alkylated product (**1l**) is observed. Increasing the illumination time leads to further alkylation of the produced mono *N*-alkylated compound into the *N,N*-dialkylated one, with, again, Pt<sub>0.5</sub>/TiO<sub>2</sub> UV100 showing the highest selectivity (see **Table 3.5**, entries with even numbers).

These differences in the selectivity of the photocatalytic *N*-alkylation reaction employing TiO<sub>2</sub> modified with Pt, Pd, Au, or Ag nanoparticles can be explained by the difference in the work function of these metals. The work functions of Pt, Pd, Au, and Ag are reported to be 5.65, 5.12, 5.10, and 4.26 eV, respectively[182]. The higher the work function the higher the amount of the electrons that is trapped by the metal nanoparticles from the conduction band of the irradiated TiO<sub>2</sub>. Consequently, employing metals with higher work function will enhance the amount of adsorbed H<sup>•</sup> radicals formed upon trapping an photogenerated electron by proton, that is generated via the photocatalytic oxidation of alcohol (*c.f.* Eqs. 4.2, 4.14, and 4.19), which in turn, will enhance the imine hydrogenation see Eq. 4.25.

To investigate the effect of the illumination on the hydrogenation of C=N double bond, the reaction between the aminoaromatic compound (**1c**) and acetaldehyde (**1d**) was carried out in the dark under H<sub>2</sub> atmosphere and in the presence of TiO<sub>2</sub>(UV100) or M<sub>0.5</sub>/TiO<sub>2</sub>(UV100) (M= Pt, Pd, Au or Ag). As can be seen from the data included in **Table 4.4**, only trace of the *N*-

alkylated compound (**11**) is produced over bare TiO<sub>2</sub>, while the metal (Pt or Pd) island loaded on its surface catalyzes this alkylation reaction even in the dark. However, in the case of (Au or Ag) the catalysts show low activity for the *N*-alkylation reaction of the aminoaromatic compound (**1c**) with acetaldehyde in the dark. The selectivity of the dark reaction towards the mono-*N*-alkylated product (**11**) also follows the order: Pt>Pd>Au>Ag which is similar to that obtained for the photocatalytic reactions.

**Table 4.4:** *N*-alkylation of the *m*-toluidine (**1c**) with acetaldehyde in the presence of different metal loaded TiO<sub>2</sub>.

Entry <sup>[a]</sup>	Catalyst	t [h]	Products / μmol <sup>[b]</sup>	
			<b>11</b>	<b>1m</b>
1	TiO <sub>2</sub> (UV100)	2	3	<1
3	Pt <sub>0.5</sub> /TiO <sub>2</sub> (UV100)	2	72	2
5	Pd <sub>0.5</sub> /TiO <sub>2</sub> (UV100)	2	27	42
7	Ag <sub>0.5</sub> /TiO <sub>2</sub> (UV100)	2	3	<1
9	Au <sub>0.5</sub> /TiO <sub>2</sub> (UV100)	2	7	1

[a] Reaction conditions: catalyst (25 mg), *m*-toluidine (**1c**) (100 μmol) and acetaldehyde (300 μmol) in 10 ml EtOH, under H<sub>2</sub> atmosphere at RT.

[b] Determined by GC.

#### 4.8 Effect of the deposition of bimetallic (Pt-Ag) nanoparticles

The activity of TiO<sub>2</sub> UV100 loaded with bimetallic (Pt-Ag) islands photocatalysts has been tested in the photocatalytic production of the mono *N*-alkylated compound (**11**) starting from the nitroaromatic compound (**1a**) and ethanol. The produced amounts of (**11**) as a function of the illumination time employing Ag<sub>m</sub>/Pt<sub>n</sub>/TiO<sub>2</sub> and Pt<sub>n</sub>/Ag<sub>m</sub>/TiO<sub>2</sub> (where n and m are the weight % ratio of Pt and Ag, respectively) are illustrated in **Figure 3.17** and **Figure 3.18**, respectively. As can be seen from **Figure 3.17** the deposition of small amount (0.1wt.%) of silver on the surface of Pt<sub>0.5</sub>/TiO<sub>2</sub> enhance the produced yield of (**11**) from 66% to 76% after 3h of illumination. This enhancement may be interpreted by decreasing the activity of the Pt

particles to carry out the further *N*-alkylation reaction of the produced *N*-alkylated product (**1l**) into *N,N*-dialkylated one (**1m**). However, increasing the loaded amounts of Ag to (0.3wt.%) has negatively affected the selectivity towards the formation of (**1l**). On the other hand, it can be noticed that no significant change in the time course of (**1l**) production takes place at Ag loaded amount  $\geq 0.3\text{wt.}\%$ . This can be explained by assuming that the Ag is deposited layer-by-layer on the surface of Pt particles, but not on the bare surface of  $\text{TiO}_2$ , to yield a Pt core Ag shell nanoparticles on the surface of  $\text{TiO}_2$ . As reported in the literature[183], The deposition of Ag on Pt electrodes or polycrystalline platinum demonstrated that the Pt-Ag bond is stronger than Ag-Ag bond. Therefore, two dimensional growth of Ag on Pt nanoparticles will be preferred. Such a structure has also been reported by Tada et al.[72, 73]. Consequently, at higher Ag loadings, the whole surface of Pt will be covered by Ag converting its electronic properties from that of bare Pt to bare Ag. However, these catalysts, at higher Ag loadings, are still more active to produce (**1l**) than the bare  $\text{Ag}_{0.5}/\text{TiO}_2$  (cf. **Figure 3.18**) which indicates that the presence of the core of Pt enhances the efficiency of the Ag for the hydrogenation of the *in situ* produced imine (**1f**). Pt displays a higher work function (5.65 eV) than that of Ag (4.26 eV) thus Pt will trap higher number of electrons from the conduction band than Ag will do. Thus, the presence of Pt as a core may enhance the number of electrons that trapped from the conduction band to Ag.

On the other hand, the direct interaction between Pt and  $\text{TiO}_2$  surface seems to be important to get the required activity for the conversion of the nitroaromatic compound (**1a**) into the mono *N*-alkylated product (**1l**). The produced amount of (**1l**) after 2h of illumination is more than 2 times higher employing  $\text{Pt}_{0.5}/\text{TiO}_2$  instead of  $\text{Pt}_{0.5}/\text{Ag}_{0.5}/\text{TiO}_2$  (cf. **Figure 3.17** and **Figure 3.18**). Similarly, the liberated amount of  $\text{H}_2$  over the reaction mixture was ca. 4 times higher employing  $\text{Pt}_{0.5}/\text{TiO}_2$  as the photocatalyst than that obtained employing  $\text{Pt}_{0.5}/\text{Ag}_{0.5}/\text{TiO}_2$  (cf. **Table 3.8**).

#### 4.9 *N*-alkylation of various nitroaromatic compounds by different alcohols

In order to evaluate the general applicability of this photocatalytic *N*-alkylation method, various types of nitroaromatic compounds as well as different alcohols were studied. As can be seen from **Table 3.7**, the photocatalytic *N*-alkylation was successfully achieved in most cases with moderate to very good isolated yields.

However, the time required to achieve a complete conversion of the nitroaromatic compound (**1a**) increases by increasing the length of the aliphatic chain of the alcohol. This is due to the difference in the alcohols properties, such as viscosity, polarity, polarisability, and reduction potential. The effect of the alcohol parameters on the rate of the nitroaromatic compounds reductions has been reported by Breyova et al.[67]. They observed that the solvent viscosity significantly affected the rate of 4-nitrophenol photocatalytic reduction employing TiO<sub>2</sub> and a linear dependence was obtained, whereas, the rate of the photocatalytic reduction increases with increasing polarity of the alcohol.

On the other hand, only trace amounts of the mono *N*-alkylated products are produced when branched or aromatic alcohols are used, while the main products in these cases are the imines in the case of 3-methyl-butanol or benzyl alcohol or even the aminoaromatic compound in the case of iso-propanol (entries 4-6 in **Table 3.7**) meaning that a steric effects also play a role on the formation of the *N*-alkylated products. It can also be observed from **Table 3.7** that the position of the methyl group in the nitroaromatic compound and its number do not affect the reaction sequence, thus, in all cases the mono *N*-alkylated products were obtained in very good yields (entries 1, 7-9 in **Table 3.7**). Interestingly, *N*-ethyl-*m*-ethyl-benzene was obtained when *m*-nitrostyrene was used as a substrate (entry 10 in **Table 3.7**). Thus, the Pt<sub>0.5</sub>/TiO<sub>2</sub>(UV100) is not only able to photocatalytically hydrogenate the C=N double bond but also the C=C one.

An overview of the suggested reaction mechanism of the photocatalytic conversion of the nitroaromatic compound (**1a**) employing  $\text{TiO}_2$  modified with metal nanoparticles is summarized in **Figure 4.11**.

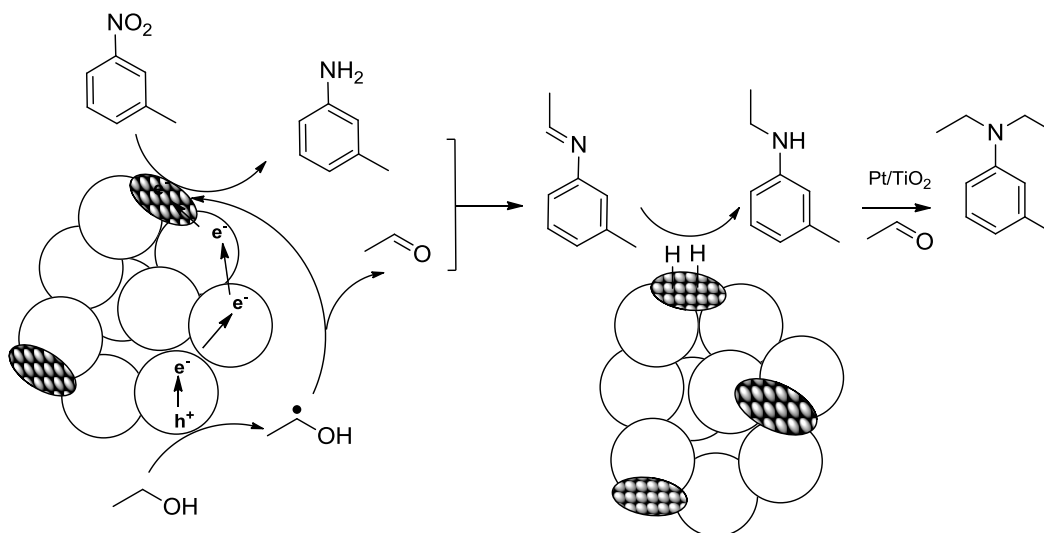


**Figure 4.11:** Proposed mechanism for the one-pot  $N$ -alkylation of  $m$ -nitrotoluene promoted by  $\text{TiO}_2$  loaded with metal nano particles catalyst under photoirradiation.

Different transformations in this “one pot” system can be achieved by employing both the photocatalytic and the catalytic action of  $\text{TiO}_2$  and metal nanoparticles, respectively: (i) the dehydrogenation of alcohol to the corresponding aldehyde consuming the photogenerated valence band holes of the illuminated  $\text{TiO}_2$ , (ii) the reduction of the nitro group of the nitroaromatic compound to an amino group either by the photogenerated conduction band electrons or through electrons initially trapped at the metal deposits on the semiconductor’s surface, and (iii) the hydrogenation of the imine, which is produced from the condensation of the aldehyde and the aminoaromatic compound, on the surface of metal nanoparticles at the  $\text{TiO}_2$  surface yielding the corresponding  $N$ -alkylated product. Prolonged illumination time then leads to the conversion of  $N$ -alkylated product into  $N,N$ -dialkylated one.



## 5 Summary and conclusions

The photocatalytic conversion of nitroaromatic compounds in alcoholic suspensions of TiO<sub>2</sub> can be successfully employed to obtain valuable nitrogen-containing organic compounds in one-pot reactions. In general, different transformations in these “one pot” systems can be achieved by employing both the photocatalytic and the catalytic action of TiO<sub>2</sub> or of modified TiO<sub>2</sub>. The oxidation of an alcohol to the corresponding aldehyde consuming the photogenerated valence band holes of the illuminated TiO<sub>2</sub>, the simultaneous reduction of the nitro group of the nitroaromatic compound to the amino group either by the photogenerated conduction band electrons or through electrons initially trapped at metal deposits on the semiconductor’s surface, and the condensation of the aldehyde with the amino compound to produce the corresponding imine all occur in one system (or “one-pot”). Afterwards, the resulting imine can suffer one of the following fates: it may undergo a cyclization reaction when a Brønsted acid is presented in the reaction media, or it may be hydrogenated to the corresponding secondary and tertiary amine when TiO<sub>2</sub> is modified with metal nanoparticles. These possible transformations are summarized in **Figure 5.1**.

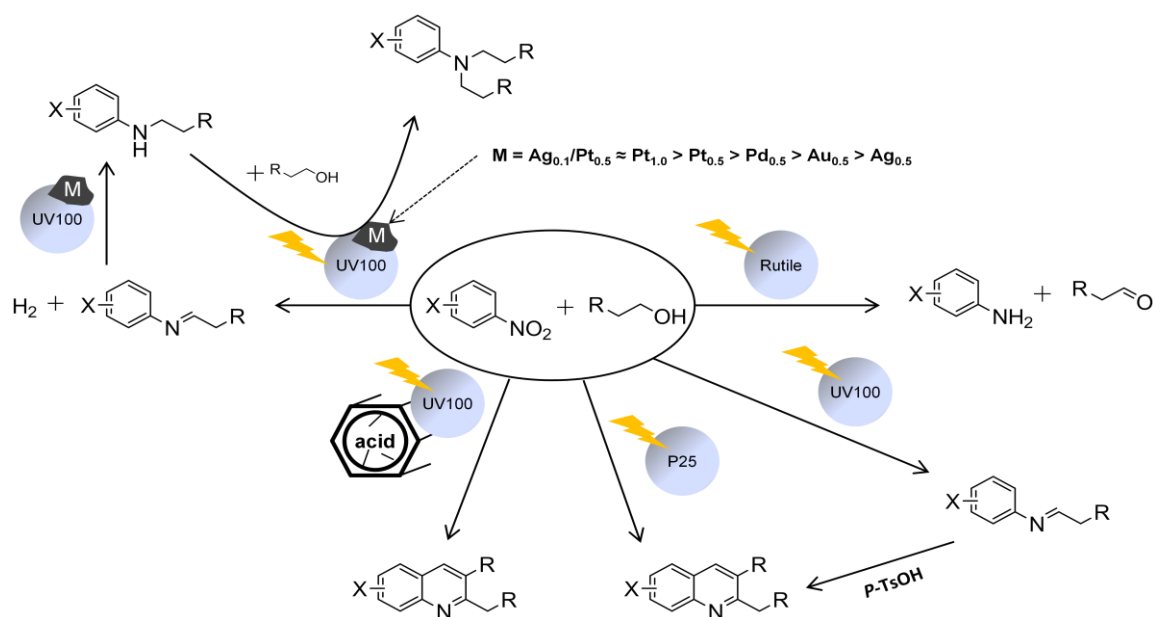


**Figure 5.1:** Schematic summarization of the fates of the nitroaromatic compounds in alcohols upon illumination in the presence of different bare or modified TiO<sub>2</sub> photocatalysts.

The distribution of the obtained products is strongly influenced by the type of the employed TiO<sub>2</sub> (i.e., bare or modified).

The surface properties of the photocatalyst play an important role for the reaction pathway and strongly affect the selectivity of the products. The poor acidity of rutile can explain the selectivity of the photocatalytic conversion of *m*-nitrotoluene towards the corresponding aminoaromatic compound (*m*-toluidine). The catalytic condensation of the photocatalytically produced aldehyde and aminoaromatic compound occurs on the Lewis acid site on anatase TiO<sub>2</sub> producing the corresponding imine (*N*-ethylidene-3-methylaniline). In the case of the anatase-rutile mixture TiO<sub>2</sub> P25 the imine, which is produced on the Lewis acid sites, can suffer a cyclization reaction to yield the corresponding quinoline (2,7-dimethylquinoline) which is readily explained by the presence of Brønsted acid sites on TiO<sub>2</sub> P25 surface.

The presence of small amounts (5 mol%) of an acidic co-catalyst, i.e., the free organic acid (*p*-TsOH), enhances the yield of the photocatalytically produced quinoline (2,7-dimethylquinoline) in the case of Sachtleben Hombikat UV100 from 4% to approx. 48%. Increasing the amounts of the added acid does not result in a simultaneous increase in the yield of the produced quinoline. However, the ratio of the cyclization products (quinolines, tetrahydroquinolines, and ethoxy-tetrahydroquinolines) of the different substituted nitrobenzenes depends on the position of the substituent (*o*-, *m*-, and *p*-) or on its type (methyl or hydroxyl).

Moreover, TiO<sub>2</sub> (Sachtleben Hombikat UV100) was successfully modified with arenesulfonic acid functionalized mesoporous SiO<sub>2</sub> to obtain a bifunctional acidic photocatalyst. The thus synthesized catalyst can be efficiently employed to convert *m*-nitrotoluene into 2,7-dimethylquinoline with 54% yield.

The cyclization of the photocatalytically produced imine was found to follow the Povarov mechanism in which the imine condenses with the enol ether (formed via the reaction of the photocatalytically generated aldehyde with the alcohol through the formation of the acetal) to form 4-ethoxy-2,7-dimethyl-1,2,3,4-tetrahydroquinoline which can be converted to 2,7-dimethyl-1,2-dihydroquinoline upon splitting off an alcohol molecule. Disproportionation or oxidation of this dihydroquinoline will, consequently, lead to the formation of 2,7-dimethylquinoline (see **Figure 4.5**).

The presence of precious metal nanoparticles as co-catalyst on the surface of TiO<sub>2</sub> directs the photocatalytic reaction towards *N*-alkylation and *N,N*-dialkylation. TiO<sub>2</sub> photocatalytically modified with Pt nanoparticles is found to be more selective for the photocatalytic mono *N*-alkylation reaction than TiO<sub>2</sub> photocatalytically loaded with Pd, Au, and Ag. Higher Pt loading results in a higher selectivity towards the mono *N*-alkylated product, the respective selectivity increased from 50% to 80% when the Pt loading increased from 0.3% to 1.0%. Moreover, Pt/TiO<sub>2</sub> catalysts prepared by the photodeposition method were found to be more active and selective towards the *N*-alkylation reaction than the one obtained from the mixed solids method. Furthermore, the illumination time controls the selectivity of the formation of the mono *N*-alkylated product, i.e., prolonged illumination time leads to the complete conversion of the mono *N*-alkylated product into the *N,N*-dialkylated one.

Loading of (0.1 wt.%) Ag over (0.5 wt.%) Pt/TiO<sub>2</sub> increased the selectivity of the formation of the mono *N*-alkylated product from 66% to 76%, while this selectivity decreased by increasing the loaded amount of Ag beyond 0.1 wt.%. In contrast, the presence of Ag nanoparticles covered with a Pt shell on the surface of TiO<sub>2</sub> inhibits the activity of the Pt nanoparticles for the hydrogenation of the C=N bond in the *in situ* produced imine.

## 6 References

1. Ciamician, G., "The photochemistry of the future". *Science*, **1912**, 36, 385-394
2. Coyle, E. E. ; Oelgemoller, M., "Micro-photochemistry: photochemistry in microstructured reactors. The new photochemistry of the future?". *Photochemical & Photobiological Sciences*, **2008**, 7, 1313-1322.
3. Albini, A. ; Fagnoni, M., "Green chemistry and photochemistry were born at the same time". *Green Chemistry*, **2004**, 6, 1-6.
4. Nebbia, G. ; Kauffman, G. B., "Prophet of solar energy: A retrospective view of Giacomo Luigi Ciamician (1857-1922), the founder of green chemistry, on the 150th anniversary of his birth ". *The Chemical Educator*, **2007**, 12, 362-369.
5. Ravelli, D.; Dondi, D.; Fagnoni, M. ; Albini, A., "Photocatalysis: A multi-faceted concept for green chemistry". *Chemical Society Reviews*, **2009**, 38, 1999-2011.
6. Fagnoni, M.; Dondi, D.; Ravelli, D. ; Albini, A., "Photocatalysis for the formation of the C-C bond". *Chemical Reviews*, **2007**, 107, 2725-2756.
7. Albini, A., "Catalysis of photochemical-reactions: Opportunities and pitfalls". *Journal of Chemical Education*, **1986**, 63, 383-386.
8. Kisch, H. ; Hopfner, M., "Novel organic syntheses through semiconductor photocatalysis", in "Electron Transfer in Chemistry", V. Balzani, Editor. 2008, Wiley-VCH Verlag GmbH: Germany. p. 232-275.
9. Nozik, A. J., "Photoelectrochemistry - applications to solar-energy conversion". *Annual Review of Physical Chemistry*, **1978**, 29, 189-222.
10. Tran, P. D.; Wong, L. H.; Barber, J. ; Loo, J. S. C., "Recent advances in hybrid photocatalysts for solar fuel production". *Energy & Environmental Science*, **2012**, 5, 5902-5918.
11. Hoffmann, M. R.; Martin, S. T.; Choi, W. Y. ; Bahnemann, D. W., "Environmental applications of semiconductor photocatalysis". *Chemical Reviews*, **1995**, 95, 69-96.
12. Fox, M. A. ; Dulay, M. T., "Heterogeneous photocatalysis". *Chemical Reviews*, **1993**, 93, 341-357.
13. Mills, A.; Davies, R. H. ; Worsley, D., "Water-purification by semiconductor photocatalysis". *Chemical Society Reviews*, **1993**, 22, 417-425.
14. Linsebigler, A. L.; Lu, G. Q. ; Yates, J. T., "Photocatalysis on TiO<sub>2</sub> surfaces - principles, mechanisms, and selected results". *Chemical Reviews*, **1995**, 95, 735-758.
15. Matsuoka, M.; Kitano, M.; Takeuchi, M.; Tsujimaru, K.; Anpo, M. ; Thomas, J. M., "Photocatalysis for new energy production - Recent advances in photocatalytic water splitting reactions for hydrogen production". *Catalysis Today*, **2007**, 122, 51-61.

16. Abe, R., "Development of a new system for photocatalytic water splitting into H<sub>2</sub> and O<sub>2</sub> under visible light irradiation". *Bulletin of the Chemical Society of Japan*, **2011**, 84, 1000-1030.
17. Sayama, K.; Mukasa, K.; Abe, R.; Abe, Y. ; Arakawa, H., "A new photocatalytic water splitting system under visible light irradiation mimicking a Z-scheme mechanism in photosynthesis". *Journal of Photochemistry and Photobiology a-Chemistry*, **2002**, 148, 71-77.
18. Kandiel, T. A.; Dillert, R. ; Bahnemann, D. W., "Enhanced photocatalytic production of molecular hydrogen on TiO<sub>2</sub> modified with Pt-polypyrrole nanocomposites". *Photochemical & Photobiological Sciences*, **2009**, 8, 683-690.
19. Palmisano, G.; Augugliaro, V.; Pagliaro, M. ; Palmisano, L., "Photocatalysis: a promising route for 21<sup>st</sup> century organic chemistry". *Chemical Communications*, **2007**, 3425-3437.
20. Renz, C., "Lichtreaktionen der Oxyde des Titans, Cers und der Erdsäuren". *Helvetica Chimica Acta*, **1921**, 4, 961-968.
21. Goodeve, C. F., "The absorption spectra and photo-sensitising activity of white pigments ". **1937**, 33, 340-347.
22. Goodeve, C. F. ; Kitchener, J. A., "The mechanism of photosensitisation by solids". *Transactions of the Faraday Society*, **1938**, 34, 902-908.
23. Carey, J. H.; Lawrence, J. ; Tosine, H. M., "Photodechlorination of PCB's in the presence of titanium dioxide in aqueous suspensions". *Bulletin of Environmental Contamination and Toxicology*, **1976**, 16, 697-701.
24. Frank, S. N. ; Bard, A. J., "Heterogeneous photocatalytic oxidation of cyanide ion in aqueous-solutions at TiO<sub>2</sub> powder". *Journal of the American Chemical Society*, **1977**, 99, 303-304.
25. McLintock, I. S. ; Ritchie, M., "Reactions on titanium dioxide: Photo-adsorption and oxidation of ethylene and propylene". *Transactions of the Faraday Society*, **1965**, 61, 1007-1016.
26. Thompson, T. L. ; Yates, J. T., "Surface science studies of the photoactivation of TiO<sub>2</sub>-new photochemical processes". *Chemical Reviews*, **2006**, 106, 4428-4453.
27. McCullagh, C.; Skillen, N.; Adams, M. ; Robertson, P. K. J., "Photocatalytic reactors for environmental remediation: a review". *Journal of Chemical Technology & Biotechnology*, **2011**, 86, 1002-1017.
28. Colina-Marquez, J.; Machuca-Martinez, F. ; Puma, G. L., "Radiation absorption and optimization of solar photocatalytic reactors for environmental applications". *Environmental Science & Technology*, **2010**, 44, 5112-5120.
29. Fujishima, A. ; Honda, K., "Electrochemical photolysis of water at a semiconductor electrode". *Nature*, **1972**, 238, 37-38.

30. Frank, S. N. ; Bard, A. J., "Semiconductor electrodes .12. Photoassisted oxidations and photoelectrosynthesis at polycrystalline TiO<sub>2</sub> electrodes". *Journal of the American Chemical Society*, **1977**, 99, 4667-4675.
31. Reiche, H. ; Bard, A. J., "Heterogeneous photosynthetic production of amino-acids from methane-ammonia-water at Pt-TiO<sub>2</sub>. Implications in chemical evolution". *Journal of the American Chemical Society*, **1979**, 101, 3127-3128.
32. Dunn, W. W.; Aikawa, Y. ; Bard, A. J., "Heterogeneous photosynthetic production of amino-acids at Pt-TiO<sub>2</sub> suspensions by near ultraviolet-light". *Journal of the American Chemical Society*, **1981**, 103, 6893-6897.
33. Onoe, J.; Kawai, T. ; Kawai, S., "Peptide formation from amino-acid with particulate semiconductor photocatalysts". *Chemistry Letters*, **1985**, 1667-1670.
34. Fox, M. A. ; Chen, C. C., "Mechanistic features of the semiconductor photocatalyzed olefin-to-carbonyl oxidative cleavage". *Journal of the American Chemical Society*, **1981**, 103, 6757-6759.
35. Fox, M. A., "Organic heterogeneous photocatalysis: Chemical conversions sensitized by irradiated semiconductors". *Accounts of Chemical Research*, **1983**, 16, 314-321.
36. Fox, M. A. ; Abdelwahab, A. A., "Selectivity in the TiO<sub>2</sub>-mediated photocatalytic oxidation of thioethers". *Tetrahedron Letters*, **1990**, 31, 4533-4536.
37. Bahnemann, D. W.; Monig, J. ; Chapman, R., "Efficient photocatalysis of the irreversible one-electron and 2-electron reduction of halothane on platinized colloidal titanium-dioxide in aqueous suspension". *Journal of Physical Chemistry*, **1987**, 91, 3782-3788.
38. Ohtani, B.; Osaki, H.; Nishimoto, S. ; Kagiya, T., "Photocatalytic Formation of Schiff-Bases from Primary Amines by Platinized-TiO<sub>2</sub> Suspension in Acetonitrile". *Chemistry Letters*, **1985**, 1075-1078.
39. Ohtani, B.; Osaki, H.; Nishimoto, S. ; Kagiya, T., "A Novel Photocatalytic Process of Amine N-Alkylation by Platinized Semiconductor Particles Suspended in Alcohols". *Journal of the American Chemical Society*, **1986**, 108, 308-310.
40. Nishimoto, S. I.; Ohtani, B.; Yoshikawa, T. ; Kagiya, T., "Photocatalytic conversion of primary amines to secondary-amines and cyclization of polymethylene-alpha,omega-diamines by an aqueous suspension of TiO<sub>2</sub>/Pt". *Journal of the American Chemical Society*, **1983**, 105, 7180-7182.
41. Hopfner, M.; Weiss, H.; Meissner, D.; Heinemann, F. W. ; Kisch, H., "Semiconductor photocatalysis type B: synthesis of unsaturated alpha-amino esters from imines and olefins photocatalyzed by silica-supported cadmium sulfide". *Photochemical & Photobiological Sciences*, **2002**, 1, 696-703.
42. Pehlivanugullari, H. C.; Sumer, E. ; Kisch, H., "Semiconductor photocatalysis type B: synthesis of unsaturated alpha-cyano-homoallylamines from imines and olefins

- photocatalysed by silica- and cellulose-supported cadmium sulphide". *Research on Chemical Intermediates*, **2007**, 33, 297-309.
43. Cermenati, L.; Richter, C. ; Albini, A., "Solar light induced carbon-carbon bond formation via TiO<sub>2</sub> photocatalysis". *Chemical Communications*, **1998**, 805-806.
  44. Marinkovic, S.; Brule, C.; Hoffmann, N.; Prost, E.; Nuzillard, J. M. ; Bulach, W., "Origin of chiral induction in radical reactions with the diastereoisomers (5R)- and (5S)-5-l-menthyloxyfuran-2[5H]-one". *Journal of Organic Chemistry*, **2004**, 69, 1646-1651.
  45. Palmisano, L.; Augugliaro, V.; Bellardita, M.; Di Paola, A.; Lopez, E. G.; Loddo, V.; Marci, G.; Palmisano, G. ; Yurdakal, S., "Titania photocatalysts for selective oxidations in water". *Chemosuschem*, **2011**, 4, 1431-1438.
  46. Bard, A. J., "Photoelectrochemistry". *Science*, **1980**, 207, 139-144.
  47. Okura, I. ; Kaneko, M., "photocatalysis: science and technology". 2002, Verlag Berlin Heidelberg New York: *Springer*.
  48. Xu, Y. ; Schoonen, M. A. A., "The absolute energy positions of conduction and valence bands of selected semiconducting minerals". *American Mineralogist*, **2000**, 85, 543-556.
  49. Fox, M. A. ; Chanon, M., "Photoinduced electron transfer. Part A: Conceptual basis". 1988, New York: *Elsevier*.
  50. Zhang, Z. ; Yates, J. T. J., "Band bending in semiconductors: chemical and physical consequences at surfaces and interfaces.". *Chemical Reviews*, **2012**, in press.
  51. Krol, R. v. d., "Principles of Photoelectrochemical Cells", in "Photoelectrochemical Hydrogen Production", R.v.d. Krol and M. Grätzel, Editors. 2012, *Springer*: US.
  52. Gratzel, M., "Photoelectrochemical cells". *Nature*, **2001**, 414, 338-344.
  53. Munuera, G.; Gonzalezzeipe, A. R.; Soria, J. ; Sanz, J., "Photo-adsorption and photo-desorption of oxygen on highly hydroxylated TiO<sub>2</sub> surfaces .3. Role of H<sub>2</sub>O<sub>2</sub> in photo-desorption of O<sub>2</sub>". *Journal of the Chemical Society-Faraday Transactions I*, **1980**, 76, 1535-1546.
  54. Howe, R. F. ; Grätzel, M., "Electron-paramagnetic-res observation of trapped electrons in colloidal TiO<sub>2</sub>". *Journal of Physical Chemistry*, **1985**, 89, 4495-4499.
  55. Bahnemann, D. W.; Hilgendorff, M. ; Memming, R., "Charge carrier dynamics at TiO<sub>2</sub> particles: Reactivity of free and trapped holes". *Journal of Physical Chemistry B*, **1997**, 101, 4265-4275.
  56. Wang, C. Y.; Pagel, R.; Dohrmann, J. K. ; Bahnemann, D. W., "Antenna mechanism and deaggregation concept: novel mechanistic principles for photocatalysis". *Comptes Rendus Chimie*, **2006**, 9, 761-773.

- 
57. Wang, C. Y.; Pagel, R.; Dohrmann, J. K. ; Bahnemann, D. W., "Antenna mechanism and de-aggregation concept: Novel mechanistic principles for photocatalysis". *Materials Science Forum*, **2007**, 544-545, 17-22.
  58. Kormann, C.; Bahnemann, D. W. ; Hoffmann, M. R., "Preparation and characterization of quantum-size titanium-dioxide". *Journal of Physical Chemistry*, **1988**, 92, 5196-5201.
  59. Hoffman, A. J.; Yee, H.; Mills, G. ; Hoffmann, M. R., "Photoinitiated Polymerization of methyl-methacrylate Using Q-Sized ZnO Colloids". *Journal of Physical Chemistry*, **1992**, 96, 5540-5546.
  60. Fox, M. A., "Synthetic applications of photocatalytic oxidation and reduction reactions of organic reactants on irradiated semiconductor surfaces", in "Electron Transfer in Chemistry", V. Balzani, Editor. 2008, *Wiley-VCH Verlag GmbH, Weinheim: Germany*. p. 271-311.
  61. Kandiel, T. A.; Feldhoff, A.; Robben, L.; Dillert, R. ; Bahnemann, D. W., "Tailored titanium dioxide nanomaterials: Anatase nanoparticles and brookite nanorods as highly active photocatalysts". *Chemistry of Materials*, **2010**, 22, 2050-2060.
  62. Hirakawa, T.; Koga, C. F.; Negishi, N.; Takeuchi, K. ; Matsuzawa, S., "An approach to elucidating photocatalytic reaction mechanisms by monitoring dissolved oxygen: Effect of H<sub>2</sub>O<sub>2</sub> on photocatalysis". *Applied Catalysis B-Environmental*, **2009**, 87, 46-55.
  63. Jaeger, C. D. ; Bard, A. J., "Spin trapping and electron-spin resonance detection of radical intermediates in the photo-decomposition of water at TiO<sub>2</sub> particulate systems". *Journal of Physical Chemistry*, **1979**, 83, 3146-3152.
  64. Cunningham, J. ; Srijaranai, S., "Isotope-effect evidence for hydroxyl radical involvement in alcohol photo-oxidation sensitized by TiO<sub>2</sub> in aqueous suspension". *Journal of Photochemistry and Photobiology a-Chemistry*, **1988**, 43, 329-335.
  65. Kominami, H.; Iwasaki, S. I.; Maeda, T.; Imamura, K.; Hashimoto, K.; Kera, Y. ; Ohtani, B., "Photocatalytic reduction of nitrobenzene to aniline in an aqueous suspension of titanium(IV) oxide particles in the presence of oxalic acid as a hole scavenger and promotive effect of dioxygen in the system". *Chemistry Letters*, **2009**, 38, 410-411.
  66. Imamura, K.; Iwasaki, S.; Maeda, T.; Hashimoto, K.; Ohtani, B. ; Kominami, H., "Photocatalytic reduction of nitrobenzenes to aminobenzenes in aqueous suspensions of titanium(IV) oxide in the presence of hole scavengers under deaerated and aerated conditions". *Physical Chemistry Chemical Physics*, **2011**, 13, 5114-5119.
  67. Brezova, V.; Blazkova, A.; Surina, I. ; Havlinova, B., "Solvent effect on the photocatalytic reduction of 4-nitrophenol in titanium dioxide suspensions". *Journal of Photochemistry and Photobiology a-Chemistry*, **1997**, 107, 233-237.



68. Fox, M. A. ; Chanon, M., "Photoinduced electron transfer. part D: Photoinduced electron transfer reactions, inorganic substrates and applications". 1988, New York: *Elsevier*. 271-276.
69. Kraeutler, B. ; Bard, A. J., "Heterogeneous photocatalytic preparation of supported catalysts: Photodeposition of platinum on TiO<sub>2</sub> powder and other substrates". *Journal of the American Chemical Society*, **1978**, 100, 4317-4318.
70. Ismail, A. A. ; Bahnemann, D. W., "One-step synthesis of mesoporous platinum/titania nanocomposites as photocatalyst with enhanced photocatalytic activity for methanol oxidation". *Green Chemistry*, **2011**, 13, 428-435.
71. Kandiel, T. A.; Ismail, A. A. ; Bahnemann, D. W., "Mesoporous TiO<sub>2</sub> nanostructures: a route to minimize Pt loading on titania photocatalysts for hydrogen production". *Physical Chemistry Chemical Physics*, **2011**, 13, 20155-20161.
72. Tada, H.; Ishida, T.; Takao, A.; Ito, S.; Mukhopadhyay, S.; Akita, T.; Tanaka, K. ; Kobayashi, H., "Kinetic and DFT studies on the Ag/TiO<sub>2</sub>-photocatalyzed selective reduction of nitrobenzene to aniline". *Chemphyschem*, **2005**, 6, 1537-1543.
73. Tada, H.; Takao, A.; Akita, T. ; Tanaka, K., "Surface properties and photocatalytic activity of Pt-core/Ag-shell nanoparticle-loaded TiO<sub>2</sub>". *Chemphyschem*, **2006**, 7, 1687-1691.
74. Ohtani, B.; Pal, B. ; Ikeda, S., "Photocatalytic organic syntheses: selective cyclization of amino acids in aqueous suspensions". *Catalysis Surveys from Asia*, **2003**, 7, 165-176.
75. Shiraishi, Y. ; Hirai, T., "Selective organic transformations on titanium oxide-based photocatalysts". *Journal of Photochemistry and Photobiology C-Photochemistry Reviews*, **2008**, 9, 157-170.
76. Lang, X. J.; Ji, H. W.; Chen, C. C.; Ma, W. H. ; Zhao, J. C., "Selective Formation of Imines by Aerobic Photocatalytic Oxidation of Amines on TiO<sub>2</sub>". *Angewandte Chemie International Edition*, **2011**, 50, 3934-3937.
77. Park, K. H.; Joo, H. S.; Ahn, K. I. ; Jun, K., "One-Step Synthesis of 4-Ethoxy-1,2,3,4-Tetrahydroquinoline from Nitroarene and Ethanol - a TiO<sub>2</sub> Mediated Photocatalytic Reaction". *Tetrahedron Letters*, **1995**, 36, 5943-5946.
78. Hakki, A.; Dillert, R. ; Bahnemann, D., "Photocatalytic conversion of nitroaromatic compounds in the presence of TiO<sub>2</sub>". *Catalysis Today*, **2009**, 144, 154-159.
79. Zhang, T. Y.; You, L. Y. ; Zhang, Y. L., "Photocatalytic reduction of p-chloronitrobenzene on illuminated nano-titanium dioxide particles". *Dyes Pigm.*, **2006**, 68, 95-100.
80. Almquist, C. B. ; Biswas, P., "The photo-oxidation of cyclohexane on titanium dioxide: An investigation of competitive adsorption and its effects on product formation and selectivity". *Applied Catalysis a-General*, **2001**, 214, 259-271.

81. Mu, W.; Herrmann, J. M. ; Pichat, P., "Room-temperature photocatalytic oxidation of liquid cyclohexane into cyclohexanone over neat and modified TiO<sub>2</sub>". *Catalysis Letters*, **1989**, 3, 73-84.
82. Worsley, D.; Mills, A.; Smith, K. ; Hutchings, M. G., "Acid enhancement effect in the clean oxidation of toluenes photocatalyzed by TiO<sub>2</sub>". *Chemical Communications*, **1995**, 1119-1120.
83. Soana, F.; Sturini, M.; Cermenati, L. ; Albin, A., "Titanium dioxide photocatalyzed oxygenation of naphthalene and some of its derivatives". *Journal of the Chemical Society-Perkin Transactions 2*, **2000**, 4, 699-704.
84. Ohno, T.; Tokieda, K.; Higashida, S. ; Matsumura, M., "Synergism between rutile and anatase TiO<sub>2</sub> particles in photocatalytic oxidation of naphthalene". *Applied Catalysis a-General*, **2003**, 244, 383-391.
85. Higashida, S.; Harada, A.; Kawakatsu, R.; Fujiwara, N. ; Matsumura, M., "Synthesis of a coumarin compound from phenanthrene by a TiO<sub>2</sub>-photocatalyzed reaction". *Chemical Communications*, **2006**, 2804-2806.
86. Palmisano, G.; Addamo, M.; Augugliaro, V.; Caronna, T.; Garcia-Lopez, E.; Loddo, V. ; Palmisano, L., "Influence of the substituent on selective photocatalytic oxidation of aromatic compounds in aqueous TiO<sub>2</sub> suspensions". *Chemical Communications*, **2006**, 1012-1014.
87. Yoshida, H.; Yuzawa, H.; Aoki, M.; Otake, K.; Itoh, H. ; Hattori, T., "Photocatalytic hydroxylation of aromatic ring by using water as an oxidant". *Chemical Communications*, **2008**, 4634-4636.
88. Pavlik, J. W. ; Tantayanon, S., "Photocatalytic oxidations of lactams and N-acylamines". *Journal of the American Chemical Society*, **1981**, 103, 6755-6757.
89. Fox, M. A. ; Younathan, J. N., "Radical cation intermediates in the formation of Schiff-bases on irradiated semiconductor powders". *Tetrahedron*, **1986**, 42, 6285-6291.
90. Lang, X. J.; Ji, H. W.; Chen, C. C.; Ma, W. H. ; Zhao, J. C., "Selective formation of imines by aerobic photocatalytic oxidation of amines on TiO<sub>2</sub>". *Angewandte Chemie International Edition*, **2011**, 50, 3934-3937.
91. Tsukamoto, D.; Ikeda, M.; Shiraishi, Y.; Hara, T.; Ichikuni, N.; Tanaka, S. ; Hirai, T., "Selective photocatalytic oxidation of alcohols to aldehydes in water by TiO<sub>2</sub> partially coated with WO<sub>3</sub>". *Chemistry-a European Journal*, **2011**, 17, 9816-9824.
92. Wardman, P., "Reduction potentials of one-electron couples involving free-radicals in aqueous-solution". *Journal of Physical and Chemical Reference Data*, **1989**, 18, 1637-1755.
93. Kawai, T. ; Sakata, T., "Conversion of carbohydrate into hydrogen fuel by a photocatalytic process". *Nature*, **1980**, 286, 474-476.

94. Hussein, F. H.; Pattenden, G.; Rudham, R. ; Russell, J. J., "Photo-oxidation of alcohols catalyzed by platinized titanium-dioxide". *Tetrahedron Letters*, **1984**, 25, 3363-3364.
95. Hussein, F. H. ; Rudham, R., "Photocatalytic dehydrogenation of liquid propan-2-ol by platinized anatase and other catalysts". *Journal of the Chemical Society-Faraday Transactions I*, **1984**, 80, 2817-2825.
96. Wang, C. Y.; Pagel, R.; Bahnemann, D. W. ; Dohrmann, J. K., "Quantum yield of formaldehyde formation in the presence of colloidal TiO<sub>2</sub>-based photocatalysts: Effect of intermittent illumination, platinization, and deoxygenation". *Journal of Physical Chemistry B*, **2004**, 108, 14082-14092.
97. Furukawa, S.; Shishido, T.; Teramura, K. ; Tanaka, T., "Photocatalytic oxidation of alcohols over TiO<sub>2</sub> covered with Nb<sub>2</sub>O<sub>5</sub>". *Acs Catalysis*, **2012**, 2, 175-179.
98. Augugliaro, V.; Caronna, T.; Loddo, V.; Marci, G.; Palmisano, G.; Palmisano, L. ; Yurdakal, S., "Oxidation of aromatic alcohols in irradiated aqueous suspensions of commercial and home-prepared rutile TiO<sub>2</sub>: A selectivity study". *Chemistry-a European Journal*, **2008**, 14, 4640-4646.
99. Chen, J.; Ollis, D. F.; Rulkens, W. H. ; Bruning, H., "Photocatalyzed oxidation of alcohols and organochlorides in the presence of native TiO<sub>2</sub> and metallized TiO<sub>2</sub> suspensions. Part (I): Photocatalytic activity and pH influence". *Water Research*, **1999**, 33, 661-668.
100. Chen, J.; Ollis, D. F.; Rulkens, W. H. ; Bruning, H., "Photocatalyzed oxidation of alcohols and organochlorides in the presence of native TiO<sub>2</sub> and metallized TiO<sub>2</sub> suspensions. Part (II): Photocatalytic mechanisms". *Water Research*, **1999**, 33, 669-676.
101. Wang, C. Y.; Bottcher, C.; Bahnemann, D. W. ; Dohrmann, J. K., "In situ electron microscopy investigation of Fe(III)-doped TiO<sub>2</sub> nanoparticles in an aqueous environment". *Journal of Nanoparticle Research*, **2004**, 6, 119-122.
102. Wang, C. Y.; Groenzin, H. ; Shultz, M. J., "Competitive adsorption: Water and methanol on TiO<sub>2</sub> detected by sum frequency generation". *Abstracts of Papers of the American Chemical Society*, **2004**, 227, U811-U811.
103. Wang, C. Y.; Groenzin, H. ; Shultz, M. J., "Direct observation of competitive adsorption between methanol and water on TiO<sub>2</sub>: An in situ sum-frequency generation study". *Journal of the American Chemical Society*, **2004**, 126, 8094-8095.
104. Miyake, M.; Yoneyama, H. ; Tamura, H., "2 Step oxidation reactions of alcohols on an illuminated rutile electrode". *Chemistry Letters*, **1976**, 635-640.
105. Yamagata, S.; Nakabayashi, S.; Sancier, K. M. ; Fujishima, A., "Photocatalytic oxidation of alcohols on TiO<sub>2</sub>". *Bulletin of the Chemical Society of Japan*, **1988**, 61, 3429-3434.

106. Bahnemann, D.; Henglein, A.; Lilie, J. ; Spanhel, L., "Flash-photolysis observation of the absorption-spectra of trapped positive holes and electrons in colloidal TiO<sub>2</sub>". *Journal of Physical Chemistry*, **1984**, 88, 709-711.
107. Ohtani, B.; Kakimoto, M.; Nishimoto, S. ; Kagiya, T., "Photocatalytic reaction of neat alcohols by metal-loaded titanium(IV) oxide particles". *Journal of Photochemistry and Photobiology a-Chemistry*, **1993**, 70, 265-272.
108. Valenzuela, M. A.; Rios-Berny, O.; Flores, S. O. ; Cordova, I., "Synthesis of imines from nitrobenzene and TiO<sub>2</sub> particles suspended in alcohols via semiconductor photocatalysis type B". *Tetrahedron Letters*, **2010**, 51, 2730-2733.
109. Navio, J. A.; Marchena, F. J.; Roncel, M. ; Delarosa, M. A., "A laser flash-photolysis study of the reduction of methyl viologen by conduction-band electrons of TiO<sub>2</sub> and Fe-Ti oxide photocatalysts". *Journal of Photochemistry and Photobiology a-Chemistry*, **1991**, 55, 319-322.
110. Yamataka, H.; Seto, N.; Ichihara, J.; Hanafusa, T. ; Teratani, S., "Reduction of C-C multiple bonds Using an illuminated semiconductor catalyst". *Chemical Communications*, **1985**, 788-789.
111. Anpo, M.; Aikawa, N. ; Kubokawa, Y., "Photocatalytic hydrogenation of alkynes and alkenes with water over TiO<sub>2</sub>-Pt: Loading effect on the primary processes". *Journal of Physical Chemistry*, **1984**, 88, 3998-4000.
112. Anpo, M.; Aikawa, N.; Kodama, S. ; Kubokawa, Y., "Photocatalytic hydrogenation of alkynes and alkenes with water over TiO<sub>2</sub>. Hydrogenation accompanied by bond fission". *Journal of Physical Chemistry*, **1984**, 88, 2569-2572.
113. Brown, G. T. ; Darwent, J. R., "Photoreduction of methyl-orange sensitized by colloidal titanium-Dioxide". *Journal of the Chemical Society-Faraday Transactions I*, **1984**, 80, 1631-1643.
114. Ohtani, B.; Goto, Y.; Nishimoto, S. ; Inui, T., "Photocatalytic transfer hydrogenation of Schiff bases with propan-2-ol by suspended semiconductor particles loaded with platinum deposits". *Journal of the Chemical Society-Faraday Transactions*, **1996**, 92, 4291-4295.
115. Park, J. W.; Hong, M. J. ; Park, K. K., "Photochemical reduction of 1,2-diketones in the presence of TiO<sub>2</sub>". *Bulletin of the Korean Chemical Society*, **2001**, 22, 1213-1216.
116. Escobar, E. A.; Zapata, M. A. V.; Hernandez, S. A.; Valle, S. O. F.; Berny, O. R.; Angeles, V. J. G. ; Reyes, I. C., "Photocatalytic reduction of benzophenone on TiO<sub>2</sub>: Effect of preparation method and reaction conditions". *Journal of the Mexican Chemical Society*, **2010**, 54, 133-138.
117. Joycepruden, C.; Pross, J. K. ; Li, Y. Z., "Photoinduced reduction of aldehydes on titanium-dioxide". *Journal of Organic Chemistry*, **1992**, 57, 5087-5091.

118. Kraeutler, B. ; Bard, A. J., "Heterogeneous photocatalytic synthesis of methane from acetic-acid: New Kolbe reaction pathway". *Journal of the American Chemical Society*, **1978**, 100, 2239-2240.
119. Ohtani, B.; Iwai, K.; Nishimoto, S. ; Sato, S., "Role of platinum deposits on titanium(IV) oxide particles: Structural and kinetic analyses of photocatalytic reaction in aqueous alcohol and amino acid solutions". *Journal of Physical Chemistry B*, **1997**, 101, 3349-3359.
120. Mahdavi, F.; Bruton, T. C. ; Li, Y. Z., "Photoinduced reduction of nitro-compounds on semiconductor particles". *Journal of Organic Chemistry*, **1993**, 58, 744-746.
121. Kemula, W. ; Krygowski, T. M., "Nitro compounds", in "Encyclopedia of electrochemistry", A.J. Bard and H.E. Lund, Editors. 1979, *M. Dekker*: New York. p. 77-130.
122. Ferry, J. L. ; Glaze, W. H., "Photocatalytic reduction of nitro organics over illuminated titanium dioxide: Role of the TiO<sub>2</sub> surface". *Langmuir*, **1998**, 14, 3551-3555.
123. Zhang, T. Y.; You, L. Y. ; Zhang, Y. L., "Photocatalytic reduction of *p*-chloronitrobenzene on illuminated nano-titanium dioxide particles". *Dyes and Pigments*, **2006**, 68, 95-100.
124. Imamura, K.; Hashimoto, K. ; Kominami, H., "Chemoselective reduction of nitrobenzenes to aminobenzenes having reducible groups by a titanium(IV) oxide photocatalyst under gas- and metal-free conditions". *Chemical Communications*, **2012**, 48, 4356-4358.
125. Tada, H.; Ishida, T.; Takao, A. ; Ito, S., "Drastic enhancement of TiO<sub>2</sub>-photocatalyzed reduction of nitrobenzene by loading Ag clusters". *Langmuir*, **2004**, 20, 7898-7900.
126. Shiraishi, Y.; Ikeda, M.; Tsukamoto, D.; Tanaka, S. ; Hirai, T., "One-pot synthesis of imines from alcohols and amines with TiO<sub>2</sub> loading Pt nanoparticles under UV irradiation". *Chemical Communications*, **2011**, 47, 4811-4813.
127. Shiraishi, Y.; Sugano, Y.; Tanaka, S. ; Hirai, T., "One-pot synthesis of benzimidazoles by simultaneous photocatalytic and catalytic reactions on Pt/TiO<sub>2</sub> nanoparticles". *Angewandte Chemie-International Edition*, **2010**, 49, 1656-1660.
128. Denmark, S. E. ; Venkatraman, S., "On the mechanism of the Skraup-Doebner-Von Miller quinoline synthesis". *Journal of Organic Chemistry*, **2006**, 71, 1668-1676.
129. Marco-Contelles, J.; Perez-Mayoral, E.; Samadi, A.; Carreiras, M. D. ; Soriano, E., "Recent Advances in the Friedlander Reaction". *Chemical Reviews*, **2009**, 109, 2652-2671.
130. Li, L. ; Jones, W. D., "Mechanistic investigation of the cobalt-catalyzed selective conversion of diallylanilines to quinolines involving C-N and C-H activations". *Journal of the American Chemical Society*, **2007**, 129, 10707-10713.

131. Byun, E.; Hong, B.; De Castro, K. A.; Lim, M. ; Rhee, H., "One-Pot Reductive mono-*N*-alkylation of aniline and nitroarene derivatives using aldehydes". *Journal of Organic Chemistry*, **2007**, 72, 9815-9817.
132. Cho, C. S.; Kim, D. T.; Kim, T. J. ; Shim, S. C., "Ruthenium-catalyzed synthesis of quinolines from anilines and tris(3-hydroxypropyl)amine via amine exchange reaction". *Bulletin of the Korean Chemical Society*, **2003**, 24, 1026-1028.
133. Glushkov, V. A. ; Tolstikov, A. G., "Synthesis of substituted 1,2,3,4-tetrahydroquinolines by the Povarov reaction. New potential of a classical reaction". *Uspekhi Khimii*, **2008**, 77, 138-160.
134. Blank, B.; Madalska, M. ; Kempe, R., "An efficient method for the selective iridium-catalyzed monoalkylation of (hetero)aromatic amines with primary alcohols". *Advanced Synthesis & Catalysis*, **2008**, 350, 749-758.
135. Guillena, G.; Ramon, D. J. ; Yus, M., "Hydrogen autotransfer in the *N*-alkylation of amines and related compounds using alcohols and amines as electrophiles". *Chemical Reviews*, **2010**, 110, 1611-1641.
136. Ismail, A. A.; Bahnemann, D. W.; Robben, L.; Yarovy, V. ; Wark, M., "Palladium doped porous titania photocatalysts: impact of mesoporous order and crystallinity". *Chemistry of Materials*, **2010**, 22, 108-116.
137. Kraeutler, B. ; Bard, A. J., "Heterogeneous photocatalytic preparation of supported catalysts - photodeposition of platinum on TiO<sub>2</sub> powder and other substrates". *Journal of the American Chemical Society*, **1978**, 100, 4317-4318.
138. Green, I. X.; Buda, C.; Zhang, Z.; Neurock, M. ; Yates, J. T., "IR spectroscopic measurement of diffusion kinetics of chemisorbed pyridine through TiO<sub>2</sub> Particles". *Journal of Physical Chemistry C*, **2010**, 114, 16649-16659.
139. Kim, S.; Wang, X. Y.; Buda, C.; Neurock, M.; Koper, O. B. ; Yates, J. T., "IR Spectroscopic measurement of diffusion kinetics of chemisorbed pyridine through nanocrystalline MgO Particles. The involvement of surface defect sites in slow diffusion". *Journal of Physical Chemistry C*, **2009**, 113, 2219-2227.
140. Wang, X. C.; Yu, J. C.; Liu, P.; Wang, X. X.; Su, W. Y. ; Fu, X. Z., "Probing of photocatalytic surface sites on SO<sub>4</sub><sup>2-</sup>/TiO<sub>2</sub> solid acids by in situ FT-IR spectroscopy and pyridine adsorption". *Journal of Photochemistry and Photobiology a-Chemistry*, **2006**, 179, 339-347.
141. Bezrodna, T.; Puchkovska, G.; Shimanovska, V.; Chashechnikova, I.; Khalyavka, T. ; Baran, J., "Pyridine-TiO<sub>2</sub> surface interaction as a probe for surface active centers analysis". *Applied Surface Science*, **2003**, 214, 222-231.
142. Kulkarni, A. P. ; Muggli, D. S., "The effect of water on the acidity of TiO<sub>2</sub> and sulfated titania". *Applied Catalysis a-General*, **2006**, 302, 274-282.

143. Green, I. X.; Buda, C.; Zhang, Z.; Neurock, M. ; Yates, J. T., "IR spectroscopic measurement of diffusion kinetics of chemisorbed pyridine through TiO<sub>2</sub> particles". *Journal of Physical Chemistry C*, **2010**, 114, 16649-16659.
144. Bello, D.; Ramon, R. ; Lavilla, R., "Mechanistic variations of the Povarov multicomponent reaction and related processes". *Current Organic Chemistry*, **2010**, 14, 332-356.
145. Ikeda, S.; Kobayashi, H.; Ikoma, Y.; Harada, T.; Torimoto, T.; Ohtani, B. ; Matsumura, M., "Size-selective photocatalytic reactions by titanium(IV) oxide coated with a hollow silica shell in aqueous solutions". *Physical Chemistry Chemical Physics*, **2007**, 9, 6319-6326.
146. Oki, A. R.; Xu, Q.; Shpeizer, B.; Clearfield, A.; Qiu, X.; Kirumakki, S. ; Tichy, S., "Synthesis, characterization and activity in cyclohexene epoxidation of mesoporous TiO<sub>2</sub>-SiO<sub>2</sub> mixed oxides". *Catalysis Communications*, **2007**, 8, 950-956.
147. Kim, Y. K.; Kim, E. Y.; Whang, C. M.; Kim, Y. H. ; Lee, W. I., "Microstructure and photocatalytic property of SiO<sub>2</sub>-TiO<sub>2</sub> under various process condition". *Journal of Sol-Gel Science and Technology*, **2005**, 33, 87-91.
148. Zhao, D. Y.; Feng, J. L.; Huo, Q. S.; Melosh, N.; Fredrickson, G. H.; Chmelka, B. F. ; Stucky, G. D., "Triblock copolymer syntheses of mesoporous silica with periodic 50 to 300 angstrom pores". *Science*, **1998**, 279, 548-552.
149. Clark, J. H., "Solid acids for green chemistry". *Accounts of Chemical Research*, **2002**, 35, 791-797.
150. Mbaraka, I. K. ; Shanks, B. H., "Acid strength variation due to spatial location of organosulfonic acid groups on mesoporous silica". *Journal of Catalysis*, **2006**, 244, 78-85.
151. Liu, J.; Yang, Q. H.; Kapoor, M. P.; Setoyama, N.; Inagaki, S.; Yang, J. ; Zhang, L., "Structural relation properties of hydrothermally stable functionalized mesoporous organosilicas and catalysis". *Journal of Physical Chemistry B*, **2005**, 109, 12250-12256.
152. Jackson, M. A.; Mbaraka, I. K. ; Shanks, B. H., "Esterification of oleic acid in supercritical carbon dioxide catalyzed by functionalized mesoporous silica and an immobilized lipase". *Applied Catalysis a-General*, **2006**, 310, 48-53.
153. Rac, B.; Molnar, A.; Forgo, P.; Mohai, M. ; Bertoti, I., "A comparative study of solid sulfonic acid catalysts based on various ordered mesoporous silica materials". *Journal of Molecular Catalysis A-Chemical*, **2006**, 244, 46-57.
154. Dufaud, V. ; Davis, M. E., "Design of heterogeneous catalysts via multiple active site positioning in organic-inorganic hybrid materials". *Journal of the American Chemical Society*, **2003**, 125, 9403-9413.

155. Das, D.; Lee, J. F. ; Cheng, S. F., "Sulfonic acid functionalized mesoporous MCM-41 silica as a convenient catalyst for Bisphenol-A synthesis". *Chemical Communications*, **2001**, 2178-2179.
156. Van Rhijn, W. M.; De Vos, D. E.; Sels, B. F.; Bossaert, W. D. ; Jacobs, P. A., "Sulfonic acid functionalised ordered mesoporous materials as catalysts for condensation and esterification reactions". *Chemical Communications*, **1998**, 317-318.
157. Melero, J. A.; Stucky, G. D.; van Grieken, R. ; Morales, G., "Direct syntheses of ordered SBA-15 mesoporous materials containing arenesulfonic acid groups". *Journal of Materials Chemistry*, **2002**, 12, 1664-1670.
158. Wang, X. G.; Cheng, S. F.; Chan, J. C. C. ; Chao, J. C. H., "Template-free synthesis of mesoporous phenylsulfonic acid functionalized silica". *Microporous and Mesoporous Materials*, **2006**, 96, 321-330.
159. Xu, Z. P. ; Braterman, P. S., "High affinity of dodecylbenzene sulfonate for layered double hydroxide and resulting morphological changes". *Journal of Materials Chemistry*, **2003**, 13, 268-273.
160. Pejov, L.; Ristova, M. ; Soptrajanov, B., "Quantum chemical study of *p*-toluenesulfonic acid, *p*-toluenesulfonate anion and the water-*p*-toluenesulfonic acid complex. Comparison with experimental spectroscopic data". *Spectrochimica Acta Part A-Molecular and Biomolecular Spectroscopy*, **2011**, 79, 27-34.
161. Yang, Q. H.; Kapoor, M. P.; Shirokura, N.; Ohashi, M.; Inagaki, S.; Kondo, J. N. ; Domen, K., "Ethane-bridged hybrid mesoporous functionalized organosilicas with terminal sulfonic groups and their catalytic applications". *Journal of Materials Chemistry*, **2005**, 15, 666-673.
162. Bibent, N.; Mehdi, A.; Silly, G.; Henn, F. ; Devautour-Vinot, S., "Proton conductivity versus acidic strength of one-pot synthesized acid-functionalized SBA-15 mesoporous silica". *European Journal of Inorganic Chemistry*, **2011**, 3214-3225.
163. Zhao, W.; Salame, P.; Launay, F.; Gedeon, A. ; Hao, Z., "Sulfonic acid functionalised SBA-15 as catalysts for Beckmann rearrangement and esterification reaction". *Journal of Porous Materials*, **2008**, 15, 139-143.
164. Agrawal, A. ; Tratnyek, P. G., "Reduction of nitro aromatic compounds by zero-valent iron metal". *Environmental Science & Technology*, **1996**, 30, 153-160.
165. Schwarz, H. A. ; Dodson, R. W., "Reduction potentials of CO<sub>2</sub><sup>-</sup> and the alcohol radicals". *Journal of Physical Chemistry*, **1989**, 93, 409-414.
166. Jagannadham, V. ; Ststeenken, "One-electron reduction of nitrobenzenes by alpha-hydroxyalkyl radicals via addition elimination - an example of an organic inner-sphere electron-transfer reaction". *Journal of the American Chemical Society*, **1984**, 106, 6542-6551.

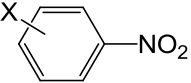
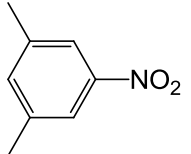
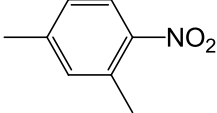
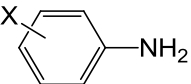
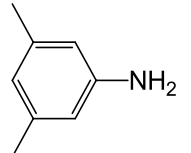
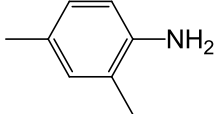
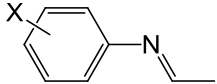


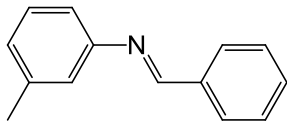
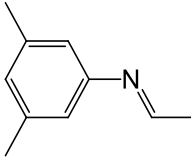
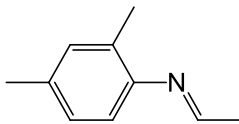
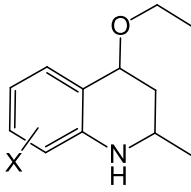
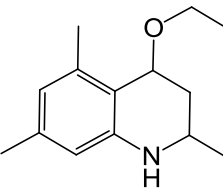
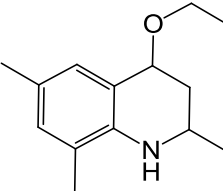
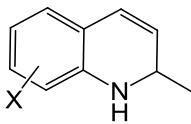
167. Panayotov, D. A.; Burrows, S. P. ; Morris, J. R., "Photooxidation mechanism of methanol on rutile TiO<sub>2</sub> nanoparticles". *Journal of Physical Chemistry C*, **2012**, 116, 6623-6635.
168. Kavan, L.; Gratzel, M.; Gilbert, S. E.; Klemenz, C. ; Scheel, H. J., "Electrochemical and photoelectrochemical investigation of single-crystal anatase". *Journal of the American Chemical Society*, **1996**, 118, 6716-6723.
169. Kwon, M. S.; Kim, S.; Park, S.; Bosco, W.; Chidrala, R. K. ; Park, J., "One-pot synthesis of imines and secondary amines by Pd-catalyzed coupling of benzyl alcohols and primary amines". *Journal of Organic Chemistry*, **2009**, 74, 2877-2879.
170. Weingart, H.; Chupp, J. P. ; White, W. A., "Ketimine Syntheses . Use of Titanium Tetrachloride in a New Procedure for Their Preparation". *Journal of Organic Chemistry*, **1967**, 32, 3246-&.
171. Forrest, T. P.; Dauphinee, G. A. ; Miles, W. F., "On the mechanism of Doebner-Miller reaction". *Canadian Journal of Chemistry*, **1969**, 47, 2121.
172. Jia, C. S.; Zhang, Z.; Tu, S. J. ; Wang, G. W., "Rapid and efficient synthesis of poly-substituted quinolines assisted by p-toluene sulphonic acid under solvent-free conditions: comparative study of microwave irradiation versus conventional heating". *Organic & Biomolecular Chemistry*, **2006**, 4, 104-110.
173. Povarov, L. S., "α,β-Unsaturated ethers and their analogues in reactions of diene synthesis". *Russian Chemical Reviews*, **1967**, 36, 656-670.
174. Geng, X.; Li, S. S.; Bian, X. Q.; Xie, Z. Y. ; Wang, C. D., "TMSCl-Catalyzed synthesis of substituted quinolines from arylimines and enolizable aldehydes". *Arkivoc*, **2008**, 50-57.
175. He, L.; Wang, J. Q.; Gong, Y.; Liu, Y. M.; Cao, Y.; He, H. Y. ; Fan, K. N., "Titania-supported iridium subnanoclusters as an efficient heterogeneous catalyst for direct synthesis of quinolines from nitroarenes and aliphatic alcohols". *Angewandte Chemie International Edition*, **2011**, 50, 10216-10220.
176. Luo, S. C. ; Falconer, J. L., "Aldol condensation of acetaldehyde to form high molecular weight compounds on TiO<sub>2</sub>". *Catalysis Letters*, **1999**, 57, 89-93.
177. Luo, S. C. ; Falconer, J. L., "Acetone and acetaldehyde oligomerization on TiO<sub>2</sub> surfaces". *Journal of Catalysis*, **1999**, 185, 393-407.
178. Idriss, H. ; Barteau, M. A., "Selectivity and mechanism shifts in the reactions of acetaldehyde on oxidized and reduced TiO<sub>2</sub>(001) surfaces". *Catalysis Letters*, **1996**, 40, 147-153.
179. Forrest, T. P.; Dauphinee, G. A. ; Deraniyagala, S. A., "On the mechanism of disproportionation reactions of 1,2-dihydroquinolines". *Canadian Journal of Chemistry*, **1985**, 63, 412-415.

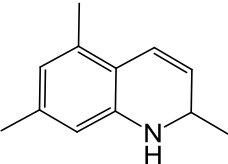
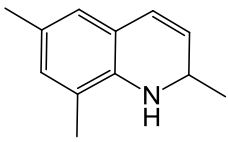
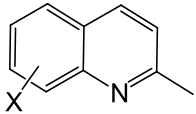
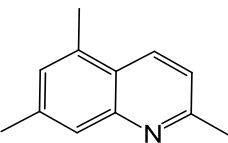
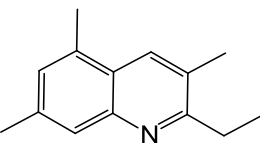
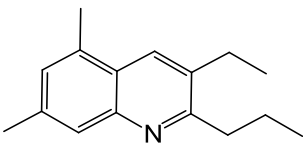
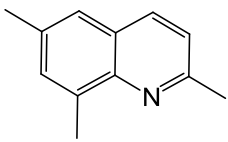
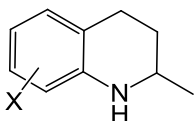
- 
180. Forrest, T. P.; Dauphinee, G. A. ; Miles, W. F., "Mechanism and stereochemistry of the hydrolysis of 4-arylamino-1,2,3,4-tetrahydroquinolines". *Canadian Journal of Chemistry*, **1973**, 52.
  181. Shiraishi, Y.; Ikeda, M.; Tsukamoto, D.; Tanaka, S. ; Hirai, T., "One-pot synthesis of imines from alcohols and amines with TiO<sub>2</sub> loading Pt nanoparticles under UV irradiation". *Chemical Communications*, **2011**, 47, 4811-4813.
  182. Michaelson, H. B., "Work function of elements and its periodicity". *Journal of Applied Physics*, **1977**, 48, 4729-4733.
  183. Mascaro, L. H.; Santos, M. C.; Machado, S. A. S. ; Avaca, L. A., "Underpotential deposition of silver on polycrystalline platinum studied by cyclic voltammetry and rotating ring-disc techniques". *Journal of the Chemical Society-Faraday Transactions*, **1997**, 93, 3999-4003.

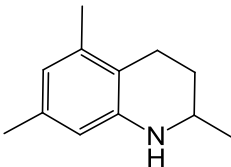
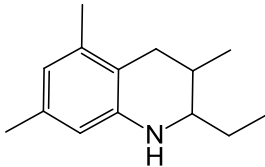
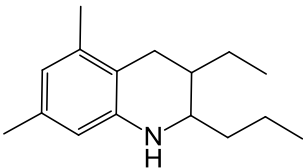
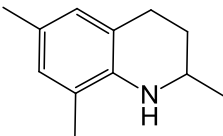
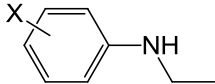
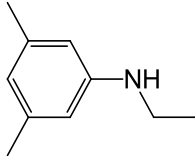
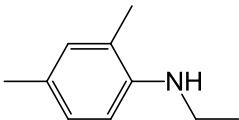
## 7 Appendix

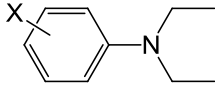
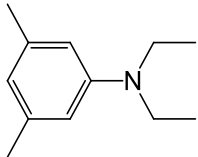
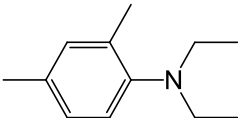
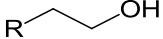
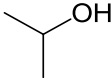
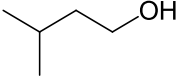
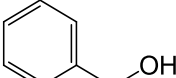
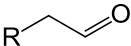
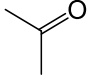
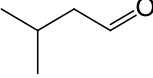
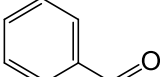
### 7.1 Names, structures, and abbreviations of the studied and the produced compounds

Compound	Substituent	Name	Symbol
	X = <i>m</i> -CH <sub>3</sub>	<i>m</i> -nitrotoluene	<b>1a</b>
	<i>p</i> -CH <sub>3</sub>	<i>p</i> -nitrotoluene	<b>2a</b>
	<i>o</i> -CH <sub>3</sub>	<i>o</i> -nitrotoluene	<b>3a</b>
	H	nitrobenzene	<b>4a</b>
	<i>m</i> -CH=CH <sub>2</sub>	3-vinyl-1-nitrobenzene	<b>5a</b>
		3,5-dimethyl-1-nitrobenzene	<b>6a</b>
		2,4-dimethyl-1-nitrobenzene	<b>7a</b>
	X = <i>m</i> -CH <sub>3</sub>	<i>m</i> -toluidine	<b>1c</b>
	<i>p</i> -CH <sub>3</sub>	<i>p</i> -toluidine	<b>2c</b>
	<i>o</i> -CH <sub>3</sub>	<i>o</i> -toluidine	<b>3c</b>
	H	aniline	<b>4c</b>
	<i>m</i> -CH=CH <sub>2</sub>	3-vinylaniline	<b>5c</b>
		3,5-dimethyl-1-nitrobenzene	<b>6c</b>
		2,4-dimethyl-1-nitrobenzene	<b>7c</b>
	X = <i>m</i> -CH <sub>3</sub>	<i>N</i> -ethylidene-3-methylaniline	<b>1f</b>
	<i>p</i> -CH <sub>3</sub>	<i>N</i> -ethylidene-4-methylaniline	<b>2f</b>
	<i>o</i> -CH <sub>3</sub>	<i>N</i> -ethylidene-2-methylaniline	<b>3f</b>
	H	<i>N</i> -ethylideneaniline	<b>4f</b>

	$m\text{-CH=CH}_2$	3-vinylaniline	<b>5f</b>
		N-benzylidene-3-methylaniline	<b>6f</b>
		3,5-dimethyl-1-nitrobenzene	<b>7f</b>
		2,4-dimethyl-1-nitrobenzene	<b>8f</b>
	X = $m\text{-CH}_3$	4-ethoxy-2,7-dimethyl-1,2,3,4-tetrahydroquinoline	<b>1g</b>
	$p\text{-CH}_3$	4-ethoxy-2,6-dimethyl-1,2,3,4-tetrahydroquinoline	<b>2g</b>
	$o\text{-CH}_3$	4-ethoxy-2,8-dimethyl-1,2,3,4-tetrahydroquinoline	<b>3g</b>
	H	4-ethoxy-2-methyl-1,2,3,4-tetrahydroquinoline	<b>4g</b>
	$m\text{-CH=CH}_2$	4-ethoxy-2-methyl-7-vinyl-1,2,3,4-tetrahydroquinoline	<b>5g</b>
		4-ethoxy-2,5,7-trimethyl-1,2,3,4-tetrahydroquinoline	<b>6g</b>
		4-ethoxy-2,6,8-trimethyl-1,2,3,4-tetrahydroquinoline	<b>7g</b>
	X = $m\text{-CH}_3$	2,7-dimethyl-1,2-dihydroquinoline	<b>1i</b>
	$p\text{-CH}_3$	2,6-dimethyl-1,2-dihydroquinoline	<b>2i</b>
	$o\text{-CH}_3$	2,8-dimethyl-1,2-dihydroquinoline	<b>3i</b>

	H	2-methyl dimethyl-1,2-dihydroquinoline	<b>4i</b>
	<i>m</i> -CH=CH <sub>2</sub>	2-methyl-7-vinyl-1,2-dihydroquinoline	<b>5i</b>
		2,5,7-trimethyl-1,2-dihydroquinoline	<b>6i</b>
		2,6,8-trimethyl-1,2-dihydroquinoline	<b>7i</b>
	X = <i>m</i> -CH <sub>3</sub>	2,7-dimethylquinoline	<b>1j</b>
	<i>p</i> -CH <sub>3</sub>	2,6-dimethylquinoline	<b>2j</b>
	<i>o</i> -CH <sub>3</sub>	2,8-dimethylquinoline	<b>3j</b>
	H	2-methylquinoline	<b>4j</b>
	<i>m</i> -CH=CH <sub>2</sub>	2-methyl-7-vinylquinoline	<b>5j</b>
		2,5,7-trimethylquinoline	<b>6j</b>
		2-ethyl-3,5,7-trimethylquinoline	<b>7j</b>
		3-ethyl-5,7-dimethyl-2-propylquinoline	<b>8j</b>
		2,6,8-trimethylquinoline	<b>9j</b>
	X = <i>m</i> -CH <sub>3</sub>	2,7-dimethyl-1,2,3,4-tetrahydroquinoline	<b>1k</b>
	<i>p</i> -CH <sub>3</sub>	2,6-dimethyl-1,2,3,4-	<b>2k</b>

		tetrahydroquinoline	
<i>o</i> -CH <sub>3</sub>		2,8-dimethyl-1,2,3,4-tetrahydroquinoline	<b>3k</b>
H		2-methyl-1,2,3,4-tetrahydroquinoline	<b>4k</b>
<i>m</i> -CH=CH <sub>2</sub>		2-methyl-7-vinyl-1,2,3,4-tetrahydroquinoline	<b>5k</b>
		2,5,7-trimethyl-1,2,3,4-tetrahydroquinoline	<b>6k</b>
		2-ethyl-3,5,7-trimethyl-1,2,3,4-tetrahydroquinoline	<b>7k</b>
		3-ethyl-5,7-dimethyl-2-propyl-1,2,3,4-tetrahydroquinoline	<b>8k</b>
		2,6,8-trimethyl-1,2,3,4-tetrahydroquinoline	<b>9k</b>
	X = <i>m</i> -CH <sub>3</sub>	<i>N</i> -ethyl- <i>m</i> -toluidine	<b>11</b>
	<i>p</i> -CH <sub>3</sub>	<i>N</i> -ethyl- <i>p</i> -toluidine	<b>21</b>
	<i>o</i> -CH <sub>3</sub>	<i>N</i> -ethyl- <i>o</i> -toluidine	<b>31</b>
	H	<i>N</i> -ethylaniline	<b>41</b>
	<i>m</i> -CH=CH <sub>2</sub>	<i>N</i> -ethyl-3-vinylaniline	<b>51</b>
	<i>m</i> -C <sub>2</sub> H <sub>5</sub>	<i>N</i> -ethyl-3-ethylaniline	<b>61</b>
		<i>N</i> -ethyl-3,5-dimethylaniline	<b>71</b>
		<i>N</i> -ethyl-2,4-dimethylaniline	<b>81</b>

	X = <i>m</i> -CH <sub>3</sub>	<i>N,N</i> -diethyl- <i>m</i> -toluidine	<b>1m</b>
	<i>p</i> -CH <sub>3</sub>	<i>N,N</i> -diethyl- <i>p</i> -toluidine	<b>2m</b>
	<i>o</i> -CH <sub>3</sub>	<i>N,N</i> -diethyl- <i>o</i> -toluidine	<b>3m</b>
	H	<i>N,N</i> -diethyl-aniline	<b>4m</b>
	<i>m</i> -CH=CH <sub>2</sub>	<i>N,N</i> -diethyl-3-vinylaniline	<b>5m</b>
	<i>m</i> -C <sub>2</sub> H <sub>5</sub>	<i>N,N</i> -diethyl-3-ethylaniline	<b>6m</b>
		<i>N,N</i> -diethyl-3,5-dimethylaniline	<b>7m</b>
		<i>N,N</i> -diethyl-2,4-dimethylaniline	<b>8m</b>
	R = H	ethanol	<b>1b</b>
	CH <sub>3</sub>	<i>n</i> -propanol	<b>2b</b>
	C <sub>2</sub> H <sub>5</sub>	<i>n</i> -butanol	<b>3b</b>
		<i>i</i> -propanol	<b>4b</b>
		3-methylbutanol	<b>5b</b>
		benzylalcohol	<b>6b</b>
	R = H	acetaldehyde	<b>1d</b>
	CH <sub>3</sub>	propionaldehyde	<b>2d</b>
	C <sub>2</sub> H <sub>5</sub>	butyraldehyde	<b>3d</b>
		acetone	<b>4d</b>
		3-methylbutanal	<b>5d</b>
		benzaldehyde	<b>6d</b>

## 7.2 List of abbreviations and symbols

A	Electron acceptor
A	Anatase
a.u.	Arbitrary unit
Ar	Argon
BET	Brunauer-Emmett-Teller
con.	Concentration
CB	Conduction band
cf.	Latin: confer (English: compare)
cm	Centimeter
$c_0$	Initial concentration
$^{\circ}\text{C}$	Degres Celsius
d	Diameter
D	Electron donor
DF-TEM	Dark-field transmission electron microscopy
DTA	Differential thermal analysis
E	Energy
$E_{\text{CB}}$	Conduction band potential
$E_f$	Fermi level energy
$E_g$	Bandgap energy
$E_{\text{red}}$	Standard redox potential
EDXS	Energy dispersive X-ray spectroscopy
e	Electron
et al.	Latin: et alii (English: and others)
eV	Electron volt
e.g.	Latin: exempli gratia (English: for example)
FT-IR	Infrared spectroscopy
g	Gram
GC	Gas chromatography
GC-FID	Gas chromatography-flame ionization detector
GC-MS	Gas chromatography-mass spectroscopy
h	Hour
h	Planck constant
$h^+$	Valence band hole
HRTEM	High resolution transmission electron microscopy
i. e.	Latin: id est (English: that is)
k	Rate konstant
kV	Kilovolt
l	Liter
M	Molar (moles per liter)
mM	Millimolar (millimoles per liter)
mg	Milligram
mol	Mole



---

mmol	Millimole
ml	Milliliter
mW	Milliwatt
min	Minute
NAC	Nitroaromatic compound
NHE	Normal hydrogen electrode
nm	Nanometer
NMR	Nuclear magnetic resonance
R	Rutile
T	Temperature
TCD	Thermal conductivity detector
TEM	Transmission electron microscopy
V	Volt
VB	Valence band
UV	Ultraviolet light
UV(A)	Near ultraviolet light (315-380 nm)
UV-Vis	Ultraviolet and visible light
W	Watt
wt%	Weight percentage
XRD	X-ray diffraction
$\lambda$	Wavelength
$\mu\text{l}$	microliter
$\mu\text{mol}$	Micromole
$\nu$	Frequency
$\zeta$	Photonic efficiency

---

### 7.3 Publications

A. Hakki, C. Hachem, M.A. Monajed, F. Karabet, "Photocatalytic Degradation of Phenolic Compounds in Olive Mill Wastewater". *Damascus University Journal for the Basic Sciences* 20 (2004) 155-175

A. Hakki, R. Dillert, D. Bahnemann, "Photocatalytic Conversion of Nitroaromatic Compounds in the Presence of TiO<sub>2</sub>". *Catalysis Today* 144 (2009) 154–159

A. A. Ismail, A. Hakki, D. Bahnemann, "Mesostructure Au/TiO<sub>2</sub> Nanocomposites for Highly Efficient Catalytic Reduction of *p*-Nitrophenol". *Journal of Molecular Catalysis A: Chemical* 358 (2012) 145–151

A. Hakki, R. Dillert, D. Bahnemann, "Factors Affecting the Selectivity of the Photocatalytic Conversion of Nitroaromatic Compounds over TiO<sub>2</sub> to Valuable Nitrogen Containing Organic Compounds". *Physical Chemistry Chemical Physics*. 15 (2013) 2992-3002.

A. Hakki, R. Dillert, D. Bahnemann, "Arenesulfonic Acid Functionalized Mesoporous Silica Decorated with Titania: A New Efficient Heterogeneous Catalyst for the One-pot Photocatalytic Synthesis of Quinolines from Nitroaromatic Compounds and Alcohols". *ACS Catalysis*. 3 (2013) 565–572.

## 7.4 Presentations

A. Hakki, R. Dillert, D. Bahnemann, “Photocatalytic One-pot N-alkylation of Nitroaromatic Compounds Using Pt/TiO<sub>2</sub>”. Oral presentation at Symposium D: Novel synthesis processes and design of nanomaterials for catalytic applications, E-MRS Fall Meeting, **2008**, (Warsaw).

A. Hakki, R. Dillert, D. Bahnemann, “Controlling the Selectivity of Photocatalytic N-Alkylation of Nitroaromatic Compounds Using Pt/TiO<sub>2</sub>”. Oral presentation at 6<sup>o</sup> European Meeting on Solar Chemistry and Photocatalysis: Environmental Applications SPEA 6, **2010**, (Prague)

A. Hakki, R. Dillert, D. Bahnemann, “Photocatalytic One-Pot Synthesis of Alkylated Quinolines Mediated by TiO<sub>2</sub>/SiO<sub>2</sub>”. Oral presentation at GDCh Wissenschaftsforum Chemie **2011**, (Bremen)

A. Hakki, R. Dillert, D. Bahnemann, “Photocatalytic Conversion of Nitroaromatic Compounds in the Presence of TiO<sub>2</sub>”. Poster presentation at 5<sup>o</sup> European Meeting on Solar Chemistry and Photocatalysis: Environmental Applications SPEA5, **2008**, (Palermo)

A. Hakki, R. Dillert, D. Bahnemann, “Effect of Photodeposited Metal Nanoparticles on the Selectivity of the Photocatalytic Conversion of Nitroaromatic Compounds over TiO<sub>2</sub>”. Poster presentation at Photocatalytic Products and Technologies Conference - PPTC'09, **2009**, (Portugal).

A. Hakki, R. Dillert, D. Bahnemann, “Photocatalytic One-Pot Synthesis of Polyalkylated Quinolines Mediated By TiO<sub>2</sub>”. Poster presentation at ICP2009. XXIV International Conference on Photochemistry, **2009**, (Toledo)

A. Hakki, R. Dillert, D. Bahnemann, “Selectivity of the Photocatalytic One-pot Organic Synthesis Using Modified TiO<sub>2</sub>”. Poster presentation at 2<sup>nd</sup> European Symposium on Photocatalysis JEP **2011**, (Bordeux).

## 7.5 Curriculum vitae

### Personals

<b>Name</b>	Amer Hakki
<b>Date of Birth</b>	08.01.1978
<b>Gender</b>	Male
<b>Nationality</b>	Syrian

### Academic qualifications

**2007-2013** PhD student, Institut für Technische Chemie, Gottfried Wilhelm Leibniz Universität Hannover, Germany. *“Novel Photocatalytic Organic Synthesis: Cyclization and N-alkylation of Nitroaromatic Compounds”*.

**2002-2004** M.Sc. Chemistry, Department of Chemistry, Faculty of Sciences, Damascus University, Damascus, Syria. *“Treatment of Olive Mill Wastewater Using Photocatalytic Advanced Oxidation Processes in Presence of Semiconductors”*.

**2001-2004** Special Diploma in educational skills, Faculty of Education, Damascus University, Damascus, Syria.

**1999-2000** High Diploma in Chemistry, Department of Chemistry, Faculty of Sciences, Damascus University, Damascus, Syria. *“Kinetic Study of Autoxidation of Cyclohexane Using Molecular Oxygen”*.

**1995-1999** BSc Applied Chemistry, Department of Chemistry, Faculty of Sciences, Damascus University, Damascus, Syria.

### Experiences

**1999- 2006** Supervised practical lessons in the laboratory of the Department of Chemistry Faculty of Sciences, Damascus University, Damascus, Syria.